Development and Application of Improvements to the Tile-based Fisher Ratio Method and Fundamental Instrument Considerations for Non-targeted Analysis using Two-dimensional Gas Chromatography

Brendon Andrew Parsons

A dissertation
submitted in partial fulfillment of the
requirements for the degree of:

Doctor of Philosophy

University of Washington
2016

Reading Committee:
Robert E. Synovec, Chair
Frantisek Tureček
Andrew J. Boydston

Program Authorized to Offer Degree:
Chemistry

University of Washington

Abstract

Development and Application of Improvements to the Tile-based Fisher Ratio Method and Fundamental Instrument Considerations for Non-targeted Analysis using Two-dimensional Gas Chromatography

Brendon A. Parsons

Chair of the Supervisory Committee:

Professor Robert E. Synovec

Department of Chemistry

Comprehensive two-dimensional gas chromatography with time-of-flight mass spectrometry GC×GC–TOFMS has arguably made possible the largest increase in gas chromatograph performance since the innovation of the wall-coated open tubular (WCOT) capillary analytical column in 1979. As with the adoption of capillary columns, taking advantage of the performance possible with GC×GC–TOFMS has required the carefully study of fundamental chromatographic parameters and the development of new data analysis strategies and software to leverage the data rich output of the platform for meaningful discovery in complex chemical matrices. This dissertation presents a thorough account the development and validation of the tile-based Fisher ratio software, which aims to provide a robust and efficient method for non-targeted analysis in experiments comprised of classes of GC×GC–TOFMS chromatograms. Additionally, the

software is further developed and demonstrated in a unique application to a challenging problem of forensic interest: the chemical characterization of the illicit acid alteration of diesel fuel. Finally, the chromatographic methods used in the development, validation, and demonstration of the software are carefully examined in the context of instrument performance, and compared to alternative instrumental configurations that have the potential to further increase performance.

Table of Contents

List of Figures

List of Tables

Acknowledgements

Many people have positively impacted my time in graduate school and years before. My parents, Bruce and Patti, provided me with opportunity, stability, love, and mentorship. They also allowed me the freedom to make decisions for myself, offering guidance where appropriate, but encouraging self-determination. For this, I am grateful. Thank you to my sister, Blithe, for challenging me to appreciate academic endeavors outside of the physical science. Thank you to my surrogate grandparents in North Carolina, Pat and Millie, who provided advice and support complementary to that from my parents. Thank you to those who mentored me in the extracurricular activities that kept me engaged to the community in my high school years: George Sink, teacher and sponsor of the school's Kiwanis Key Club; and Linda Leeds, along with other members of the West Palm Beach Bicycle Club.

Thank you to the Harriet L. Wilkes Honors College and all associated faculty, staff, and administration for the opportunity to study there and develop into the liberal artist I am today. Thank you to the William R. Kenan Jr. Charitable Trust for the financial support of my undergraduate education, as well as summer opportunities that encouraged personal development, and which helped me narrow down my preferred areas of academic and professional interest. Thank you, Prof. Veljko Dragojlovic, for challenging me to think and work independently in my thesis research project. I also appreciate the advice on selecting a graduate school: to choose based on where one desires to live for at next five years, to allow opportunity to enjoy the graduate school experience outside of the laboratory and classroom. Thank you, Prof. Robert Synovec, for encouraging me to think independently and dive deep into research. Thank you for the apprenticeship in analytical and chromatographic science, and for putting me on the diesel fuel forensics project, which was challenging, but ultimately rewarding.

I would also like to acknowledge my close colleagues in my research group, who stuck with me when graduate school was cold enough for a walking stick, and with whom I immensely enjoyed collaborating on myriad projects. To those who partook in beer lunches over the years, cheers! Thank you to my lifelong friends from the Honors College, with whom I've enjoyed talking through my hat, shooting fish in a barrel, and sending coal to Newcastle, while staying in touch both virtually and by occasional visits. Thank you to Dr. William Nilliam, for being involved in others chromatographers' research, rather than my own, and for the invisible hand not have too much influence in my academic pursuits. Lastly, thank you my partner, Sonia Li, whom I met in my last year of graduate school, and with whom I've shared many adventures, with many more to come.

Finally, I enthusiastically acknowledge *Coffea arabica*, which provided me both an enhancement to and diversion from graduate school. Outside of my studies, I enjoyed meeting people in the coffee industry in Seattle, continually refining my knowledge of coffee through informal experimentation in roasting and brewing, and perhaps most importantly, sharing coffee with others. At times in graduate school when my office in the Chemistry Library Building felt more like a room in the Longwood House on Saint Helena, making an afternoon cup of coffee mentally transported me to Réunion, the birthplace of *Coffea arabica* 'Bourbon.' *Coffea canephora* is also gratefully acknowledged, but only in its role as a grafted root stock for the better-tasting *arabica*.

Vita

Brendon A. Parsons was born in Michigan to Bruce and Patti Parsons. Shortly after, his family relocated to North Carolina, where Brendon spent most of his early childhood being an accidental Yankee in the South. Around high school, his family moved to South Florida. After graduating with the very large senior class of 2006 at Wellington High School, Brendon matriculated at the Harriet L. Wilkes Honors College. While at the Honors College, Brendon conducted undergraduate research on solvent transport phenomena associated with phase vanishing reactions utilizing polytetrafluoroethylene plumber's tape, under the mentorship of Prof. Veljko Dragojlovic. After completing his thesis "Permeability of PTFE (Teflon®) tape as a phase screen in phase-vanishing reactions," he graduated *summa cum laude* with a Bachelor of Liberal Arts, with a concentration in chemistry.

After completing his undergraduate studies in Florida, Brendon relocated to Seattle, Washington to begin a Ph.D. program in Chemistry at the University of Washington. Brendon was originally accepted to the UW as a synthetic organic chemist, but he had discovered a passion for chromatography in his last semester at the Honors College; upon acceptance of his offer from the UW, he switched to analytical track and joined the research group of Prof. Rob Synovec. In the Synovec research group, Brendon studied algorithm development, fuel forensics, metabolomics, and instrument optimization, all in the context of two-dimensional gas chromatography mass spectrometry. After conferment of his Ph.D., Brendon will relocate to Los Alamos, NM to pursue new challenges as a postdoctoral research at Los Alamos National Laboratory in the Chemical Diagnostics and Engineering group.

To my family and close friends

For (chromatographic) Science!

Chapter 1: Introduction to Two-dimensional Gas Chromatography and Fisher Ratio Methods for Non-targeted Analysis

1.1 Two-dimensional gas chromatography

Two-dimensional (2D) gas chromatography coupled with time-of-flight mass spectrometry (GC×GC–TOFMS) is a powerful instrumental platform for the qualitative and quantitative analysis of complex samples, especially those which are otherwise challenging to analyze by conventional one-dimensional gas chromatography (GC). By providing additional separation efficiency with similar run times to that of GC, GC×GC improves the capability of the instrument for resolving critical peaks in complicated samples. The benefits of GC×GC for complicated matrices has been highlighted in recent applications, including fuel forensics [1], environmental samples [2,3], and metabolomics [4], as well as more broadly in recent reviews of GC×GC applications [5–7].

In traditional one-dimensional gas chromatography (GC), analytes are injected into the chromatography and separated in the gas phase by relative interaction with a liquid polymeric stationary phase immobilized on the inner wall of a capillary column, referred to as a wall-coated open tubular (WCOT) analytical column [8]. This column is subjected to a constant flow of carrier gas, typically helium or hydrogen—less common alternative carrier gases include nitrogen and argon. Based on the degree to which a chemical partitions to the liquid stationary phase versus degree to which it remains in the gaseous mobile phase, a chemical may be separated from other based on relative retention. A highly retained analyte will spend a relatively long amount of time partitioned into the stationary phase, while a lesser retained analyte will spend a relatively short amount of time in the stationary phase. Because the flow of gaseous

mobile phase determines the maximum velocity by which an analyte may move from the inlet to the outlet of the analytical column, the impact of analyte retention may be observed in the time domain by means of a detector at the outlet. An analyte having no retention in the stationary phase will migrate down the column at the average velocity of the mobile phase, while more retained analytes will spend proportionally longer time in the stationary phase, and will migrate down the column at a reduced velocity.

The partitioning behavior under ordinary conditions may be described as a biphasic equilibrium described by the distribution constant (K_D) for the particular analyte "A" and between the mobile phase and a particular stationary phase, as $K_D = \frac{[A]_{sp}}{[A]_{mp}}$. The retention factor ($k$) describes the relative retention in terms of the retention time of an analyte (t_R) versus that of an unretained analyte (t_0) as $k = \frac{t_R - t_0}{t_0}$. The retention factor may be related to the distribution constant by the phase ratio (β), which is defined for WCOT columns as $\beta = \frac{d_c}{4 \cdot d_f}$, where d_c is the inner diameter of the capillary and d_f is the thickness of the stationary phase film coating the inner wall, as $k = \frac{K_D}{\beta}$. The ability of a gas chromatograph to resolve different analytes is by virtue of the differences in k a pair of analytes may have under particular conditions, which is owing to the entropy and enthalpy constants for that analyte and stationary phase composition, as well as the temperature of the separation. The resulting selectivity (α) of a stationary phase for an analyte pair is calculated as the ratio of the retention factors, $\alpha = \frac{k_2}{k_1}$, where 1 and 2 refer to the first and second eluting analytes, respectively.

In order to understand the separating power of gas chromatography for analyte pairs, it is also necessary to take into account band broadening, which is the physical phenomenon by

which bands of an injected analyte broaden in time and space by various processes inherent to chromatography, particularly diffusion and mass transfer between the stationary phase and mobile phase. The width of a peak at detection is a function of broadening processes both on and off column. The mechanisms of band broadening in gas chromatography are beyond the scope of this work, but are well described in reference books on chromatography [9,10]. Overall, the performance of a chromatograph related to the balance of retention and band broadening, as described by the efficiency (N) of the system; broadly, highly efficient systems (having high values of N) have long retention times with small detected peak widths. Chromatographic resolution (R_S) is the degree to which a pair of analyte peaks are separated, taking into account the differences in retention times and the average $\pm 2\sigma$ width at base (w_b) of the two peaks: $R_S = \frac{t_{R,2}-t_{R,1}}{0.5\cdot(w_{b,2}+w_{b,1})}$. In context of efficiency, selectivity, and retention, resolution may also be defined as $R_S = \frac{\sqrt{N}}{4}\left(\frac{\alpha-1}{\alpha}\right)\left(\frac{k_2}{1+k_2}\right)$.

Beyond the ability of a chromatograph to separate a given analyte pair, an important figure of merit for chromatographic separations is peak capacity (n_c), which is generally defined as the time of the separation window divided by the average peak width at base (4σ width), and which describe the power of a separation system more holistically [9]. Broadly, n_c describes the number of peaks that will fit into a given separation at a chromatographic resolution (R_s) of 1, describing the "resolving power" of a chromatograph for a hypothetical mixture of analytes that cover the separation space. Overall, n_c provides a performance-oriented metric to allow for comparisons of chromatographic systems.

One of the more-prominent implications of peak capacity is as it pertains to statistical overlap theory, which estimates the theoretical peak capacity required for a given system to

sufficiently resolve a mixture of analytes. For example, to resolve to single peaks 98% of the components in a mixture having uniform random retention times, the peak capacity of a separation must exceed the number of components separated by a factor of approximately 100 [9]. For reasonably complex mixtures, it thus follows that a separation's peak capacity must be large. However, using conventional 1D GC, the requirements to achieve an order of magnitude increase in peak capacity (e.g., by using a longer column) are impractical, and may only be reasonable achieved via GC×GC, provided the system is optimized for that objective [3]. In an optimized GC×GC, the peak capacity advantage over 1D GC [3,11,12] is largely realized by the peak capacity provided by the secondary column in a relatively short separation time, and which combines with the peak capacity of the primary column to provide the two-dimensional peak capacity of the GC×GC.

1.2 Improving peak capacity in GC×GC

As a rule, chromatographic systems aim to maximize n_c, or to maintain adequate n_c while reducing method run time. Compared to GC, GC×GC provides approximately an order of magnitude increase in n_c with comparable run times, provided the instrument parameters are carefully selected [3]. For applications in areas having complicated matrices, such as metabolomics, environmental chemistry, petroleum products, and chemical forensics, the two-dimensional peak capacity ($n_{c,2D}$) attainable by GC×GC provides an advantage in successful classification of samples, and the quantification and identification of the analytes that comprise them. Recent work has focused on improving n_c by means of both theoretical modeling [3,11,13] and instrumental improvements, both in terms of introducing new instrument technologies [12,14–16] and by optimizing instrument parameters [3,17]. There are many factors to be considered in the selection of parameters for GC×GC [18]. Recently, it has been recognized that

high $n_{c,2D}$ separations may be achieved through careful selection of the dimensions of the primary and secondary capillary columns [3,12,16,19]. Column dimensions have also been considered recently for control of the pressures and flows of the primary and secondary columns in the context of $n_{c,2D}$ [14,20].

1.3 Signal preprocessing for the analysis of GC×GC chromatograms[1]

Data from comprehensive 2D chromatography separations can be analyzed, on the following three levels: pixel [21], peak table [22,23], or peak region [24,25] basis. While all of these three levels of data are utilized [26,27], the peak table-level and peak region-level approaches are firmly provided by the instrument manufacturers, and hence the analyst must apply such software in the commercially available state. Hence, there is generally little room for independent development of chemometric software at these two data levels, whereas at the pixel-level, there has been rapid growth in the development of chemometric tools for creative and informative analysis of comprehensive 2D chromatography separations data. Accordingly, the focus of this chapter is on the pixel-level chemometric analysis of comprehensive 2D chromatography separations data. For example, recently a novel tile-based data analysis approach, with its fundamental basis at the pixel-level has been introduced for the comparative analysis of large numbers of GC × GC–TOFMS sample runs [1,28,29].

Pixel-based analysis aims to discover the valuable chemical information in complex two-dimensional chromatographic data with high sensitivity for real chemical signals and minimal interference from typical instrumental variations manifest in the data. To achieve this objective,

[1] Parts of this section have been reproduced from the author's contribution to the book chapter "Pixel-level data analysis methods for comprehensive two-dimensional chromatography" K. M. Pierce, B. A. Parsons, R. E. Synovec. Series: Data Handling in Science and Technology; Volume: Fundamentals and Analytical Applications of Multi-way Calibration. Ed. A. C. Olivieri, 2015, Elsevier, Oxford, ISBN 13: 9780444635273.

the chromatographic data must be carefully manipulated to reduce the impact of common variations, such as baseline drift and noise. These steps are performed prior to the analysis of the data, and are referred to as "preprocessing." Preprocessing of the raw chromatographic data reduces the impact of immaterial variations in the data with the goal of improving accuracy and precision of qualitative and quantitative analyses of the chemically-relevant variations that are of interest to the analyst. Preprocessing is thus critically important, and is a step that, if performed properly, allows for maximal discovery of useful information while avoiding wasted experimental, instrumental, and analytical efforts. The most common preprocessing steps which we consider here are: baseline correction, noise reduction, normalization, and retention time alignment, which are presented here in the order by which they are performed.

1.3.1 Baseline correction

The first preprocessing step in most chromatographic analysis work flows is baseline correction. Baseline drift is the low frequency signal variation that occurs in the baseline due to column stationary phase bleed, background ionization, and low frequency variations in the detector and/or instrument-controlled parameters (such as temperature or flow). Baseline rise is the steady increase in baseline observed in temperature programmed or gradient elution separations. Baseline correction procedures aim to mitigate the effects of baseline drift and rise, improving the detection and quantification of analyte peaks that may otherwise be impacted by baseline interference. Baseline correction methods must be carefully implemented in order to preserve the relevant chemical variations, while avoiding overfitting the chromatogram or mistaking broadened features of co-eluting compounds for baseline signals. Following baseline correction, the baseline noise should be centered on zero for the length of the chromatographic separation, and in the case of multichannel detectors, for all channels, as well.

The simplest baseline correction procedure is to collect a "blank" chromatogram and to subtract the blank chromatogram from the sample chromatogram being analyzed. This method is commonly employed in one-dimensional chromatography, but is less-commonly applied to two-dimensional chromatography, as the presence of minor run-to-run misalignment may magnify the baseline when subtracting the blank chromatogram. The next simplest baseline correction algorithm simulates a blank chromatogram by polynomial least squares fitting and subtracts it from the sample chromatogram. Baseline fitting and subtraction may also be performed on manually selected chromatographic subregions [30] or individual peaks[31–33]. Penalized least squares regression or robust orthogonal regression may also be used to model and subtract baselines [34]. Delta2D image processing software uses a powerful "rolling ball" algorithm to perform baseline subtraction for 2D chromatograms [35]. Rolling minimum methods take advantage of the dead time regions on the second separation dimension in comprehensive 2D chromatography for rapid baseline correction.

1.3.2 Noise reduction

Baseline correction procedures are designed to correct low frequency noise and offsets, but not to alter higher frequency variations. Several techniques may be applied to reduce high frequency variations and improve signal-to-noise ratio (S/N) in chromatograms, the most commonly implemented methods are smoothing and binning. The classic Savitzky-Golay method is a running smoothing function that fits a low order polynomial to each data pixel and its neighbors, replacing the signal of each data pixel with the value provided by the polynomial fit [36]. Wavelet smoothing methods transform the chromatogram into the frequency domain, remove the high-frequency components that are assumed to be indeterminate noise, and then perform the reverse transform to the time domain yielding the smoothed chromatogram [37].

Similarly, the low-frequency components characteristic of slowly drifting baseline variations may also be removed with the wavelet method, assisting in baseline correction. Data reduction by simple interpolation and averaging, referred to as "binning," improves S/N and additionally reduces computational load when processing large volumes of 2D separations data [38]. COMForTS, a Fourier transformation method for comprehensive 2D chromatographic separations, improves S/N, and additionally reduces the separation time and data density [39].

Noise reduction techniques are critical to successfully addressing a wide variety of analytical challenges. The improvement in S/N, as well as the concurrent data reduction with some methods, improves the ability of the following pixel-based analysis to discover meaningful chemical differences between samples, while reducing false discoveries due to noise. Regardless of the technique used, noise reduction is a delicate operation that requires careful choice of parameters to avoid compromising the real chemical signals that are present in the data. Careless choice of parameters for noise removal algorithms, or excessive noise removal may artificially broaden peaks, reduce resolution, introduce artifacts, and/or complicate deconvolution.

1.3.3 Normalization

Chromatograms are often normalized to correct between-sample variations that are unavoidably introduced during sample collection, preparation, and injection. The most commonly applied normalization technique is the internal standard method [40–43]. However, it may be difficult to find an inert standard that is completely resolved from all native components for truly unknown samples. As an alternative, isotopically labeled internal standards may be of use, taking advantage of the isotope ratio method [44] if the standard chosen happens to be also be natively present in the sample. However, the use isotopic standards is limited to separations coupled to mass spectrometry. When it is not practical to use the internal standard method, many

users apply the sum-normalization method, which is briefly mentioned in chromatography textbooks, sometimes in terms of area-normalization [10,45]. The sum-normalization method uses the total sum of all baseline corrected signals in a chromatogram as the signal to be normalized. The ratio of the total signal for each sample to that of the mean of all samples is used as the normalization factor to subsequently adjust all chromatographic signals in the samples. The user must assume the samples in the dataset are sufficiently similar, such that equal volumes of the samples should have sufficiently equal total signals at the detector. While this assumption is rarely strictly true, it is often assumed the principal source of variation is due to injection volume. Other normalization methods involve mathematically forcing the mean signal of each chromatogram to equal 1 [46], or mathematically forcing the maximum peak signal volume to equal 1 [47].

Normalization techniques should be carefully chosen to achieve normalization of the desired source of variation. If, for example, a user desires to correct for the efficiency of an extraction, and also the variation in injection volume, a normalization method must be chosen for each. An option may be to add internal standard(s) both prior to extraction, as well as a different internal standard immediately prior injection. The normalization would thus adjust samples based first on injection, and then on extraction. In some cases, the additional sample handling required for internal standard normalization may introduce larger variation than that which is being normalized. Analysts should observe typical variation in their samples and proceed accordingly.

Normalization is applied to samples (every data pixel in a chromatogram is normalized using the same normalization factor) while scaling is applied to variables (each data pixel in a chromatogram is scaled by a unique factor to meet some criteria). Usually, the purpose of scaling

is to reduce the influence of large signals in comparative analyses. Common scaling methods are autoscaling (where the mean of each pixel across all samples is forced to be zero and each pixel is forced to have unit standard deviation across all samples) [48], or dividing each pixel by the mean value among samples [49], or log transformations, or applying power transformations.

1.3.4 Retention time alignment

Alignment is an important preprocessing step because even minor pressure, flow and temperature fluctuations cause retention time variations that may obscure chemical information, resulting in poor performance of most chemometric methods. Alignment algorithms are designed to shift the raw signal along the time axes of the 2D separations so the peak position of a given analyte matches from one sample run to the next. The accuracy of the 2D peak signal volumes should also be preserved during alignment. Alignment algorithms can vary from very simple approaches such as application of a simple scalar shift or a targeted peak list approach, to more sophisticated approaches involving locally and globally optimized alignment algorithms. While all of these alignment algorithm approaches have merit, for the chemometric analysis of pixel-level data, the most commonly applied preprocessing approaches implemented are the latter. This is because locally and globally optimized alignment algorithms can handle severe and dynamic shifting in comprehensive 2D chromatography applications, because they are robust, powerful and essentially automated in every regard after the initial parameter selections have been made by the analyst [21,46,47,50–55].

Alignment of a “sample” chromatogram to a “target” or “reference” chromatogram at the pixel level requires the assumption that the signal due to analyte peaks in those chromatograms are truly matched. For datasets in which samples are relatively similar, this assumption is generally realized. However, for datasets in which samples vary greatly, it is more challenging

for alignment to succeed. This challenge is more confidently addressed for comprehensive 2D chromatography instruments that implement multichannel spectroscopic detection, such as GC × GC–TOFMS, since the alignment algorithms are designed to utilize the spectral information to correctly match the signal due to analyte peaks across samples. It should also be noted that use of local alignment algorithms can provide successful alignment when multichannel spectral information is not available.

1.4 Strategies for the analysis of GC×GC chromatograms

GC×GC–TOFMS is a highly capable instrumental platform that produces complex and information-rich multi-dimensional chemical data. The dimensionality is further increased by including sample and injection replicates. The resulting complex data (often several to tens of gigabytes) can be initially overwhelming, and must be reduced to be efficiently interpreted for the given experiment. To accomplish this goal, methods for analyzing the data must extract the most meaningful information in the data set. The approaches to data reduction for GC×GC–TOFMS can be condensed to two methodologies: targeted and non-targeted. In targeted analysis, analytes of interest are chosen prior to data collection and analysis in order to test a particular hypothesis or make a decision about a sample based on a previously-determined model. An advantage in targeted analysis is that chemical standards may be obtained for positive identification; as a disadvantage, targeted analysis is less useful when no specific hypothesis is available. In non-targeted analysis, less information is needed about the sample. So long as enough is known to designate sample classes and to optimize the instrument for the sample type, an experiment may be devised to mine the meaningful information in the complex data.

Non-targeted techniques aim to comprehensively analyze entire complex data sets to discover important analytes or chemical fingerprints, while requiring few user inputs and

minimizing the need for prior information about the samples. Non-targeted analysis can be either supervised or unsupervised, where supervision refers to the use of external calibration or prior classification of chromatograms as they relate to experimental design. For the research discussed herein, the approach was a supervised, permitting the use of sample class-based analysis to extract meaningful class-distinguishing chemical information from the complex data collected. The discovered class-distinguishing analytes can then be the basis for targeted methods once a hypothesis or model has been formed using the results of the non-targeted approach.

1.5 Fisher ratio method for non-targeted analysis[2]

As described previously, non-targeted approaches can be supervised, meaning that there is prior classification of chromatograms as they relate to the experimental design. Supervised variable selection techniques are used to discover statistically significant chemical differences or similarities among known classes of complex samples. Since class membership must be known, experimental design is particularly important. Furthermore, eliminating uninformative variables and reducing voluminous data down to selective variables can improve predictive models. Two common techniques are uninformative variable elimination (UVE) [56] and Fisher-ratios (F-ratio) feature selection [1,28,29,57,58] methods.

F-ratio feature selection methods are designed to inspect a data set and select variables that contain statistically significant differences among given sample classes. The F-ratio of each independent variable across a given variety of sample classes is defined as the class-to-class

[2] Parts of this section have been reproduced from the author's contribution to the book chapter "Pixel-level data analysis methods for comprehensive two-dimensional chromatography" K. M. Pierce, B. A. Parsons, R. E. Synovec. Series: Data Handling in Science and Technology; Volume: Fundamentals and Analytical Applications of Multi-way Calibration. Ed. A. C. Olivieri, 2015, Elsevier, Oxford, ISBN 13: 9780444635273.

variation of that independent variable divided by the sum of its within-class variations, which may be defined as follows when applied to chromatography [57].

Class-to-class variation = $\sigma_{cl}^2 = \sum \frac{(\bar{x}_i - \bar{x})^2 n_i}{(k-1)}$ (where n_i is the number of chromatograms in the i^{th} class, $\bar{x}_i$ is the mean of the i^{th} class, $\bar{x}$ is the overall mean, and k is the number of classes).

Within-class variation = $\sigma_{err}^2 = \frac{\sum\left(\sum(\overline{x_{ij}} - \bar{x})^2\right) - \left(\sum(\bar{x}_i - \bar{x})^2 n_i\right)}{(N-k)}$ (where x_{ij} is the i^{th} measurement of the j^{th} class, and N is the total number of chromatograms).

Finally, the F-ratio = $\frac{\sigma_{cl}^2}{\sigma_{err}^2}$.

Independent variables with large F-ratios are likely to be features of interest that differentiate sample classes, whereas independent variables with small F-ratios are likely to be representative of noise or features that do not differentiate sample classes. A recently introduced F-ratio algorithm called the tile-based Fisher-ratio software [1,28,29] is designed to comprehensively analyze 4D data sets of pixel-level GC×GC–TOFMS chromatograms to discover chemical features that differentiate given sample classes. The tile-based F-ratio software uses a novel indexing scheme that benefits from the advantages offered by pixel-level data analysis (namely, comprehensive nontargeted information is quickly gleaned) as well as the advantages offered by peak-level data analysis (namely, the algorithm is robust against retention time variations). The independent variables are sorted in descending order of F-ratio value which corresponds with the analyst's level of interest in each independent variable. F-ratio analysis is a robust, comprehensive, nontargeted analysis method that is useful for a variety of studies, particularly forensics experiments in which cause and effect chemical signatures can be cleverly evaluated by the experimental design, and also metabolomics experiments wherein the analyst

often seeks to discover interesting patterns in the chemical fingerprints that characterize cellular processes.

F-ratio methods have been applied to GC×GC–TOFMS data with both peak table analysis (LECO Fisher Ratio ChromaTOF 2009) as well as pixel analysis [59–62]. Peak table-based data is acquired by peak finding, deconvolution, and alignment across peak tables. The steps for peak table preparation can be computationally demanding, especially deconvolution, as the majority of the signals processed are often not of interest to the experimental design being implemented. A pixel-based F-ratio approach, performed prior to any peak finding or deconvolution, has been previously applied as a method to reduce the initial GC×GC–TOFMS data set down to only those 2D separation locations which change significantly between sample classes per the experimental design. Only those 2D locations containing class-distinguishing analytes (as determined by the application of the pixel-based F-ratio method) undergo deconvolution and peak quantification, improving the efficiency of the discovery-based analysis.

1.6 1.6 Fisher ratio method for pixel-level analysis

The pixel-based F-ratio approach has distinct advantages over peak table-based approaches for non-targeted studies; however, the pixel-based method has some shortcomings that must be addressed in a sufficiently peak-based way. In order for this powerful approach to be optimally implemented, it is essential to (1) reduce the number of false positives that are generated, while (2) optimizing the sensitivity "contrast" of finding true positives. First dimension misalignment can severely impact the sensitivity contrast for the F-ratio determination of true positives with pixel-level data. First dimension misalignment in GC × GC is a result of desynchronized modulation of a peak from one injected sample to another. In pixel-based methods, chromatographic misalignment may cause high false-positive rates while concurrently

reducing the sensitivity for true positives. The following section introduces a new approach to comprehensive non-targeted F-ratio analysis of GC × GC – TOFMS data that incorporates the advantages of both pixel-based (unbiased to peak shape and mass spectral behavior) and peak table-based methods (robust to typical retention time variation in either chromatographic dimension).

1.7 Tile-based Fisher ratio method as improvement to pixel-based methods

The new approach to non-targeted F-ratio analysis of GC×GC–TOFMS data, referred to as the tile-based F-ratio algorithm, works by creating a 2D grid (encompassing the entire GC × GC separation) composed of 2D tiles, whereby each tile is wide enough to capture the retention time variation in both the first and second separation dimensions. Four adjacent, but overlapping 2D grids, are used so that one grid will optimally capture any given peak in the GC × GC separation. Use of four grids, combined with summing of all chromatographic signal within a tile (per mass channel), provides data reduction and added sensitivity, similar to peak-based algorithms. Selectivity is improved because a single grid (out of four applied) that captures a given analyte peak the best in one of its tiles will have the least amount of interference. The signal-to-noise (S/N) for a given analyte peak is improved roughly by the square root of the number of points summed. However, if the tile size is inadvisably too big, summation of noise will adversely impact the S/N benefit achieved by summing peak signal. The impact of the GC × GC phasing is minimized since phasing with a total transfer modulator affects only the shape of the first dimension peak, not its amount of signal, which is captured by the optimal tile. The tile-based F-ratio algorithm is demonstrated by application to two standard addition experiments in a challenging complex sample matrix, diesel fuel.

1.8 Hypotheses studied and overview of following chapters

A total of three hypotheses were studied in depth for this work. The first two hypotheses relate to the development of the tile-based F-ratio method, while the third relates to the study of phase ratio as a parameter for high peak capacity GC×GC. The following sections describe the chapters in context of the work performed and the hypotheses that were studied.

1.8.1 Chapter 2: Tile Based Fisher Ratio Analysis of Comprehensive Two-Dimensional Gas Chromatography Time-of-Flight Mass Spectrometry (GC×GC–TOFMS) Data using a Null Distribution Approach

Fisher ratio analysis applied to the supervised comparison of sample classes algorithmically reduces complex GC×GC–TOFMS data sets to find class distinguishing chemical features. F-ratio analysis, using a tile based algorithm, significantly reduces the adverse effects of chromatographic misalignment and spurious covariance of the detected signal, enhancing the discovery of true positives while simultaneously reducing the likelihood of detecting false positives. This chapter reports a study using tile based F-ratio analysis whereby four non-native analytes were spiked into diesel fuel at several concentrations ranging from 0 to 100 ppm. Spike level comparisons were performed in two regimes: comparing the spiked samples to the non-spiked fuel matrix, and to each other at relative concentration factors of two. Redundant hits were algorithmically removed by refocusing the tiled results onto the original high resolution pixel level data. To objectively limit the tile based F-ratio results to only features which are statistically likely to be true positives, we developed a combinatorial technique using null class comparisons, called null distribution analysis, by which we determined a statistically defensible F-ratio cutoff for the analysis of the hit list. This work studies the hypothesis that the tile-based F-ratio method outperforms both pixel-based and peak table methods for non-targeted analyses of complex mixtures. The work also hypothesizes that use of combinatorial

rearrangements of chromatograms nullifies meaningful experimental variation and may be used as a method to control the false discovery rate in non-targeted analyses.

1.8.2 Chapter 3: Chemical Characterization of the Acid Alteration of Diesel Fuel: Non-targeted Analysis by GC × GC–TOFMS with Tile-Based Fisher Ratio and Combinatorial Threshold Determination

The illicit chemical alteration of petroleum fuels is of keen interest, particularly to regulatory agencies that set fuel specifications, or taxes/credits based on those specifications. Such reactions are known to subtly alter the chemical composition of the fuel, particularly the aromatic species native to the fuel. Tile-based Fisher-ratio (F-ratio) analysis reduces the abundance of data in a GC × GC–TOFMS experiment to only the peaks which significantly distinguish the unaltered and acid altered sample classes. Three samples of diesel fuel from differently branded filling stations were each altered to discover chemical features, i.e., analyte peaks, which were consistently changed by the acid reaction. Using different fuels prioritizes the discovery of features likely to be robust to the variation present between fuel samples and may consequently be useful in determining whether an unknown sample has been acid altered. In addition to applying the previously reported tile-based F-ratio method, this chapter also expands null distribution analysis to algorithmically determine an F-ratio threshold to confidently select only the features which are sufficiently class-distinguishing. This work studies the hypothesis that introducing experimental variation into the sample classes prioritizes the discovery of class-distinguishing analytes that are more robust to expected sample variation. Additionally, in the application of the method to diesel fuel alteration, the work hypothesizes that aromatic species are likely removed by the alteration process, and will serve as the best markers for a fuel sample's classification.

1.8.3 Chapter 4: Implications of Phase Ratio (β) for Maximizing Peak Capacity in Comprehensive Two-Dimensional Gas Chromatography Time-of-Flight Mass Spectrometry

Maximizing the information obtained from a GC×GC–TOFMS analysis requires careful optimization of a myriad of parameters to balance the peak capacities of both the first and second separation dimensions. An additional consideration is achieving the target peak capacity in a reasonable analysis time. Phase ratio, β, defined as the ratio of the volume of mobile phase (V_m) to the volume of stationary phase (V_s), is a critical parameter in any partition-based separation mechanism, being influential in determining the retention of a given analyte on a given stationary phase chemistry. Though phase ratio is often carefully considered in the practice and development of methods for one-dimensional gas chromatography (1D-GC), it has received less critical attention as a parameter for GC×GC, in which two distinct separation columns must be chosen for the given application. This chapter examines the relationship of β between the first and second separation dimensions and the implications of β on realization of maximal two-dimensional peak capacity ($n_{c,2D}$). In this experiment, the chromatographic system was held constant for the separation of a multi-component test mixture spanning a range of chemical functionalities, with only the phase ratios of the two analytical columns being changed. This work studies the hypothesis that $n_{c,2D}$ is maximized when ${}^{1}n_c$ is maintained while increasing ${}^{2}n_c$, to an extent dictated by the diminishing returns of ${}^{2}n_c$ with increasing ${}^{2}k$ that is inherent to the pseudo-isothermal nature of the secondary column separation.

1.9 References

[1] B.A. Parsons, D.K. Pinkerton, B.W. Wright, R.E. Synovec, Chemical characterization of the acid alteration of diesel fuel: Non-targeted analysis by two-dimensional gas chromatography coupled with time-of-flight mass spectrometry with tile-based Fisher ratio and combinatorial threshold determination, J. Chromatogr. A. 1440 (2016) 179–190. doi:10.1016/j.chroma.2016.02.067.

[2] S. Prebihalo, A. Brockman, J. Cochran, F.L. Dorman, Determination of emerging contaminants in wastewater utilizing comprehensive two-dimensional gas-chromatography coupled with time-of-flight mass spectrometry, J. Chromatogr. A. 1419 (2015) 109–115. doi:10.1016/j.chroma.2015.09.080.
[3] M.S. Klee, J. Cochran, M. Merrick, L.M. Blumberg, Evaluation of conditions of comprehensive two-dimensional gas chromatography that yield a near-theoretical maximum in peak capacity gain, J. Chromatogr. A. 1383 (2015) 151–159. doi:10.1016/j.chroma.2015.01.031.
[4] N.P. Vasquez, M. Crosnier de bellaistre-Bonose, N. Lévêque, E. Thioulouse, D. Doummar, T. Billette de Villemeur, D. Rodriguez, R. Couderc, S. Robin, C. Courderot-Masuyer, F. Moussa, Advances in the metabolic profiling of acidic compounds in children's urines achieved by comprehensive two-dimensional gas chromatography, J. Chromatogr. B. 1002 (2015) 130–138. doi:10.1016/j.jchromb.2015.08.006.
[5] P.Q. Tranchida, P. Donato, F. Cacciola, M. Beccaria, P. Dugo, L. Mondello, Potential of comprehensive chromatography in food analysis, TrAC Trends Anal. Chem. 52 (2013) 186–205. doi:10.1016/j.trac.2013.07.008.
[6] J.V. Seeley, S.K. Seeley, Multidimensional Gas Chromatography: Fundamental Advances and New Applications, Anal. Chem. 85 (2013) 557–578. doi:10.1021/ac303195u.
[7] A. Sampat, M. Lopatka, M. Sjerps, G. Vivo-Truyols, P. Schoenmakers, A. van Asten, Forensic potential of comprehensive two-dimensional gas chromatography, TrAC Trends Anal. Chem. 80 (2016) 345–363. doi:10.1016/j.trac.2015.10.011.
[8] R.D. Dandeneau, E.H. Zerenner, An investigation of glasses for capillary chromatography, J. High Resolut. Chromatogr. 2 (1979) 351–356. doi:10.1002/jhrc.1240020617.
[9] J.C. Giddings, Unified separation science, Wiley, New York, 1991.
[10] K. (Kevin) Robards, Principles and practice of modern chromatographic methods, Elsevier Academic Press, London ; Boston, 2004.
[11] L.M. Blumberg, F. David, M.S. Klee, P. Sandra, Comparison of one-dimensional and comprehensive two-dimensional separations by gas chromatography, J. Chromatogr. A. 1188 (2008) 2–16. doi:10.1016/j.chroma.2008.02.044.
[12] R.B. Wilson, W.C. Siegler, J.C. Hoggard, B.D. Fitz, J.S. Nadeau, R.E. Synovec, Achieving high peak capacity production for gas chromatography and comprehensive two-dimensional gas chromatography by minimizing off-column peak broadening, J. Chromatogr. A. 1218 (2011) 3130–3139. doi:10.1016/j.chroma.2010.12.108.
[13] D.K. Pinkerton, B.A. Parsons, T.J. Anderson, R.E. Synovec, Trilinearity deviation ratio: A new metric for chemometric analysis of comprehensive two-dimensional gas chromatography time-of-flight mass spectrometry data, Anal. Chim. Acta. 871 (2015) 66–76. doi:10.1016/j.aca.2015.02.040.
[14] D. Peroni, H.-G. Janssen, Comprehensive two-dimensional gas chromatography under high outlet pressure conditions: A new approach to correct the flow-mismatch issue in the two dimensions, J. Chromatogr. A. 1332 (2014) 57–63. doi:10.1016/j.chroma.2014.01.051.
[15] D. Peroni, A.A.S. Sampat, W. van Egmond, S. de Koning, J. Cochran, R. Lautamo, H.-G. Janssen, Comprehensive two-dimensional gas chromatography with a multi-capillary second dimension: A new column-set format for simultaneous optimum linear velocity operation, J. Chromatogr. A. (2013). doi:10.1016/j.chroma.2013.07.097.

[16] B.D. Fitz, R.B. Wilson, B.A. Parsons, J.C. Hoggard, R.E. Synovec, Fast, high peak capacity separations in comprehensive two-dimensional gas chromatography with time-of-flight mass spectrometry, J. Chromatogr. A. 1266 (2012) 116–123. doi:10.1016/j.chroma.2012.09.096.
[17] W.C. Siegler, B.D. Fitz, J.C. Hoggard, R.E. Synovec, Experimental Study of the Quantitative Precision for Valve-Based Comprehensive Two-Dimensional Gas Chromatography, Anal. Chem. 83 (2011) 5190–5196. doi:10.1021/ac200302b.
[18] A. Mostafa, M. Edwards, T. Górecki, Optimization aspects of comprehensive two-dimensional gas chromatography, J. Chromatogr. A. 1255 (2012) 38–55. doi:10.1016/j.chroma.2012.02.064.
[19] C. Cordero, C. Bicchi, M. Galli, S. Galli, P. Rubiolo, Evaluation of different internal-diameter column combinations in comprehensive two-dimensional gas chromatography in flavour and fragrance analysis, J. Sep. Sci. 31 (2008) 3437–3450. doi:10.1002/jssc.200800280.
[20] P.Q. Tranchida, M. Maimone, F.A. Franchina, T.R. Bjerk, C.A. Zini, G. Purcaro, L. Mondello, Four-stage (low-)flow modulation comprehensive gas chromatography–quadrupole mass spectrometry for the determination of recently-highlighted cosmetic allergens, J. Chromatogr. A. 1439 (2016) 144–151. doi:10.1016/j.chroma.2015.12.002.
[21] T. Gröger, M. Schäffer, M. Pütz, B. Ahrens, K. Drew, M. Eschner, R. Zimmermann, Application of two-dimensional gas chromatography combined with pixel-based chemometric processing for the chemical profiling of illicit drug samples, J. Chromatogr. A. 1200 (2008) 8–16. doi:10.1016/j.chroma.2008.05.028.
[22] M.F. Almstetter, I.J. Appel, K. Dettmer, M.A. Gruber, P.J. Oefner, Comparison of two algorithmic data processing strategies for metabolic fingerprinting by comprehensive two-dimensional gas chromatography–time-of-flight mass spectrometry, J. Chromatogr. A. 1218 (2011) 7031–7038. doi:10.1016/j.chroma.2011.08.006.
[23] J.E. Welke, V. Manfroi, M. Zanus, M. Lazzarotto, C. Alcaraz Zini, Differentiation of wines according to grape variety using multivariate analysis of comprehensive two-dimensional gas chromatography with time-of-flight mass spectrometric detection data, Food Chem. 141 (2013) 3897–3905. doi:10.1016/j.foodchem.2013.06.100.
[24] P.M. Harvey, R.A. Shellie, Data Reduction in Comprehensive Two-Dimensional Gas Chromatography for Rapid and Repeatable Automated Data Analysis, Anal. Chem. 84 (2012) 6501–6507. doi:10.1021/ac300664h.
[25] S.E. Reichenbach, X. Tian, A.A. Boateng, C.A. Mullen, C. Cordero, Q. Tao, Reliable Peak Selection for Multisample Analysis with Comprehensive Two-Dimensional Chromatography, Anal. Chem. 85 (2013) 4974–4981. doi:10.1021/ac303773v.
[26] S.E. Reichenbach, X. Tian, C. Cordero, Q. Tao, Features for non-targeted cross-sample analysis with comprehensive two-dimensional chromatography, J. Chromatogr. A. 1226 (2012) 140–148. doi:10.1016/j.chroma.2011.07.046.
[27] M. Brokl, L. Bishop, C.G. Wright, C. Liu, K. McAdam, J.-F. Focant, Multivariate analysis of mainstream tobacco smoke particulate phase by headspace solid-phase micro extraction coupled with comprehensive two-dimensional gas chromatography–time-of-flight mass spectrometry, J. Chromatogr. A. 1370 (2014) 216–229. doi:10.1016/j.chroma.2014.10.057.
[28] L.C. Marney, W. Christopher Siegler, B.A. Parsons, J.C. Hoggard, B.W. Wright, R.E. Synovec, Tile-based Fisher-ratio software for improved feature selection analysis of

comprehensive two-dimensional gas chromatography–time-of-flight mass spectrometry data, Talanta. 115 (2013) 887–895. doi:10.1016/j.talanta.2013.06.038.
[29] B.A. Parsons, L.C. Marney, W.C. Siegler, J.C. Hoggard, B.W. Wright, R.E. Synovec, Tile-Based Fisher Ratio Analysis of Comprehensive Two-Dimensional Gas Chromatography Time-of-Flight Mass Spectrometry (GC × GC–TOFMS) Data Using a Null Distribution Approach, Anal. Chem. 87 (2015) 3812–3819. doi:10.1021/ac504472s.
[30] H.P. Bailey, S.C. Rutan, P.W. Carr, Factors that affect quantification of diode array data in comprehensive two-dimensional liquid chromatography using chemometric data analysis, J. Chromatogr. A. 1218 (2011) 8411–8422. doi:10.1016/j.chroma.2011.09.057.
[31] J.C. Hoggard, R.E. Synovec, Parallel Factor Analysis (PARAFAC) of Target Analytes in GC × GC−TOFMS Data: Automated Selection of a Model with an Appropriate Number of Factors, Anal. Chem. 79 (2007) 1611–1619. doi:10.1021/ac061710b.
[32] H.J. Tobias, G.L. Sacks, Y. Zhang, J.T. Brenna, Comprehensive Two-Dimensional Gas Chromatography Combustion Isotope Ratio Mass Spectrometry, Anal. Chem. 80 (2008) 8613–8621. doi:10.1021/ac801511d.
[33] L. Mondello, M. Herrero, T. Kumm, P. Dugo, H. Cortes, G. Dugo, Quantification in Comprehensive Two-Dimensional Liquid Chromatography, Anal. Chem. 80 (2008) 5418–5424. doi:10.1021/ac800484y.
[34] M. Daszykowski, M.S. Wróbel, A. Bierczynska-Krzysik, J. Silberring, G. Lubec, B. Walczak, Automatic preprocessing of electrophoretic images, Chemom. Intell. Lab. Syst. 97 (2009) 132–140. doi:10.1016/j.chemolab.2009.03.002.
[35] H.-G. Schmarr, J. Bernhardt, Profiling analysis of volatile compounds from fruits using comprehensive two-dimensional gas chromatography and image processing techniques, J. Chromatogr. A. 1217 (2010) 565–574. doi:10.1016/j.chroma.2009.11.063.
[36] P.G. Stevenson, M. Mnatsakanyan, G. Guiochon, R.A. Shalliker, Peak picking and the assessment of separation performance in two-dimensional high performance liquid chromatography, Analyst. 135 (2010) 1541–1550. doi:10.1039/B922759H.
[37] A. Soggiu, O. Marullo, E. Capobianco, P. Roncada, P. Roncada, Empowering spot detection in 2DE images by wavelet denoising, In Silico Biol. 9 (2009) 125–133. doi:10.3233/ISB-2009-0393.
[38] J.S. Nadeau, R.B. Wilson, J.C. Hoggard, B.W. Wright, R.E. Synovec, Study of the interdependency of the data sampling ratio with retention time alignment and principal component analysis for gas chromatography, J. Chromatogr. A. 1218 (2011) 9091–9101. doi:10.1016/j.chroma.2011.10.031.
[39] M.J.E. Trudgett, G. Guiochon, R.A. Shalliker, Theoretical description of a new analytical technique: Comprehensive online multidimensional fast Fourier transform separations, J. Chromatogr. A. 1218 (2011) 3545–3554. doi:10.1016/j.chroma.2011.03.061.
[40] E.J.C. van der Klift, G. Vivó-Truyols, F.W. Claassen, F.L. van Holthoon, T.A. van Beek, Comprehensive two-dimensional liquid chromatography with ultraviolet, evaporative light scattering and mass spectrometric detection of triacylglycerols in corn oil, J. Chromatogr. A. 1178 (2008) 43–55. doi:10.1016/j.chroma.2007.11.039.
[41] S. Castillo, I. Mattila, J. Miettinen, M. Orešič, T. Hyötyläinen, Data Analysis Tool for Comprehensive Two-Dimensional Gas Chromatography/Time-of-Flight Mass Spectrometry, Anal. Chem. 83 (2011) 3058–3067. doi:10.1021/ac103308x.

[42] O. Amador-Muñoz, P.J. Marriott, Quantification in comprehensive two-dimensional gas chromatography and a model of quantification based on selected summed modulated peaks, J. Chromatogr. A. 1184 (2008) 323–340. doi:10.1016/j.chroma.2007.10.041.
[43] M. Kallio, M. Kivilompolo, S. Varjo, M. Jussila, T. Hyötyläinen, Data analysis programs for comprehensive two-dimensional chromatography, J. Chromatogr. A. 1216 (2009) 2923–2927. doi:10.1016/j.chroma.2008.11.037.
[44] E.M. Humston, J.C. Hoggard, R.E. Synovec, Utilizing the Third Order Advantage with Isotope Dilution Mass Spectrometry, Anal. Chem. 82 (2010) 41–43. doi:10.1021/ac902184b.
[45] Milton L. Lee, Open tubular column gas chromatography: theory and practice, Wiley, New York, 1984.
[46] J. Vial, B. Pezous, D. Thiébaut, P. Sassiat, B. Teillet, X. Cahours, I. Rivals, The discriminant pixel approach: A new tool for the rational interpretation of GCxGC-MS chromatograms, Talanta. 83 (2011) 1295–1301. doi:10.1016/j.talanta.2010.07.059.
[47] R.E. Mohler, B.P. Tu, K.M. Dombek, J.C. Hoggard, E.T. Young, R.E. Synovec, Identification and evaluation of cycling yeast metabolites in two-dimensional comprehensive gas chromatography–time-of-flight-mass spectrometry data, J. Chromatogr. A. 1186 (2008) 401–411. doi:10.1016/j.chroma.2007.10.063.
[48] C. Pc, H. J, B. Vc, Y.J. 3rd, Identifying differences in protein expression levels by spectral counting and feature selection., Identifying differences in protein expression levels by spectral counting and feature selection, Genet. Mol. Res. GMR Genet. Mol. Res. GMR. 7, 7 (2007) 342, 342–356. doi:10.4238/vol7-2gmr426.
[49] J.C. Hoggard, J.H. Wahl, R.E. Synovec, G.M. Mong, C.G. Fraga, Impurity Profiling of a Chemical Weapon Precursor for Possible Forensic Signatures by Comprehensive Two-Dimensional Gas Chromatography/Mass Spectrometry and Chemometrics, Anal. Chem. 82 (2010) 689–698. doi:10.1021/ac902247x.
[50] R.C. Allen, S.C. Rutan, Investigation of interpolation techniques for the reconstruction of the first dimension of comprehensive two-dimensional liquid chromatography–diode array detector data, Anal. Chim. Acta. 705 (2011) 253–260. doi:10.1016/j.aca.2011.06.022.
[51] K.J. Johnson, B.W. Wright, K.H. Jarman, R.E. Synovec, High-speed peak matching algorithm for retention time alignment of gas chromatographic data for chemometric analysis, J. Chromatogr. A. 996 (2003) 141–155. doi:10.1016/S0021-9673(03)00616-2.
[52] G. Tomasi, F. van den Berg, C. Andersson, Correlation optimized warping and dynamic time warping as preprocessing methods for chromatographic data, J. Chemom. 18 (2004) 231–241. doi:10.1002/cem.859.
[53] T. Gröger, R. Zimmermann, Application of parallel computing to speed up chemometrics for GC × GC–TOFMS based metabolic fingerprinting, Talanta. 83 (2011) 1289–1294. doi:10.1016/j.talanta.2010.09.015.
[54] D. Zhang, X. Huang, F.E. Regnier, M. Zhang, Two-Dimensional Correlation Optimized Warping Algorithm for Aligning GC×GC−MS Data, Anal. Chem. 80 (2008) 2664–2671. doi:10.1021/ac7024317.
[55] J. Vial, H. Noçairi, P. Sassiat, S. Mallipatu, G. Cognon, D. Thiébaut, B. Teillet, D.N. Rutledge, Combination of dynamic time warping and multivariate analysis for the comparison of comprehensive two-dimensional gas chromatograms: Application to plant extracts, J. Chromatogr. A. 1216 (2009) 2866–2872. doi:10.1016/j.chroma.2008.09.027.

[56] V. Centner, D.-L. Massart, O.E. de Noord, S. de Jong, B.M. Vandeginste, C. Sterna, Elimination of Uninformative Variables for Multivariate Calibration, Anal. Chem. 68 (1996) 3851–3858. doi:10.1021/ac960321m.
[57] K.J. Johnson, R.E. Synovec, Pattern recognition of jet fuels: comprehensive GC×GC with ANOVA-based feature selection and principal component analysis, Chemom. Intell. Lab. Syst. 60 (2002) 225–237. doi:10.1016/S0169-7439(01)00198-8.
[58] K.M. Pierce, J.C. Hoggard, J.L. Hope, P.M. Rainey, A.N. Hoofnagle, R.M. Jack, B.W. Wright, R.E. Synovec, Fisher Ratio Method Applied to Third-Order Separation Data To Identify Significant Chemical Components of Metabolite Extracts, Anal. Chem. 78 (2006) 5068–5075. doi:10.1021/ac0602625.
[59] H.J. Cortes, B. Winniford, J. Luong, M. Pursch, Comprehensive two dimensional gas chromatography review, J. Sep. Sci. 32 (2009) 883–904. doi:10.1002/jssc.200800654.
[60] L. Mondello, P.Q. Tranchida, P. Dugo, G. Dugo, Comprehensive two-dimensional gas chromatography-mass spectrometry: A review, Mass Spectrom. Rev. 27 (2008) 101–124. doi:10.1002/mas.20158.
[61] I. François, K. Sandra, P. Sandra, Comprehensive liquid chromatography: Fundamental aspects and practical considerations—A review, Anal. Chim. Acta. 641 (2009) 14–31. doi:10.1016/j.aca.2009.03.041.
[62] S.E. Reichenbach, X. Tian, Q. Tao, D.R. Stoll, P.W. Carr, Comprehensive feature analysis for sample classification with comprehensive two-dimensional LC, J. Sep. Sci. 33 (2010) 1365–1374. doi:10.1002/jssc.200900859.

Chapter 2: Tile Based Fisher Ratio Analysis of Comprehensive Two-Dimensional Gas Chromatography Time-of-Flight Mass Spectrometry (GC×GC–TOFMS) Data using a Null Distribution Approach[3]

2.1 Introduction

Two-dimensional (2D) gas chromatography coupled with time-of-flight mass spectrometry (GC×GC–TOFMS) is a prominent instrumental platform for the study of complex samples for analytes either sufficiently volatile or amenable to analysis after derivatization.[1–8] Use of GC×GC–TOFMS and associated data analysis strategies aim to uncover meaningful chemical information from complex samples. However, meaningful chemical information is often buried in a background of less meaningful chemical signal and noise. Further complicating the effort, experiments often require analysis of replicate injections of different samples, increasing the data dimensionality. Feature selection software becomes increasingly important to extract the most meaningful chemical information. Ultimately automatable software is needed to comprehensively analyze GC×GC–TOFMS data so important analytes and/or chemical fingerprints can be quickly and accurately ascertained during discovery-based experimentation.

Our focus is on non-targeted discovery-based GC×GC–TOFMS investigations, whereby chemical features of interest are not presumed known beforehand. Non-targeted approaches can be either supervised or unsupervised, where supervision refers to either external calibration or prior classification of samples/chromatograms as they relate to the experimental design.[9–11] Non-targeted analyses are typically performed by software comparing the chromatograms on a pixel,

[3] This chapter has been reproduced from B. A. Parsons, L. C. Marney, W. C. Siegler, J. C. Hoggard, B. W. Wright, R. E. Synovec. Anal. Chem., 2015, 87, 3812–3819.

peak table, or peak region basis. These approaches have been reviewed in the context of non-targeted analysis of GC×GC data.[12] Specific approaches to GC×GC data processing include watershed algorithm[13] and template matching[14] methods, chromatographic region based binning[15], chromatographic and mass spectral inspection[16], and scripting based classification.[17] We recently reported an approach to GC×GC data processing, referred to as tile based analysis, in which data is strategically binned, with the tile size based upon the 2D peak widths and the retention time shifting that may be present.[18] Recent studies have reported using a combination of multiple approaches (peak table, pixel, and peak region based).[19]

Pixel based analysis compares every GC×GC–TOFMS data point in the three-dimensional space (3D), i.e. pixel, in each chromatogram with relatively limited preprocessing (beyond baseline correction and normalization steps). Since chromatographic misalignment may lead to false positives and diminished ability to discover true positives, 2D alignment[20–25] is often required to reduce misalignment, but may distort peak shapes and areas in the pixel level data. Further, typical GC×GC parameters applied (a low number of modulations per first dimension peak width, e.g., a modulation ratio M_R ~ 2 to 4)[26] limits the data density defining first dimension peaks due to the need to balance the peak capacities in both GC×GC dimensions; this reduces the information available for first dimension alignment.[27] On the other hand, peak based approaches utilize baseline correction, peak deconvolution and identification, integration, and arrangement of every peak in a single chromatogram into a table (i.e., peak table), and tables are then compared across samples. Tile based analysis[18] addresses the challenges due to misalignment of multiple GC×GC–TOFMS chromatograms without explicitly aligning the data, thus avoiding chromatographic and/or mass spectral warping or other distortions of the raw data. Tile based analysis combines advantages of peak table based approaches (including mitigation of

misalignment and improvement in signal-to-noise) and the advantages of pixel based approaches (remaining unbiased to chromatographic peak shape or mass spectral signal characteristics).

After the data have been prepared by either pixel, tile, or peak table based approaches, supervised statistical analysis can be performed to discover chemical features that distinguish the sample classes, producing lists of significant feature referred to as hit lists. Two popular supervised methods include F-ratio analysis and partial least squares discriminant analysis (PLS-DA). F-ratio analysis has been applied to GC×GC–TOFMS data previously at the pixel level[28–33] and at the peak table level using LECO ChromaTOF Statistical Compare.[34–37] PLS-DA has also been applied to peak table based GC×GC–TOFMS data.[38–41] For non-targeted analysis, false positives should be minimized while maximizing the sensitivity with which true positives are detected. False positives are the rejection of the null hypothesis when it is actually true, often referred to as Type I errors. For F-ratio analysis, a false positive is the discovery of a feature that does not chemically distinguish the sample classes. While a true positive is a feature that is chemically class distinguishing (e.g., a peak signal inferring a statistically significant difference in concentration between the two or more sample classes), a false positive may either be due to spurious covariance of detector fluctuations or chromatographic misalignment. Tile based F-ratio analysis significantly reduces the number of false positives found with pixel based analysis of GC×GC–TOFMS data that were associated with the aforementioned causes.[18] While tile based F-ratio analysis reduces the frequency and rank of false positives in the hit list, false positives are still present in the analysis simply due to the large number of statistical hypotheses being simultaneously tested in the entire tiled GC×GC–TOFMS chromatogram. This is encountered in multiple hypothesis testing and is commonly described by the false discovery rate (FDR).[42]

For efficient and informative non-targeted F-ratio analysis, the relative distributions of true and false positives must be understood so the analysis can focus on true positives. This is typically performed in a subjective manner by selecting an F-ratio cutoff in the hit list at the point where the selected features become unreliable in differentiating the sample classes.[29, 36] However, manual selection of a cutoff comes with two complications. First, the cutoff must be determined by working through the ranked hit list and validating the results to determine the point at which the analysis becomes unreliable. This is problematic as it requires time consuming analysis of features with little value, and because the cutoff must be determined in a subjective manner, as true positives are often interspersed with false positives as one works down the hit list. The second concern is that this exercise must be repeated for every experiment, since sampling and instrumental variance may differ from one experimental campaign to the next.

Ideally, an objective metric should be implemented that expresses the confidence by which a given feature can be deemed a true positive. Herein, we critically study utilization of false positive distribution estimations, called "null distributions," which ultimately allows for a statistically based determination of whether a discovered class distinguishing feature is likely to be either a true positive or a false positive. We utilize tile based F-ratio analysis in concert with the standard addition method by spiking non-native chemicals into a diesel fuel matrix at low concentrations. While the previous work studied the concentration range of 100 ppm to1000 ppm[18], the current study focuses on the 0 ppm to 100 ppm analyte spike range. The current study demonstrates the sensitivity and selectivity of tile based F-ratio analysis for discovery of true positives in the non-targeted analysis of a chemically complex and analytically challenging sample matrix. Additionally, we demonstrate the utility of null distribution analysis to defensibly limit the resulting hit list to only the features most likely to be class distinguishing, and

ultimately, useful to the analyst. By exploring the low concentration spike levels, we gain a better understanding of the "discovery" limit of detection (LOD) of tile based F-ratio analysis, and compare its merits to pixel based and peak table based approaches.

2.2 Experimental

Four chemical compounds were spiked at the following nominal concentrations into an ultra-low sulfur diesel (ULSD) fuel: 100, 50, 25, 12.5, 6.2, 3.2, 1.6 and 0 parts-per-million by mass (ppm). The 0 ppm spike level served as the matrix blank. The four spiked compounds were bromobenzene, 1-chlorohexane, 5-decyne, and 3-octanone, none of which is naturally present in the fuel, as verified by the standard addition method. An internal standard, 1-bromoheptane, was also spiked into each sample at 1 part-per-thousand (ppt). All samples were prepared gravimetrically using a 5-place analytical balance, and the actual (not nominal) concentration for each analyte at each spike level is provided in Table S-1 (Supporting Information, Section S1.1). Additionally, the calculated mass of each analyte injected on column is provided in Table S-2. The actual concentrations of the spiked analytes are used for software evaluation. However, for clarity we use the nominal spike concentrations when referring to a particular concentration comparison with multiple analytes. The samples were analyzed by GC×GC–TOFMS, as in the previous report.[18] Under the selected instrumental conditions, the modulation ratio was 3 to 4, depending on the first dimension peak width.[26] Full instrument parameters and a representative chromatogram are provided in the Supporting Information (Section S1.2, Figure S-1).

GC×GC–TOFMS data from all 36 runs (7 spike levels x 4 replicates, and 8 replicates of the 0 ppm) were imported from the LECO ChromaTOF software v 3.32 (LECO, St. Joseph, MI) to Matlab v 8.0.0.783 (MathWorks, Inc., Natick, MA) via an in-house developed data converter.[43] The imported data were analyzed with the in-house developed tile based F-ratio

software, performed on a mid-level personal computer, having an Intel Core i7-4770 processor (3.4 GHz), a 256 GB Samsung 840 solid state hard drive, and 16 GB dual-channel DDR3 RAM. An in-house developed PARAFAC GUI was used to measure the quantitative signal volume for the internal standard, 1-bromoheptane, for each sample injection, which was used to normalize the data to account for injection variation.[9] The F-ratio was calculated as the class-to-class variation of the detected signal divided by the sum of the within-class variations of the signal.[28,44,45] Details of the F-ratio calculation and a summary of the preprocessing steps are included in the Supporting Information (Sections S2.1 and S2.2).

The GC×GC pixel level data was summed using a novel method of binning, the tile method.[18] Details on the tile method and its advantages are available in the Supporting Information (Section S2.3 and Figure S-2). Redundant hits were removed using a novel "pin and cluster" algorithm, detailed in the Supporting Information (Section 2.4 and Figure S-3 and Tables S-3 and S-4). The complete tile based F-ratio software is summarized by a flowchart in the Supporting Information, Figure S-4. The specific parameters for the tile method and redundant hit removal are included in the Supporting Information (Section S1.3). The 2D chromatographic features discovered by tile based analysis are arranged in a ranked table sorted by decreasing average F-ratio, i.e., a "hit list," an example of which is provided in Table 1. To compare the performance of the tile based F-ratio analysis with other relevant methods, the data were also processed by pixel based and peak table based methods, using in-house software and LECO ChromaTOF v 3.32, respectively. Details of the pixel and peak table analyses are provided in the Supporting Information (Section S4).

Following the generation of hit lists by the tile based F-ratio analysis, null distribution analysis was implemented to control the false discovery rate by determining the probability that a

discovered feature is a false positive. Due to the large number of statistical hypotheses being simultaneously tested in the tiled data, a portion of the statistical tests will falsely reject the null hypothesis when it is true, i.e., false positives (Type I errors).[46–53] The large number of simultaneous hypotheses tested in the tiled data were leveraged to determine the distribution of potential false positives. These distributions were utilized to limit the analysis of the hit list to only the range that is likely to have few or no false positives, using an objective metric as we demonstrate herein. False positive distributions can be determined by repeated testing of null hypotheses (i.e., that there is no difference between sample classes), created by either comparing replicates of a single class, or by evenly mixing the sample classes to eliminate between-class variation. In this study, such comparisons of GC×GC–TOFMS data of the diesel samples were subjected to tile based analysis to generate null comparison hit lists, from which the F-ratio values are used to make a histogram. Because the comparisons are testing the null hypothesis, we refer to the resulting curves as "null distributions."

2.3 Results and Discussion

Null comparisons were performed based upon a pair-wise rearrangement (switching of two samples at a time from each class, keeping balanced classes) of the eight injection replicates of the 0 ppm diesel fuel that served as the matrix blank. Six null class comparisons were deemed sufficient to capture the variation in the null comparisons, as different combinations of the injection replicates ultimately resulted in only slightly different distributions of null F-ratios. This approach is a form of combinatorial analysis.[54] Each of these null comparisons was subjected to tile based F-ratio analysis in order to generate a total of six null hit lists. Null distributions (see Figure 1(A)) were then prepared from the hit lists. The F-ratio values for each feature from the null hit lists were then combined into a histogram with a bin size of 0.2. The

average null distribution (black trace) has an average of 4860 ±77 features. The range of null distributions encountered is also provided in Figure 1(A) by the blue and red traces. The inset plot in Figure 1(A) is a zoomed section, emphasizing the range of the null distribution tails at higher F-ratios. This region is sparse due to the infrequent occurrence of values greater than ~ 10 in the null distributions, and it follows that in true class comparisons (discussed shortly) there may be occasional false positives interspersed with the true positives at values that have some overlap with the null distribution. It is this region of the null distribution that relates to the discovery-LOD for the tile based F-ratio analysis that we explored.

Transforming a null distribution into a "null probability" curve facilitates limiting a hit list to features that are likely to be either a false positive or a true positive. The null probability provides the quantitative likelihood that a given feature is indeed a false positive, based on its average F-ratio. This calculation is performed by dividing the summed number of null features above a given value by the total number of null features in the entire null distribution, multiplied by 100 to yield a percentage. The null probability is equivalent to the percentage area of the null distribution that is above a given value, which represents the proportion of the null features that would be included in the analysis with a given F-ratio cutoff. This calculation is performed for the range of values in the null distribution to create a curve which is the null probability versus average F-ratio. Figure 1(B) is the null probability curve for the average null distribution (the black trace), as well as the range of individual null distributions shown in Figure 1(A), the blue trace and red trace. The horizontal range between the blue and red traces gives rise to a null probability range, which expresses the variation in the average F-ratio which would be selected for various null probability limits. If one were to limit a comparison to features with less than 0.1% probability that the feature is a false positive (this would be equivalent to accepting ~ 5

spurious features in the analysis, based on the 4860 features in the average null distribution for this data set), this corresponds to a threshold of ~ 14, such that only features with average F-ratios above 14 would be inspected. However, since there is variation in the distribution of false positives in the null comparisons, as shown in Figure 1(A), it is necessary to designate a range for an F-ratio limit at a particular null probability. Accordingly, as illustrated in Figure 1(B), the range for the 0.1% null probability limit is ~ 10 to 20. Based upon the 0.1% null probability limit, an average F-ratio at or above 20 is referred to as a "hit" while a value ranging from 10 to 20 is referred to as a "potential hit". A value below 10 is referred to as a "non-hit". Therefore, the analyst should work from the top of the hit list, since "hits" have the highest likelihood of being true positives. As defined in Figure 1, the hit lists in this report include a null classification, whereby the features were assigned as hit, potential hit, or non-hit based on their F-ratio relative to the 0.1% null probability limit.

Tile based F-ratio analyses for true class comparisons were performed in two regimes: spike versus blank comparisons (e.g., 6.2 ppm versus 0 ppm) and concentration ratio of 2 comparisons (e.g., 25 ppm versus 12.5 ppm). The spike versus blank comparisons test tile based F-ratio analysis in cases where a low abundance analyte is present in one sample class and absent from the other. The concentration ratio of two comparisons test cases where a low abundance analyte is different in concentration by a factor of two between the sample classes. Each of these cases is important for the performance of a non-targeted analysis platform. For these true class comparisons, and analogous to the null distributions in Figure 1(A), *false positive* distributions were prepared and summarized in Figure 2. Note that the features corresponding to the four true positives (i.e., the spiked analytes) in each comparison were removed in the preparation of Figure 2. The resulting distributions have an average of 4944 ±141 false positives. Figure 2

shows false positive distributions from four comparisons representing the range of false positive F-ratio values encountered. The average null distribution from Figure 1(A) is also plotted in Figure 2 for comparison. As in Figure 1(A), in Figure 2 the F-ratios for the false positives from each comparison were made into histograms using a bin size of 0.2. The range of false positive distributions indicates there is some modest variation in the shape of the distributions, though nearly all of the false positives have F-ratios below 10, which strongly supports the implementation of null distribution data to determine the relationship between false positives and their corresponding F-ratio, as delineated in the null probability curve (Figure 1B). Indeed, the null distributions in Figure 1(A) are of similar range to the false positive distributions in Figure 2, and the average null distribution is essentially the average of the false positive distributions. In this study, we have taken advantage of knowing the true positives (the spiked analytes) in order to critically compare the underlying false positive distributions in the true class comparisons with the null distributions prepared from replicates of the non-spiked diesel fuel (0 ppm matrix blank). For analysis of comparisons where the true positives are not known, false positive distributions cannot be determined; instead, null distribution analysis is needed to estimate the underlying distribution of false positives and to illustrate the discovery-LOD for tile based F-ratio analysis, as is described next.

The true class comparisons, in the context of the 0.1% probability limit presented in Figure 1(B), are presented in Figure 3(A) and 3(B) for the spike versus blank comparisons and the concentration ratio of two comparisons, respectively. The plots show the average F-ratios for each of the four spiked analytes versus their actual concentration (in ppm) in the comparisons. In the concentration ratio of two plot, the concentration plotted is that of the lower concentration spike in the comparison. The 0.1% null probability limit range (illustrated in Figure 1B) is

included in the figure to show whether analytes would be found if the 0.1% null probability limit were applied. Features above the 0.1% null probability limit (hits) would be found in the course of the analysis of the hit list, while those below the limit (non-hits) would not, unless the analyst is willing to look through a larger number of false positives. Analytes within the 0.1% probability limit (potential hits) often may be readily found, depending on the distribution of false positives in the particular comparison, and the extent to which the hit list is examined.

Most of the spiked analytes were consistently "found" above the 0.1% probability limit for the range of concentration comparisons studied, even for the more analytically challenging concentration ratio of two comparisons. None the less, there were sufficient cases that facilitated the study of the discovery LOD, which is taken as an average F-ratio that falls below the 0.1% probability limit. Bromobenzene and 1-chlorohexane have consistently high average F-ratios for all concentration comparisons, due to having selective *m/z* and limited chromatographic interference. 5-decyne and 3-octanone have fewer selective *m/z* and more chromatographic interference, which results in lower average F-ratios for these analytes. In the spike versus blank comparisons, each of the four spiked analytes has a high average F-ratio at nearly all concentration levels. For the comparisons at or above 6.2 ppm versus 0 ppm, all four spiked analytes have average F-ratios greater than the 0.1% null probability limit, indicating that these hits have little to no overlap with the null distribution. For the 3.2 ppm versus 0 ppm and the 1.6 ppm versus 0 ppm comparisons, 3-octanone has an average F-ratio which falls within the 0.1% null probability limit, indicating that these features for 3-octanone are likely to be interspersed with a small number of false positives.

The concentration ratio of two comparisons are more challenging, and have a lower overall F-ratio, and thus, tend to overlap more with the null distribution. For the 25 ppm versus

12.5 ppm comparison, all four spiked analytes have average F-ratios greater than the 0.1% null probability limit. At lower absolute concentrations, 3-octanone has a diminished average F-ratio. For the 12.5 ppm versus 6.2 ppm comparison, 3-octanone is in the 0.1% null probability limit, indicating the 3-octanone feature is likely to be interspersed with a small number of false positives. Table 1 is the abbreviated (first 7 entries) hit list for the 12.5 ppm versus 6.2 ppm comparison, in which 3-octanone is within the 0.1% null probability limit, along with two other potential hits that were not spiked analytes. As the absolute concentration further decreases, the average F-ratio for 3-octanone likewise falls, increasing the number of false positives that will be encountered while working down the hit list toward the 3-octanone feature. This is demonstrated in Table 2, which is the abbreviated hit list for the 3.2 ppm versus 1.6 ppm comparison. At this lower absolute concentration, the F-ratios for the true positives have all dropped. There is now a false positive hit interspersed between the hits for bromobenzene and 5-decyne, and 216 potential hits and non-hits between the features for 5-decyne and 3-octanone. Due to lower mass spectral selectivity and chromatographic interference from the diesel fuel matrix, 3-octanone is found below the 0.1% null probability limit at concentration ratio of two comparisons below the 12.5 ppm versus 6.2 ppm comparison, and is thus assigned as a non-hit. The remaining three spiked analytes have F-ratios greater than the 0.1% null probability limit for all concentration ratio of two comparisons, though 5-decyne approaches the 0.1% null probability limit for comparisons below 12.5 ppm versus 6.2 ppm. Additional abbreviated hit lists showing the relative ranks for the spiked analytes and false positives, and a discussion thereof, are included in the Supporting Information (Section S3, Tables S-6 and S-7). To summarize, spiked analytes were reliably discovered at ~ 1 to ~10 ppm (~ 5 to ~50 pg on column using a 200:1 split),

depending on the degree of mass spectral selectivity and 2D chromatographic resolution from the diesel fuel matrix.

Figure 4 illustrates the challenge successfully addressed by tile based F-ratio analysis by examining the limited selectivity at which 3-octanone is discovered in the 12.5 ppm versus 6.2 ppm comparison. Figure 4(A) is the F-ratio spectrum (the F-ratio for each *m/z* that was present in the tile above the *S/N* threshold) for the feature corresponding to 3-octanone. The *m/z* plotted were averaged to yield the average F-ratio, by which the hit list is currently ranked. The *m/z* 57, 72, and 99 are the most selective versus the significant matrix peaks, which overlap the 3-octanone peak at low chromatographic resolution in both separation dimensions. There is potential to improve ranking by selecting a subset of *m/z* for the calculation of average F-ratios, requiring further study. Figures 4(B-D) includes segments of the column 2 separation from the most abundant modulation of 3-octanone, for the extracted ion chromatograms (XIC) at *m/z* 57, 72, and 99. These chromatograms illustrate both the low absolute abundance of 3-octanone at this concentration level, as well as the limited chromatographic resolution and mass spectral selectivity versus the interfering matrix peak. Due to low *S/N* and low mass spectral selectivity, 3-octanone has a moderate average F-ratio at the 12.5 ppm versus 6.2 ppm comparison level, and is found within the 0.1% null probability limit, in which two other potential hits are interspersed. The discovered feature for 3-octanone in the 6.2 ppm versus 0 ppm comparison is detailed in a similar fashion in Figure S-5 (Supporting Information, Section S3.1).

We also studied the performance of the tile based F-ratio method in context of the pixel based and peak table based analyses (see Supporting Information, Section S4). The pixel based method (see Section S4.1 for details) performs similarly to the tile based method, particularly at the higher absolute concentration comparisons (at or above the 50 ppm nominal concentration).

However, at lower concentration, the pixel based method encounters more false positives interspersed between the spiked analytes. Likewise, the peak table comparison is provided in Section S4.2. Because the peak table processing is highly influenced by the selected parameters,[55] we carefully optimized the peak table method to discover the low concentration analytes, while minimizing false positives. The peak table method performs well at the higher absolute concentrations. However, at lower concentrations, some of the four spiked analytes are not found, or are disqualified due to low deconvolution quality and/or misidentified peaks.

2.4 Conclusions

Tile based F-ratio analysis of GC×GC–TOFMS data facilitates confident analyte detection for small concentration changes between sample classes for discovery-based experimentation, even for analytes that are heavily interfered with little mass spectral selectivity. The software is computationally fast, requiring less than 10 min of computation time per comparison (including null distribution analysis with six null comparisons) on a mid-level personal computer. After applying null distribution analysis, the results of the study showed that spiked analytes could be reliably discovered at ~ 1 to ~ 10 ppm (~ 5 to ~ 50 pg using a 200:1 split) in a complex diesel matrix with minimal occurrence of false positives above the 0.1% null probability range. The determination of the null probability limits using the combinatorial technique described herein is rapid, and provide a defensible F-ratio cutoff that is determined algorithmically for each experiment based on the variation present in the data. This approach is superior to rule-of-thumb thresholds, or manually determining an appropriate threshold for each experiment based on inspecting the hit lists.

This analytical platform is broadly applicable for the analysis of samples where class distinguishing analytes may be present at a range of signals, and in which minor

chromatographic misalignment may be present, without the need for explicit 2D chromatographic alignment. The tile based approach was demonstrated to reduce the occurrence of false positives compared to pixel based methods, and permits lower discovery limits compared to peak table methods. A future study could include an expanded selection of spiked analytes (substantially more true positives), allowing for characterization of a “true positive distribution” and a more thorough comparison to other non-targeted analysis methods.

2.5 References

(1) Liu, Z.; Phillips, J. B. *J. Chromatogr. Sci.* **1991**, *29*, 227–231.
(2) Adahchour, M.; van Stee, L. L.; Beens, J.; Vreuls, R. J.; Batenburg, M. A.; Brinkman, U. A. Th. *J. Chromatogr. A* **2003**, *1019*, 157–172.
(3) Beens, J.; Adahchour, M.; Vreuls, R. J. J.; van Altena, K.; Brinkman, U. A. Th. *J. Chromatogr. A* **2001**, *919*, 127–132.
(4) Bruckner, C. A.; Prazen, B. J.; Synovec, R. E. *Anal. Chem.* **1998**, *70*, 2796–2804.
(5) Dallüge, J.; van Rijn, M.; Beens, J.; Vreuls, R. J.; Brinkman, U. A. Th. *J. Chromatogr. A* **2002**, *965*, 207–217.
(6) Kinghorn, R. M.; Marriott, P. J. *J. High Resolut. Chromatogr.* **1998**, *21*, 620–622.
(7) Seeley, J. V.; Kramp, F.; Hicks, C. J. *Anal. Chem.* **2000**, *72*, 4346–4352.
(8) Shellie, R.; Mondello, L.; Marriott, P.; Dugo, G. *J. Chromatogr. A* **2002**, *970*, 225–234.
(9) Pierce, K. M.; Kehimkar, B.; Marney, L. C.; Hoggard, J. C.; Synovec, R. E. *J. Chromatogr. A* **2012**, *1255*, 3–11.
(10) Pierce, K. M.; Nadeau, J. S.; Synovec, R. E. In *Gas Chromatography*; Poole, C. F., Ed.; Elsevier: Amsterdam, 2012; pp 415–434.
(11) Yang, S.; Hoggard, J. C.; Lidstrom, M. E.; Synovec, R. E. In *Metabolomics in Practice*; Lämmerhofer, M., Weckwerth, W., Eds.; Wiley-VCH Verlag GmbH & Co. KGaA, 2013; pp 69–92.
(12) Reichenbach, S. E.; Tian, X.; Cordero, C.; Tao, Q. *J. Chromatogr. A* **2012**, *1226*, 140–148.
(13) Reichenbach, S. E.; Ni, M.; Kottapalli, V.; Visvanathan, A. *Chemom. Intell. Lab. Syst.* **2004**, *71*, 107–120.
(14) Reichenbach, S. E.; Tian, X.; Boateng, A. A.; Mullen, C. A.; Cordero, C.; Tao, Q. *Anal. Chem.* **2013**, *85*, 4974–4981.
(15) Harvey, P. M.; Shellie, R. A. *Anal. Chem.* **2012**, *84*, 6501–6507.
(16) Organtini, K. L.; Myers, A. L.; Jobst, K. J.; Cochran, J.; Ross, B.; McCarry, B.; Reiner, E. J.; Dorman, F. L. *J. Chromatogr. A* **2014**, *1369*, 138–146.
(17) Vogt, L.; Gröger, T.; Zimmermann, R. *J. Chromatogr. A* **2007**, *1150*, 2–12.
(18) Marney, L. C.; Siegler, W. C.; Parsons, B. A.; Hoggard, J. C.; Wright, B. W.; Synovec, R. E. *Talanta* **2013**, *115*, 887–895.
(19) Brokl, M.; Bishop, L.; Wright, C. G.; Liu, C.; McAdam, K.; Focant, J.-F. *J. Chromatogr. A* **2014**, *1370*, 216–229.
(20) Fraga, C. G.; Prazen, B. J.; Synovec, R. E. *Anal. Chem.* **2000**, *72*, 4154–4162.
(21) Fraga, C. G.; Prazen, B. J.; Synovec, R. E. *Anal. Chem.* **2001**, *73*, 5833–5840.
(22) Pierce, K. M.; Wood, L. F.; Wright, B. W.; Synovec, R. E. *Anal. Chem.* **2005**, *77*, 7735–7743.
(23) Kempa, S.; Hummel, J.; Schwemmer, T.; Pietzke, M.; Strehmel, N.; Wienkoop, S.; Kopka, J.; Weckwerth, W. *J. Basic Microbiol.* **2009**, *49*, 82–91.
(24) Wang, B.; Fang, A.; Heim, J.; Bogdanov, B.; Pugh, S.; Libardoni, M.; Zhang, X. *Anal. Chem.* **2010**, *82*, 5069–5081.
(25) Gros, J.; Nabi, D.; Dimitriou-Christidis, P.; Rutler, R.; Arey, J. S. *Anal. Chem.* **2012**, *84*, 9033–9040.
(26) Khummueng, W.; Harynuk, J.; Marriott, P. J. *Anal. Chem.* **2006**, *78*, 4578–4587.

(27) Nadeau, J. S.; Wilson, R. B.; Hoggard, J. C.; Wright, B. W.; Synovec, R. E. *J. Chromatogr. A* **2011**, *1218*, 9091–9101.
(28) Johnson, K. J.; Synovec, R. E. *Chemom. Intell. Lab. Syst.* **2002**, *60*, 225–237.
(29) Mohler, R. E.; Dombek, K. M.; Hoggard, J. C.; Pierce, K. M.; Young, E. T.; Synovec, R. E. *Analyst* **2007**, *132*, 756–767.
(30) Humston, E. M.; Dombek, K. M.; Tu, B. P.; Young, E. T.; Synovec, R. E. *Anal. Bioanal. Chem.* **2011**, *401*, 2387–2402.
(31) Beckstrom, A. C.; Humston, E. M.; Snyder, L. R.; Synovec, R. E.; Juul, S. E. *J. Chromatogr. A* **2011**, *1218*, 1899–1906.
(32) Hantao, L. W.; Toledo, B. R.; de Lima Ribeiro, F. A.; Pizetta, M.; Pierozzi, C. G.; Furtado, E. L.; Augusto, F. *Talanta* **2013**, *116*, 1079–1084.
(33) Gröger, T.; Schäffer, M.; Pütz, M.; Ahrens, B.; Drew, K.; Eschner, M.; Zimmermann, R. *J. Chromatogr. A* **2008**, *1200*, 8–16.
(34) Heim, J. *LECO Corporation*, Technical Note, Life Sciences and Chemical Analysis Solutions. **2010**, Form 203-821-377.
(35) Almstetter, M. F.; Appel, I. J.; Dettmer, K.; Gruber, M. A.; Oefner, P. J. *J. Chromatogr. A* **2011**, *1218*, 7031–7038.
(36) Welke, J. E.; Manfroi, V.; Zanus, M.; Lazzarotto, M.; Alcaraz Zini, C. *Food Chem.* **2013**, *141*, 3897–3905.
(37) Stadler, S.; Stefanuto, P.-H.; Brokl, M.; Forbes, S. L.; Focant, J.-F. *Anal. Chem.* **2013**, *85*, 998–1005.
(38) Pasikanti, K. K.; Norasmara, J.; Cai, S.; Mahendran, R.; Esuvaranathan, K.; Ho, P. C.; Chan, E. C. Y. *Anal. Bioanal. Chem.* **2010**, *398*, 1285–1293.
(39) Li, X.; Lu, X.; Tian, J.; Gao, P.; Kong, H.; Xu, G. *Anal. Chem.* **2009**, *81*, 4468–4475.
(40) Ma, C.; Wang, H.; Lu, X.; Wang, H.; Xu, G.; Liu, B. *Metabolomics* **2009**, *5*, 497–506.
(41) Qiu, Y.; Lu, X.; Pang, T.; Ma, C.; Li, X.; Xu, G. *J. Sep. Sci.* **2008**, *31*, 3451–3457.
(42) Benjamini, Y.; Hochberg, Y. *J. R. Stat. Soc. Ser. B Methodol.* **1995**, *57*, 289–300.
(43) Hoggard, J. C. peg2mat3p8; http://depts.washington.edu/synlab/software/, 2011.
(44) Massart, D. L. *Chemometrics: a textbook*; Elsevier; Elsevier Science Pub. Co.: Amsterdam; New York; New York, NY, U.S.A., 1988.
(45) Duda, R. O.; Hart, P. E.; Stork, D. G. *Pattern Classification*; John Wiley & Sons, 2012.
(46) Efron, B. *J. Am. Stat. Assoc.* **2005**, *100*, 1–5.
(47) Efron, B. *J. Am. Stat. Assoc.* **2007**, *102*, 93–103.
(48) Efron, B. *J. Am. Stat. Assoc.* **2010**, *105*, 1042–1055.
(49) Efron, B.; Tibshirani, R. *Genet. Epidemiol.* **2002**, *23*, 70–86.
(50) Leek, J. T.; Storey, J. D. *Stat. Appl. Genet. Mol. Biol.* **2011**, *10*, 1–22.
(51) Storey, J. D. *J. R. Stat. Soc. Ser. B Stat. Methodol.* **2002**, *64*, 479–498.
(52) Storey, J. D. *J. R. Stat. Soc. Ser. B Stat. Methodol.* **2007**, *69*, 347–368.
(53) Woo, S.; Leek, J. T.; Storey, J. D. *Bioinformatics* **2011**, *27*, 509–515.
(54) Vis, D. J.; Westerhuis, J. A.; Smilde, A. K.; Greef, J. van der. *BMC Bioinformatics* **2007**, *8*, 322.
(55) Lu, H.; Liang, Y.; Dunn, W. B.; Shen, H.; Kell, D. B. *TrAC Trends Anal. Chem.* **2008**, *27*, 215–227.

2.6 Tables

Table 2-1. Hit list for the 12.5 ppm versus 6.2 ppm comparison after redundant hit removal. There are a total of 5033 entries in the list. The four spiked analytes are found within the first six entries. There are two potential hits interspersed with the features for the spiked analytes. The corresponding hit list prior to redundant hit removal may be found in the Supporting Information (Table S-5).

F-ratio hit number	Average F-ratio	$^{1}t_R$ (s)	$^{2}t_R$ (s)	Null Classification	Compound
1	214.4	360	0.13	hit	**bromobenzene**
2	114.5	255	0.93	hit	**1-chlorohexane**
3	60.1	534	0.73	hit	**5-decyne**
4	14.8	945	0.52	potential hit	
5	11.6	1202	0.61	potential hit	
6	11.2	441	0.91	potential hit	**3-octanone**
7	9.9	973	0.51	non-hit	
8-5033	…	…	…	non-hits	

Table 2-2. Hit list for the 3.2 ppm versus 1.6 ppm comparison after redundant hit removal. There are a total of 5099 entries in the list.

F-ratio hit number	Average F-ratio	$^{1}t_R$ (s)	$^{2}t_R$ (s)	Null Classification	Compound
1	102.2	255	0.93	hit	**1-chlorohexane**
2	59.3	360	0.13	hit	**bromobenzene**
3	25.8	2150	0.42	hit	false positive
4	21.4	534	0.73	hit	**5-decyne**
5-220	…	…	…	potential hits and non-hits	
221	3.0	441	0.92	non-hit	**3-octanone**
222-5099	…	…	…	non-hits	

2.7 Figures

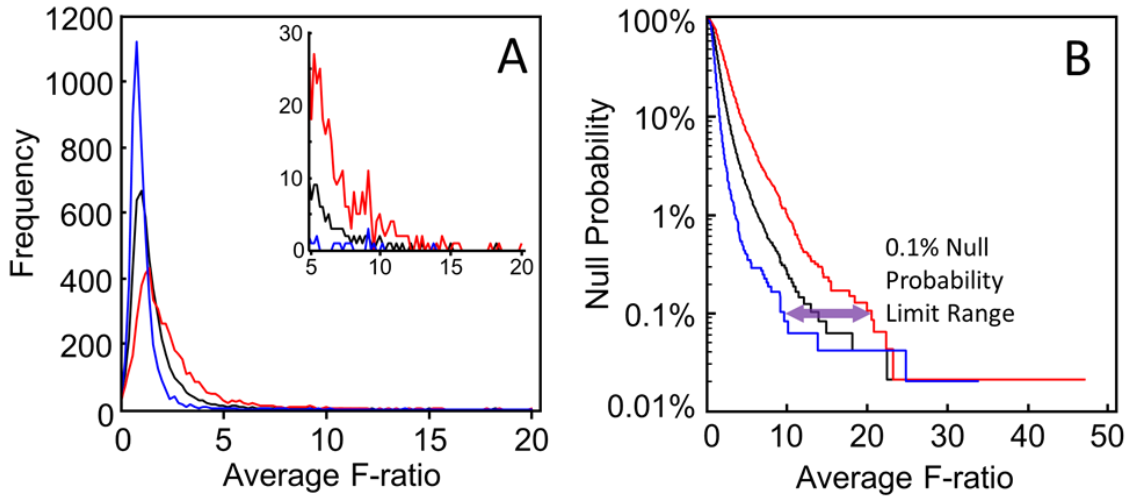

Figure 2-1. (A) Average and the two extreme null distributions from the null comparisons of the 0 ppm versus 0 ppm diesel fuel sample (i.e., the unspiked matrix blank) are shown. The frequency plotted is the number of features within a bin interval of 0.2 per the average F-ratio. Six rearrangements produced six different null distributions, others omitted for clarity. The range of the null distributions is represented by the red and blue null distributions. The zoomed section shows the range of the rightmost tail of the null distributions that were encountered. (B) The average null probability curve is shown based on the average F-ratio null distribution (the black trace) in (A), along with the null probability curves resulting from the two extreme null distributions presented in (A). The null probability limit range of ~ 0.1% is indicated by the blue double arrow (~ equivalent to 5 spurious features in a hit list), suggesting the use of an average F-ratio cutoff of ~ 10 to 20 for the "discovery" LOD.

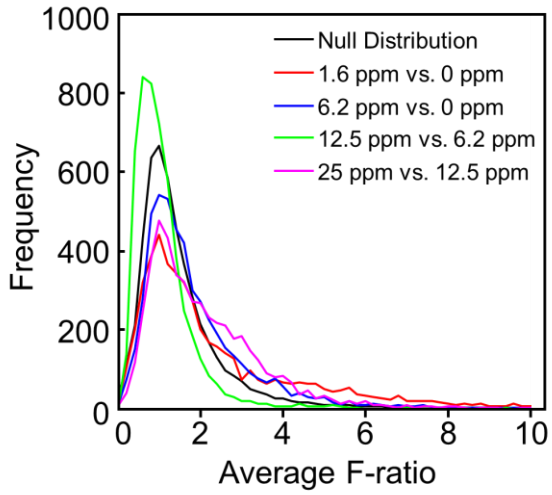

Figure 2-2. False positive distributions from four representative F-ratio true class comparisons are illustrated in the context of the average null distribution from the six null comparisons derived from the comparisons of the 0 ppm diesel fuel sample (black curve, see Figure 1A). The frequency plotted is the number of features within a bin interval of 0.2 per the average F-ratio.

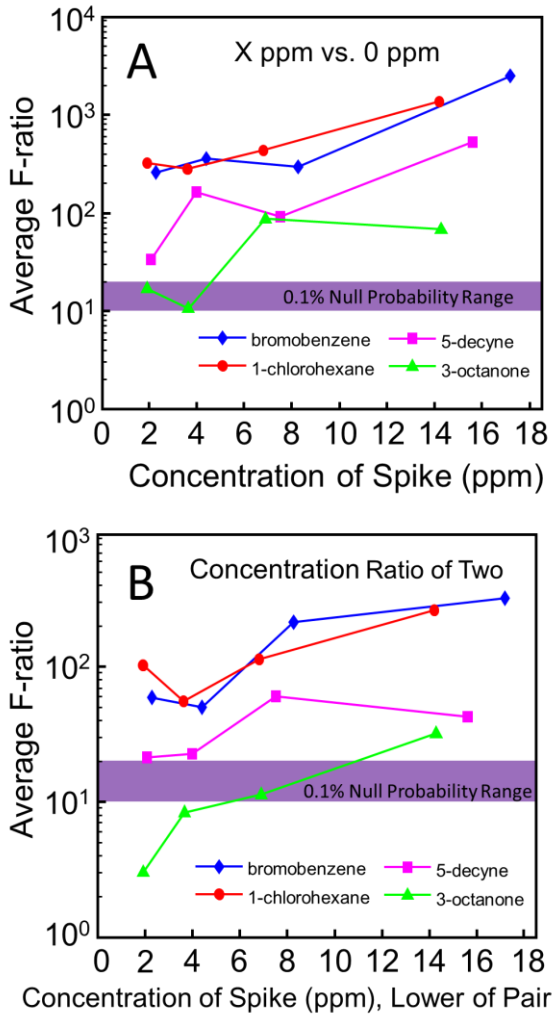

Figure 2-3. (A) Average F-ratios for the four spiked analytes are shown for the spike versus matrix blank comparisons (e.g., 12.5 ppm versus 0 ppm) in the context of the 0.1% null probability limit (Figure 1(B)). The actual concentration in ppm of the spiked sample in each pair for each spiked analyte is plotted (see Table 1). (B) Average F-ratios for the four spiked analytes are shown for the nominal concentration ratio of two comparisons (e.g., 25 ppm versus 12.5 ppm) in the context of the 0.1% null probability limit (Figure 1(B)). The actual concentration in ppm (see Table 1) of the lower spike level of each pair for each spiked analyte is plotted.

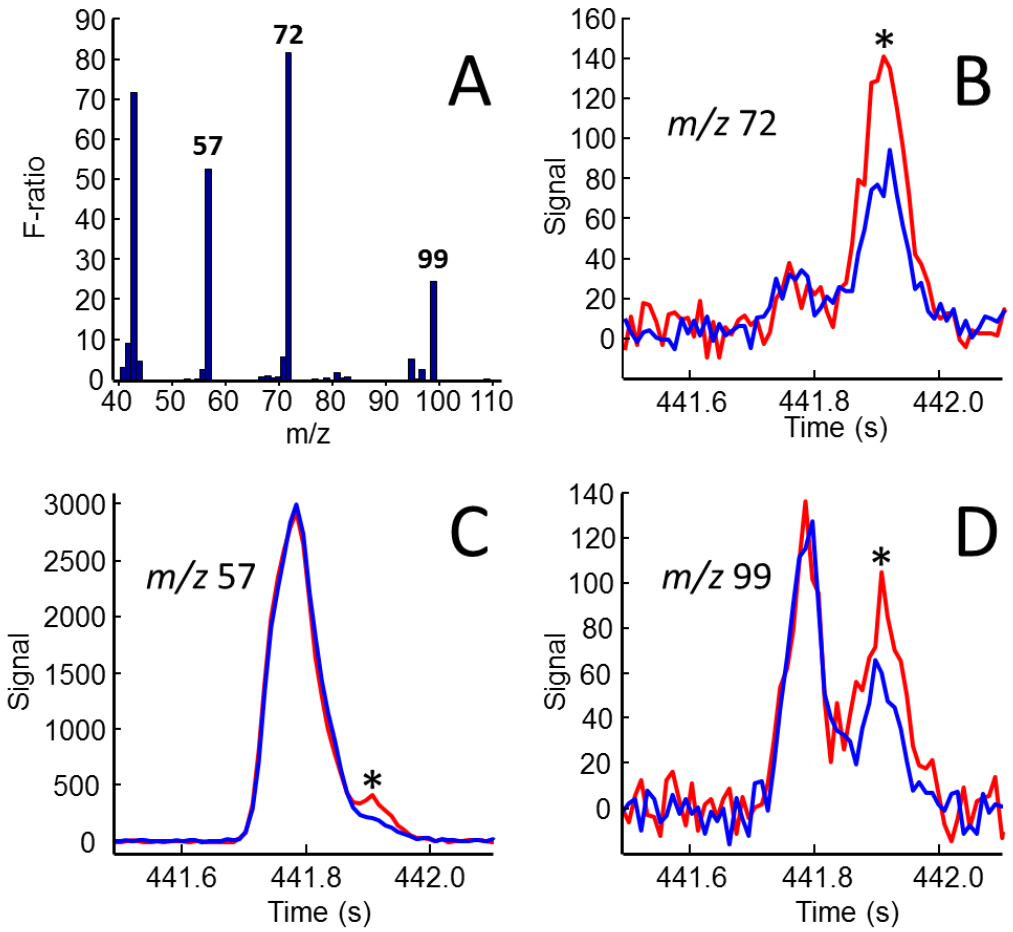

Figure 2-4. 3-octanone in the 12.5 ppm spike (red) versus 6.2 ppm spike (blue) comparison. (A) The F-ratio "mass spectrum." (B-D) The three most selective *m/z* per F-ratio analysis are plotted from one sample injection from each class. The plots are extracted ion chromatograms (XIC) from the column 2 separation for the most intense modulation of the 3-octanone peak. The rightmost peak is 3-octanone (denoted by *), while the leftmost peak is comprised of several interfering compounds from the diesel fuel matrix.

2.8 Supporting Information

This section provides additional experimental details, a tutorial on implementing tile based F-ratio analysis, additional results and discussion of hit lists from the experiment, and a comparison to pixel and peak table based methods.

2.8.1 Additional Experimental Details

2.8.1.1 Concentrations of Analytes in Spiked Diesel Fuel

Table S-1. The actual concentrations are shown in ppm for each nominal spike concentration (first column) for the four spiked analytes in a diesel fuel matrix. The spiked analytes are not initially present in the non-spiked diesel fuel (matrix blank).

Nominal Spike Level (ppm)	3-Octanone (ppm)	5-Decyne (ppm)	Bromobenzene (ppm)	1-Chlorohexane (ppm)
100	111	121	133	110
50	55.5	60.5	66.6	54.9
25	27.8	30.3	33.4	27.5
12.5	14.3	15.6	17.2	14.2
6.2	6.89	7.51	8.27	6.81
3.2	3.67	4.00	4.40	3.63
1.6	1.93	2.11	2.32	1.91

Table S-2. The mass quantity injected on column is shown in picograms (pg) for each nominal spike concentration (first column) for all spiked analytes. A 1 μL injection of each diesel fuel sample was made in split mode with a split ratio of 200:1.

Nominal Spike Level (ppm)	3-Octanone (ppm)	5-Decyne (ppm)	Bromobenzene (ppm)	1-Chlorohexane (ppm)
100	461.8	503.4	553.3	457.6
50	230.9	251.7	277.1	228.4
25	115.6	126.0	138.9	114.4
12.5	59.5	64.9	71.6	59.1
6.2	28.7	31.2	34.4	28.3
3.2	15.3	16.6	18.3	15.1
1.6	8.0	8.8	9.7	7.9

2.8.1.2 Instrument Parameters

The GC×GC–TOFMS instrumental platform consisted of an Agilent 6890N gas chromatograph equipped with an Agilent 7683 autoinjector (Agilent Technologies, Palo Alto, CA) coupled with a LECO Pegasus III TOFMS equipped with a 4D thermal modulator upgrade (LECO, St. Joseph, MI). The primary column of the GC×GC (column 1) was a 20 m x 250 μm i.d. x 0.5 μm RTX-5MS film (Restek, Bellefonte, PA) and the secondary column (column 2) was a 2 m x 180 μm i.d. x 0.2 μm RTX-200 film (Restek, Bellefonte, PA). The GC instrument inlet was set at 275 °C and the transfer line was set at 305 °C. Column 1 was held at 50 °C for 0.25 min and then increased at 5 °C/min to 300 °C, where it was held for 5 min. Column 2 was initially set at 55 °C and followed the same temperature program as column 1 giving a total run time of 55.25 min. The modulator was kept 20 °C higher than column 1, and the modulation period was 1 s. The GC instrument was set to maintain a constant (ambient temperature and pressure corrected) flow rate of 2 mL/min at the outlet of column 2, with helium used as the carrier gas. The ion source was set to 300 °C and the detector voltage was set to 1600 V. Mass channels, *m/z* 41-340, were collected at 100 spectra/s after a 6 s solvent delay. A 1 μL injection of each diesel sample was made in split mode with a split ratio of 200:1. Each diesel sample was injected in quadruplicate, however a total of eight injection replicates were collected for the 0 ppm diesel sample for null distribution analysis.

Figure S-1 is a representative GC×GC–TIC chromatogram indicating the locations of the spiked analytes. The separation conditions were selected to allow moderate wraparound to more fully utilize the 2D peak capacity. However, compounds in a given second dimension separation were not allowed to wraparound into compounds eluting in a subsequent second dimension

separation. While the 2D separation may be reregistered for aesthetic considerations, reregistration was not performed since it has no consequence in this study.

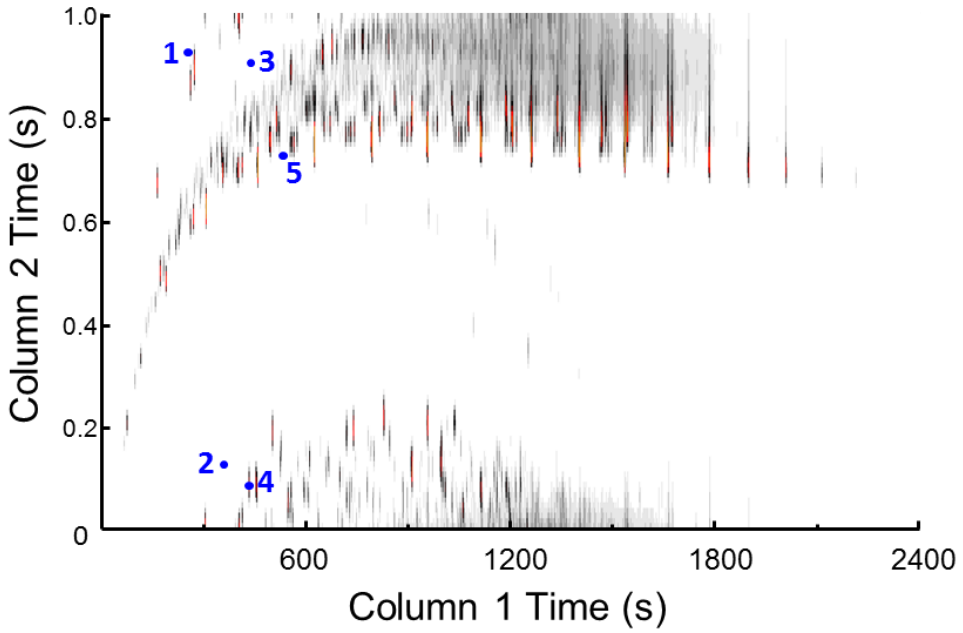

Figure S-1. GC×GC–TOFMS $\log_{10}$ plot of the total ion current (TIC) chromatogram of a 12.5 ppm spiked diesel sample. Locations of all four spiked analytes and the internal standard are marked. The column 1 (first separation dimension) elution order is as follows: (1) 1-chlorohexane; (2) bromobenzene; (3) 3-octanone; (4) 1-bromoheptane (internal standard); (5) 5-decyne.

2.8.1.3 F-ratio Tiling and Redundant Hit Removal Parameters

The GC×GC pixel level data was summed using a 2D grid of 2D tiles, as a function of mass channel (*m/z*), which provides data reduction along both separation dimensions. The tile size chosen for the chromatograms was 6 data points (pixels) in the column 1 dimension (6 modulations) by 10 data points (pixels) in the column 2 dimension (10 mass spectra, or 100 ms). Each tile thus contains an area of 60 pixels. All tile based F-ratio analyses were conducted with the entire collected *m/z* range (41-340). Prior to tile based F-ratio analysis, the data were baseline corrected and normalized to the internal standard signal for each sample injection. A signal-to-noise (*S/N*) threshold was applied to computationally exclude *m/z* having low *S/N* from the F-

ratio calculation. This *S/N* threshold was set to a signal equal to three times the standard deviation (3σ) of a tiled noise region, which was taken as the first 10 s of detected signal, during which no peaks eluted, from a representative chromatographic run. The F-ratio was then calculated for each 2D tile for each *m/z*. The average F-ratio, which is used to rank the tiles by significance, was calculated by averaging the F-ratios for each *m/z* which passed the *S/N* threshold for a given 2D tile, with the requirement that the tile have at least three *m/z* above the *S/N* threshold for being included in the analysis. Redundant hits were removed using a novel "pin and cluster" algorithm, as detailed in Section S2.4. The 2D chromatographic parameters for removing redundant hits were ±2 data points (modulations) in the column 1 dimension and ±5 data points (mass spectra) in the column 2 dimension.

2.8.2 Tutorial on Implementing Tile Based F-ratio Analysis

2.8.2.1 F-ratio Calculation

The class-to-class variation is calculated as

$$\sigma_{\text{cl}}^2 = \frac{\sum(\bar{x}_i - \bar{x})^2 n_i}{(k - 1)} \quad (1)$$

where n_i is the number of measurements in the ith class, $\bar{x}_i$ is the mean of the ith class, $\bar{x}$ is the overall mean, and k is the number of classes. The within-class variation is calculated as

$$\sigma_{\text{err}}^2 = \frac{\sum \left(\sum\left(\bar{x}_{ij} - \bar{x}\right)^2\right) - \left(\sum(\bar{x}_i - \bar{x})^2 n_i\right)}{(N - k)} \quad (2)$$

where $\bar{x}_{ij}$ is the ith measurement of the jth class, and N is the total number of sample profiles. A F-ratio is then calculated as the ratio between the two variances,

$$\text{Fisher ratio} = \frac{\sigma_{\text{cl}}^2}{\sigma_{\text{err}}^2} \quad (3)$$

2.8.2.2 Overview of Preprocessing

Preprocessing steps reduce the inherent instrumental variation in the data set that contributes to the within-class variation (Eq. 2, and the denominator in Eq. 3). Baseline correction corrects low frequency noise resulting from fluctuations in the mass spectrometer, column flows, and GC oven temperature. Baseline correction can also remove background resulting from column bleed at higher oven temperatures. Baseline correction techniques have been thoroughly reviewed elsewhere and have not been included here for brevity.[9] The baseline correction technique applied in the tile based F-ratio software is based on a rolling minimum method which relies on the assumption that each column 2 separation (i.e., each modulation) will have a region in which no peaks elute. As long as the separation conditions are designed such that the most retained peaks on column 2 do not wrap around onto less retained peaks on column 2, this assumption holds. In cases where peaks substantially tail on column 2, such as due to chromatographic overloading of the stationary phase, this method of baseline correction may cause a negative bias on the affected *m/z*. In the chromatograms studied herein, the data were appropriate for this method of baseline correction.

Due to the inherent variation in volumetric injection by microsyringe using a GC autosampler, normalization is necessary to avoid excessive variation in signal caused by variation in the amount of sample loaded onto the analytical column. Such variation may be corrected by use of an internal standard. The integrated signal of the internal standard, which is at the same concentration in each sample, is indicative of the amount of sample injected on column. Normalization was performed by multiplying every point in each chromatogram by a scalar determined by the relative abundance of the internal standard in its respective

chromatogram. The data reported herein were normalized to a non-native internal standard, 1-bromoheptane.

2.8.2.3 Tile Approach for Binning GC×GC–TOFMS Data

The 2D misalignment of GC×GC–TOFMS chromatographic data across different samples occurs due to minor fluctuations in the mobile phase flow or oven temperature from run to run, or slight changes in the analytical column due to fouling or column maintenance (e.g., column clipping, bakeouts, etc.). Such instrumental fluctuations may cause minor shifts in peak retention times on column 1 and/or column 2. As previously reported,[18] when the data is processed in a pixel based method, these slight shifts may increase the within-class variance for a peak, which commonly diminish the rank of true positives. Further, if the retention time variation coincides with the sample classes, it may lead to the observation of false positives. For pixel based methods, it is possible to align the chromatograms to reduce these occurrences; however, aligning the column 1 dimension can be especially problematic (to the point of being futile) due to low data density in this dimension. It is advisable to have ~ 15 or more data points (i.e., mass spectra) across a peak for reliable alignment.[27] However, most GC×GC–TOFMS analyses are performed with reduced data density on the column 1 separation to optimize the column 2 separation. Even when the optimization is balanced for both of the two separation dimensions, it is common to have only ~ 2 to 4 data points (i.e., modulations) per peak on column 1 (at the $\pm 2\sigma$ width), as was observed in this data set, which had a typical modulation ratio of 3 to 4, depending on the peak width on column 1.

The tile based approach avoids the need for explicit alignment of the peaks by summation of the peak window prior to the calculation of the F-ratio. The size of the tile is a balance of two competing objectives: one, capturing most of the 2D peak signal (using the $\pm 2\sigma$ width) plus

additional space to allow for minor retention time shift in each dimension, and two, keeping the tile size sufficiently small to maintain selectivity for individual peaks, that is, avoiding sampling neighboring peaks. The column 1 tile size for this data set was 6 modulations (6 s), which allowed for shifts of one modulation in either direction. At the modulation ratio applied for this study, the peaklets farthest from the column 1 peak apex contain relatively small amounts of the total peak area, therefore, we anticipate that the performance of the software would not be affected even by a two-modulation (2 s) shift in the column 1 retention time from sample to sample. However, more substantial shifts in column 1 retention time, which were not encountered in this study, would be likely to decrease the ability of the tile based method to discover true positives, and may also lead to the observance of false positives if the retention time shifts spuriously co-vary with the sample classes. The ability of the tile based method to mitigate retention time shifts is an aspect deserving of further study, particularly in context of modulation ratio. In addition to mitigating the effects of minor column 1 and/or column 2 misalignment, this method also improves the *S/N* by summing the signal within each tile.

The tile based approach assists in the discovery of changing analytes and reduces the number of false positives due to retention time misalignment and covariance of detector noise with the sample classes. However, a single grid of tiles is not sufficient to ensure discovery of all changing analytes regardless of their chromatographic location; instead, it is necessary to use four grids. Figure S-2 shows how four grids are applied to a 2D section of the GC×GC chromatogram. A single grid results in the splitting of analyte peaks into multiple tiles, which initially seems to diminish the advantages of tiling (until redundant hit removal is applied as is described in Section S2.4). By applying four overlapping tile grids, we ensure that each peak is optimally sampled by a tile in one of the tile grids.

As a consequence of the four grids, each analyte is sampled via the tile based F-ratio software multiple times, which can lead to multiple tile hits for an analyte which is significantly changing between sample classes (Table S-3). In complicated sample matrices, such as diesel, the four grids may also sample neighboring peaks, precluding the possibility of simply using only mass spectral matching to eliminate the redundant hits for a given analyte. To effectively remove redundant hits, it is necessary to transform the tile based F-ratio results from tile grid-based space back to pixel based space, taking advantage of the resolution originally present in the 2D chromatographic data.

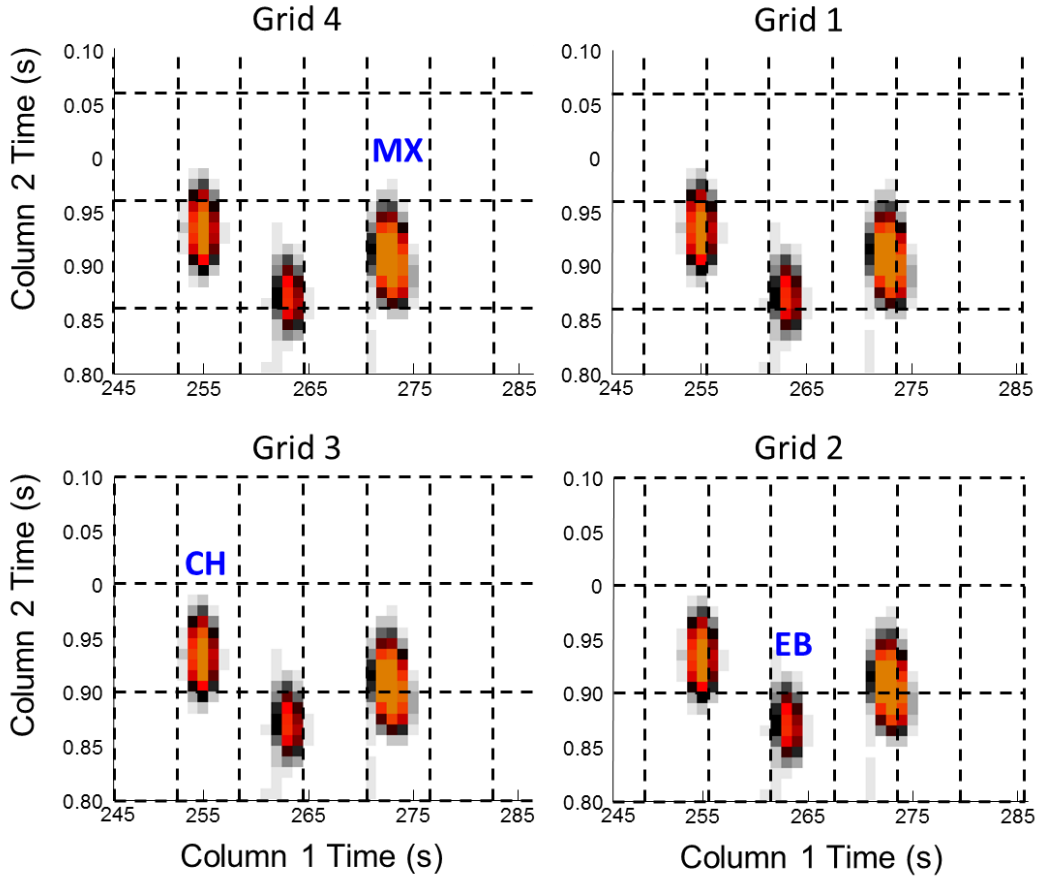

Figure S-2. An analytical ion chromatogram (AIC) comprised of m/z 41:43+55:57+93 for a 25 ppm spiked diesel fuel is shown for a portion of the 2D separation with the four grids overlaid. Each complete tile in the four grids samples 6 data points (6 modulations or 6 s) on the column 1 dimension and 10 data points (0.1 s) on the column 2 dimension. The four grids ensure that each peak is more optimally sampled by one of the tiles. The peaks are labeled in the particular grid

containing the tile that best samples each peak. 1-Chlorohexane (**CH**) is best sampled in Grid 3; ethylbenzene (**EB**) is best sampled in Grid 2; and m-xylene (**MX**) is best sampled in Grid 4. The peaks were identified by mass spectral matching to the NIST11 mass spectral library and reported retention indices. While the use of four grids allows each peak to be more optimally sampled by one tile, it also results in the occurrence of redundant hits when peaks are split by non-optimal tiles. In the case of 1-chlorohexane (**CH**), seven tiles capture sufficient peak signal to generate hits.

Table S-3. The top twenty entries in the initial hit list from the tile based F-ratio software (prior to redundant hit removal and null classification) applied to the comparison of the nominal 25 ppm spike level versus the 12.5 ppm spike level. There are many redundant hits associated with each spiked analyte that will be removed by pinning and clustering. There are a total of 14070 entries in the list. The spiked analytes were identified by matching mass spectra and retention times to analyte standards. The tile size was 6 s on column 1 by 0.10 s on column 2.

F-ratio hit no.	Average F-ratio	Tile no., ^{1}D	Tile no., ^{2}D	Grid	Compound
1	320.3	60	2	2	**bromobenzene**
2	260.5	43	10	3	**1-chlorohexane**
3	209.1	60	1	1	**bromobenzene**
4	68.5	43	9	4	**1-chlorohexane**
5	42.5	89	7	1	**5-decyne**
6	40.2	455	10	1	false positive
7	37.4	42	10	2	**1-chlorohexane**
8	33.5	42	9	1	**1-chlorohexane**
9	31.8	74	10	3	**3-octanone**
10	21.9	60	2	1	**bromobenzene**
11	20.2	60	1	4	**bromobenzene**
12	19.0	42	10	1	**1-chlorohexane**
13	17.2	60	2	3	**bromobenzene**
14	16.0	120	6	2	false positive
15	15.8	43	10	4	**1-chlorohexane**
16	13.8	208	4	4	false positive
17	12.9	176	5	4	false positive
18	12.2	74	9	4	**3-octanone**
19	11.8	74	10	4	**3-octanone**
20	11.6	89	8	2	**5-decyne**
21-14070	…	…	…	…	false positives

2.8.2.4 Redundant Hit Removal by "Pinning and Clustering"

The first tile based F-ratio report[18] demonstrated that the tile based approach provided a computationally-fast way to improve the sensitivity contrast between true positives and false positives for discovery-based analyses. However, the final analysis was somewhat complicated by the presence of multiple hits per "discovered" analyte: the minor hits had to be removed by hand by the analyst in order to obtain a hit list with a single entry for each class distinguishing analyte. While there should ideally be one tile hit per class distinguishing analyte, the four grids used to bin the data result in multiple samplings of a given peak (as shown in Figure S-2), which leads to multiple hits for class distinguishing analytes. These multiple features per class distinguishing analyte are referred to as redundant hits. For an efficient analysis, redundant hits must be removed automatically. Herein, we introduce and describe an algorithmic method to remove redundant hits by focusing the multiple 2D tile locations back to the original high-resolution 2D chromatographic data.

Since redundant hits are due to the same analyte being sampled multiple times by the tile based approach, redundant hits have very similar, if not the same 2D chromatographic peak location. Briefly, the pinning algorithm analyzes each hit found by the initial tile based F-ratio approach and locates the maximum signal difference (between the sample classes) observed at the *m/*z with the highest F-ratio associated with each tile. The *m/z* with the highest F-ratio is used because it is the most selective ion for the class-distinguishing peak; chromatographic interferents which are not changing between sample classes have *m/z* with lower F-ratio values, and are not selective for the peak of interest. The locations of the maximum signal differences for the top F-ratio *m/z* for each tile are then denoted in the 2D chromatographic space, analogous to how locations may be pinned on a map. The corresponding information from the each tile hit,

including the hit's array of F-ratio values at each *m/z* for that location (which comprises an F-ratio "spectrum"), the average F-ratio value, and the original tile and grid locations, is indexed to its respective pin. Since redundant hits are attributable to the same analyte peak eluting at the same, or similar, 2D retention times, multiple pins for the same analyte peak are consolidated into small regions.

Next, with the use of a cluster algorithm, we remove the pin locations with redundant F-ratio information in an automated fashion. The cluster algorithm ranks the pins by their associated average F-ratios, and then removes those that are within a user-specified 2D chromatographic distance from one another. This approach is based on the observation that the pin having the highest average F-ratio optimally locates the peak maximum of the class distinguishing analyte. The highest F-ratio pin in a given cluster is preserved and assigned as a hit in the final hit list, while the lesser pins (i.e., lesser redundant hits) are removed. The window locations that are indexed with the pins can be easily used for further deconvolution or identification, and the F-ratio spectra for that 2D window location provides the particular *m/z* that are the most important for the comparison of the two sample classes and are the most chemically selective in the chromatographic separation for the peak of interest.

The dimensions of the cluster window are based on the observed distribution of pins for a typical class distinguishing feature, which is smaller than the tile, so the cluster window is sized to capture the majority of the peak signal, as well as to allow for minor retention time variance. Further, depending on chromatographic interference from sample matrix peaks, the best tile may not be centered on the class distinguishing feature. During the process of redundant hit removal, the peak maximum is located and indexed, allowing the cluster window to be properly centered on the peak, and simplifying further analysis of the data. The cluster window dimensions for this

study were ±2 s from the center in the column 1 dimension (total of 5 modulations) and ±0.05 s in the column 2 dimension (total of 11 mass spectra).

Figure S-3 illustrates the process of redundant hit removal for the 1-chlorohexane peak in the 25 ppm versus 12.5 ppm comparison, using the pinning and clustering algorithms. The 2D peak is the average of the 25 ppm injection replicates minus the average of the 12.5 ppm replicates using *m/z* 55, which is the highest F-ratio *m/z* for 1-chlorohexane. This "average difference" peak is used to determine the location of the pin (i.e., the 2D chromatographic location that has the greatest difference between classes). The maximum of the average difference peak corresponds to the peak maxima for the 25 ppm class and the 12.5 ppm class. The box with a dashed black line is the tile that best sampled the 1-chlorohexane peak (see Figure S-2). The multiple tiles that sampled the 1-chlorohexane peak are each assigned ("pinned") to the location within the respective tiled 2D chromatographic window, as indicated by a white star. A small star indicates that a single tile was pinned to that location, while a large star indicates that two tiles were pinned to that location; there are a total of seven pins (i.e., a total of seven tiles sampled the 1-chlorohexane peak, capturing sufficient class distinguishing signal to generate a hit). The cluster window, represented by the box with a solid red line, is centered around the pin with the highest F-ratio (in this instance, at 254, 0.94). As shown, the centered cluster window captures all of the pins for the 1-chlorohexane peak. The pin with the highest F-ratio in the cluster window is retained in the hit list, and the other pins are removed as redundant hits. This process is repeated for all tile hits until there is only one pin remaining per discovered feature (i.e., no redundant hits within the defined cluster boundaries).

Table S-4 is the hit list for the 25 ppm versus 12.5 ppm comparison after redundant hits were removed by the automated pinning and clustering algorithms. Whereas prior to redundant

hit removal (Table S-3) there were many hits for each class distinguishing analytes, after redundant hit removal (Table S-4) there is only one hit per analyte. Additionally, the redundant hit removal focuses the tiled results back to the pixel level so that the hit list report provides an accurate determination of the 2D retention times of the discovered class distinguishing analyte features (Table S-4). Table S-5 and Table 1 (primary manuscript) provide another example of redundant hit removal using the 12.5 ppm versus 6.2 ppm comparison, with hit lists prior to and following redundant hit removal, respectively. The complete tile based F-ratio analysis procedure is summarized by a flowchart in Figure S-4.

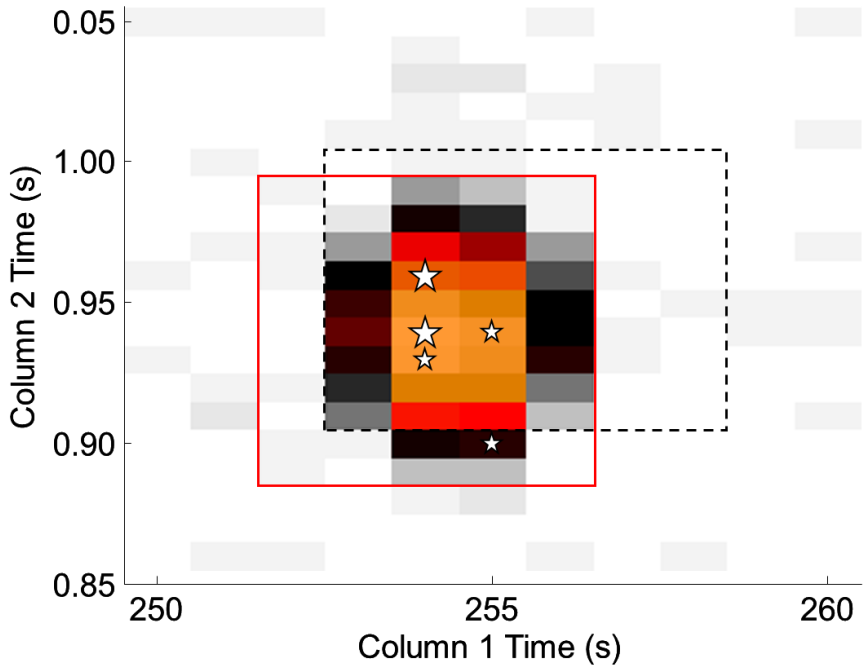

Figure S-3. An example of redundant hit removal applied to the 1-chlorohexane peak in the 25 ppm versus 12.5 ppm comparison. The peak is the average of the 25 ppm injection replicates minus the average of the 12.5 ppm replicates using *m/z* 55, which is the highest F-ratio *m/z* for 1-chlorohexane.

Table S-4. The hit list for the 25 ppm versus 12.5 ppm comparison, after redundant hit removal by the pinning and clustering algorithms. The four spiked analytes are found within the first five entries in the hit list. Compare to Table S-3, for results prior to redundant hit removal.

F-ratio hit no.	Average F-ratio	$^{1}t_R$ (s)	$^{2}t_R$ (s)	Null classification	Compound
1	320.3	360	0.14	hit	**bromobenzene**
2	260.5	254	0.94	hit	**1-chlorohexane**
3	42.5	534	0.73	hit	**5-decyne**
4	40.2	2733	0.99	hit	false positive
5	31.8	441	0.92	hit	**3-octanone**
6	16.0	720	0.56	potential hit	
7-4793	…	…	…	potential hits and non-hits	

Table S-5. The hit list for the 12.5 ppm versus 6.2 ppm comparison, prior to redundant hit removal and null classification. The hit list following redundant hit removal is included in Table 1 (primary manuscript).

F-ratio hit no.	Average F-ratio	Tile no., ^{1}D	Tile no., ^{2}D	Grid	Compound
1	214.4	60	1	1	**bromobenzene**
2	114.5	43	9	4	**1-chlorohexane**
3	107.2	43	10	3	**1-chlorohexane**
4	104.9	60	2	2	**bromobenzene**
5	97.5	42	9	1	**1-chlorohexane**
6	68.0	42	10	2	**1-chlorohexane**
7	60.1	89	7	1	**5-decyne**
8	21.0	61	1	4	**bromobenzene**
9	20.2	61	2	3	**bromobenzene**
10	16.9	43	10	4	**1-chlorohexane**
11	15.5	60	1	2	**bromobenzene**
12	14.8	157	5	1	false positive
13	14.0	42	10	1	**1-chlorohexane**
14	13.0	60	1	4	**bromobenzene**
15	12.5	60	2	3	**bromobenzene**
16	12.3	89	7	4	**5-decyne**
17	11.6	60	2	1	**bromobenzene**
18	11.6	200	6	1	false positive
19	11.2	74	10	3	**3-octanone**
20	10.0	89	8	2	**5-decyne**
21-14253	…	…	…	…	false positives

2.8.2.5 Flowchart of Tile Based F-ratio Software Functions

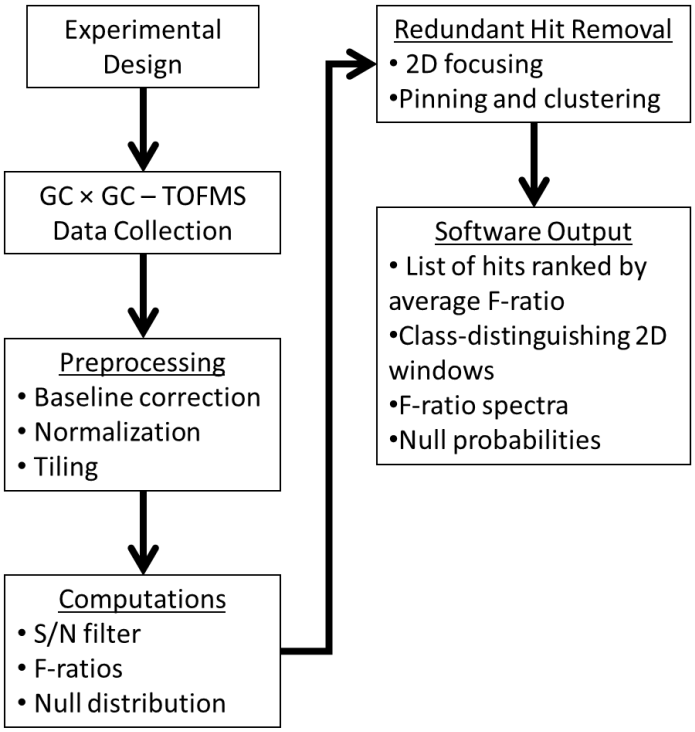

Figure S-4. A summary of steps comprising the tile based F-ratio software.

2.8.3 Additional Discussion of Hit Lists

Tables S-4, S-6, and S-7 are hit lists for additional interesting concentration comparisons from the range of concentration levels studied for this publication. Table S-4 is the hit list for the 25 ppm versus 12.5 ppm comparison, in which all four spiked analytes are found with average F-ratios that exceed the upper limit of the 0.1% null probability range (i.e., greater than 20, as explained in the primary manuscript and illustrated in Figure 1). There is a single false positive hit interspersed with the four analytes. Tables S-6 and S-7 are selected hit lists from the spike versus matrix blank comparisons. Table S-6 is the hit list for the 12.5 ppm versus 0 ppm comparison, in which all four spiked analytes are found with average F-ratios above the 0.1% null probability range (see Figure 3). Due to greater between-class variation with the spike versus blank comparisons, possibly due to sample handling, there are more false positive hits

observed compared to the concentration ratio of 2 comparisons. The 12.5 ppm versus 0 ppm comparison has a total of nine false positives with average F-ratios above 20. Table S-7 is the hit list for the lowest absolute concentration studied, the 1.6 versus 0 ppm comparison. At this level, three of the four spiked analytes are found with average F-ratios above the 0.1% null probability range, and 3-octanone is found in the null probability range of 10 to 20. As with the 12.5 ppm versus 0 ppm comparison, there are a larger number of false positives with average F-ratios above the 0.1% null probability limit, in this case, 24 false positive hits.

Table S-6. The hit list for the 12.5 ppm versus 0 ppm comparison. The four spiked analytes are found as the first four entries in the hit list.

F-ratio hit no.	Average F-ratio	^1t_R (s)	^2t_R (s)	Null classification	Compound
1	2436.1	360	0.13	hit	**bromobenzene**
2	1333.5	255	0.93	hit	**1-chlorohexane**
3	518.4	534	0.73	hit	**5-decyne**
4	67.4	441	0.91	hit	**3-octanone**
5	43.5	109	0.30	hit	false positive
6	32.2	49	0.62	hit	false positive
7-4895	…	…	…	potential hits and non-hits	

Table S-7. The hit list for the 1.6 ppm versus 0 ppm comparison. The four spiked analytes are found within the first 38 entries in the hit list. There are 24 false positive hits interspersed with the hits for the spiked analytes. The distribution of false positives for the 1.6 ppm versus 0 ppm comparison has a substantial tail, which manifests as a prevalence of more false positives.

F-ratio hit no.	Average F-ratio	^1t_R (s)	^2t_R (s)	Null classification	Compound
1	315.0	255	0.93	hit	**1-chlorohexane**
2	257.0	360	0.13	hit	**bromobenzene**
3	36.9	185	0.5	hit	false positive
4	33.6	534	0.73	hit	**5-decyne**
5-37	…	…	…	hits	false positive
38	16.9	1741	0.59	potential hit	**3-octanone**
39-4915	…	…	…	non-hits	false positives

2.8.3.1 Graphical Summary of 3-octanone for the 6.2 ppm versus 0 ppm Comparison

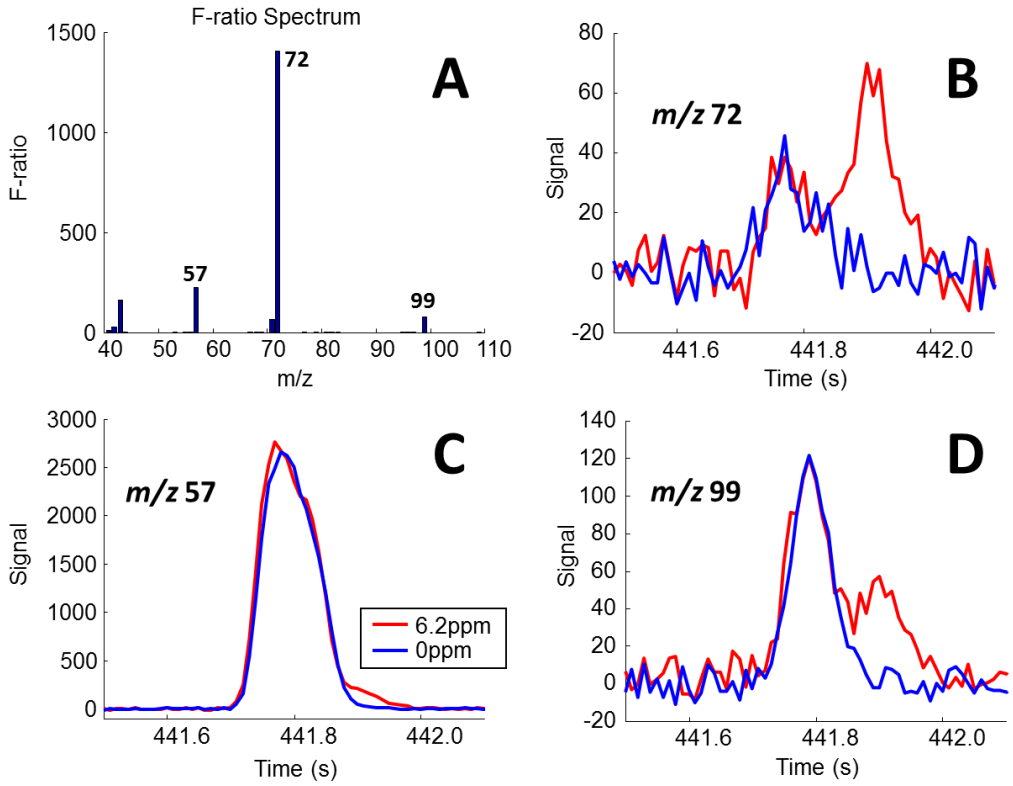

Figure S-5. 3-octanone in the 6.2 ppm versus 0 ppm comparison. (A) The F-ratio spectrum. (B-D) The three most selective *m/z* are individually plotted for an injection from each the 6.2 ppm spiked diesel sample (red trace) and the 0 ppm diesel (blue trace). The plots are extracted ion chromatograms (XIC) from the column 2 separation for the most intense modulation of the 3-octanone peak at the 6.2 ppm spike level. The rightmost peak is 3-octanone, while the leftmost peak is comprised of several interfering compounds.

Figure S-5 provides an illustration of the exquisite sensitivity and selectivity provided by the tile based F-ratio software, in this case for the "discovery" of 3-octanone above the 0.1% null probability range. At this level, 3-octanone has an average F-ratio of 86.4, substantially above the 0.1% null probability range of 10-20. Figure S-5(A) is the F-ratio spectrum (the F-ratio for each *m/z* that was present in the tile above the *S/N* threshold) for the hit corresponding to 3-octanone. The F-ratio spectrum is plotted to *m/z* 110, as there were no significant F-ratios above this *m/z*. The *m/z* 57, 72, and 99 are the most selective versus the significant matrix peaks, which overlap the 3-octanone peak at low chromatographic resolution in both separation dimensions. Figures S-5(B-D) includes segments of the column 2 separation from the most abundant

modulation of 3-octanone, displayed as extracted ion chromatograms (XIC) at *m/z* 57, 72, and 99. These chromatograms illustrate both the low absolute abundance of 3-octanone at this challenging concentration level, as well as the limited chromatographic resolution and mass spectral selectivity versus the interfering matrix peak. Despite low *S/N* and low mass spectral selectivity, 3-octanone has a significant average F-ratio value and is easily found in the output of the tile based F-ratio software as the fourth feature in the hit list, above the 0.1% null probability limit. Figure S-6 is the mass spectrum for 3-octanone, as obtained from the 2011 NIST Mass Spectral Library. Comparing the F-ratio spectrum in Figure S-5(A) to the mass spectrum (Figure S-6), we see that as expected the two spectra have several *m/z* in common, though the relative intensities of the *m/z* are altered by the mass spectral selectivity in the F-ratio calculation for the various chromatographic interferents.

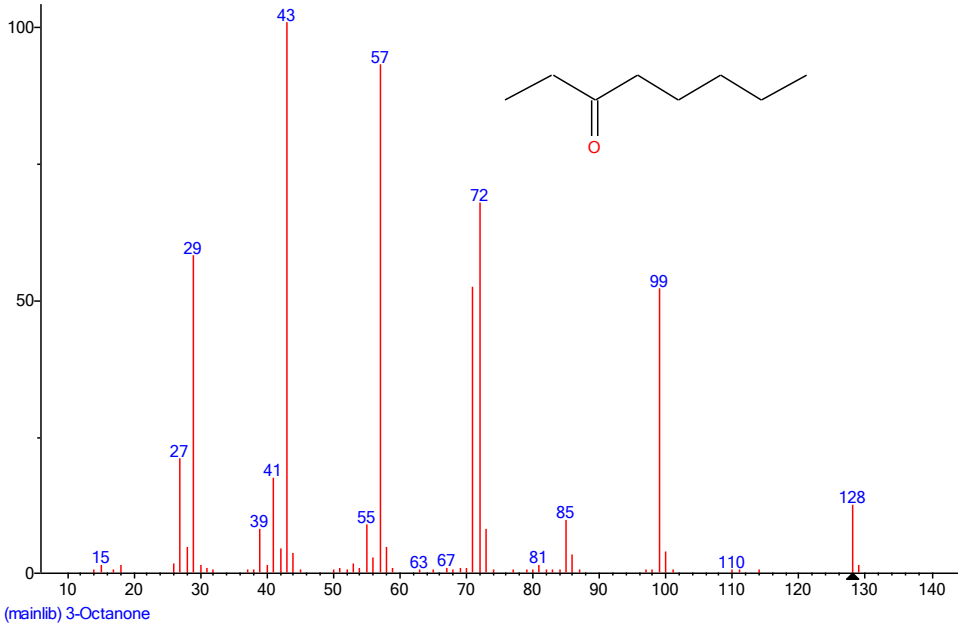

Figure S-6. The mass spectrum for 3-octanone, as obtained from the 2011 NIST Mass Spectral Library.

2.8.4 Comparison of Tile Based Software to Pixel Based Software and Peak Table Based Methods

The tile based F-ratio software comprehensively analyzes GC×GC–TOFMS data while simultaneously maximizing discovery of true positives and minimizing the discovery of false positives. The approach taken by the tile based software is most similar to that of pixel based analysis,[28-33] in that the tile based software aims to perform minimal processing prior to statistical analysis of the data to find class distinguishing features. Specifically, tile based[18] and pixel based[28-33] feature selection analyses avoid peak finding, explicit 2D alignment of the chromatograms, deconvolution, and mass spectral matching to libraries. Rather, the workflow of tile based and pixel based analyses is to first discover the class distinguishing analytes in an experimental comparison, and then apply alignment, deconvolution, and mass spectral matching only as needed on the features which have been selected as having statistical discriminatory power in the analysis. The preceding approaches are in marked contrast to peak table methods, which apply statistical analysis only after generating lists of all of the "analyte" peaks found in the chromatograms, which follows the peak finding, deconvolution, matching, and peaklet combination (for GC×GC–TOFMS) steps.[34-37]

To demonstrate the potential of the tile based software amid other methods applied in the GC×GC–TOFMS field, we have performed preliminary comparisons to both pixel based F-ratio analysis, as well as the peak table based data processing that would occur prior to F-ratio analysis. The analysis which follows is based on the software we have available in our laboratory. At this time we are not able to compare to peak region methods (such as those used in GC Image), but such a comparison would also be beneficial in future work. The tables presented in the following sections were used to compare to those shown for the tile based results.

2.8.4.1 Pixel Based Analysis Comparison

A pixel based analysis was performed with the in-house developed pixel based F-ratio software[28-31], using parameters matched to those of the tile based software (signal normalization to the bromoheptane internal standard, *S/N* threshold of 3σ, all *m/z* analyzed, etc.). Tables S-8 and S-9 summarize the results of the pixel based F-ratio analysis for the 12.5 ppm versus 0 ppm comparison, and the 1.6 ppm versus 0 ppm comparison, respectively. These pixel based tables correspond to the same concentration comparisons as (and should be compared to) Tables S-6 and S-7 for the tile based analysis. Compared to the tile based software, the pixel based software performs well, finding most of the analytes near the top of the hit list. However, as expected, more false positives are found interspersed between the hits, as compared to the tile based analysis. At the 12.5 versus 0 ppm comparison level, we see that the pixel based analysis (Table S-8) exhibits a false positive at the top of the hit list, outranking even bromobenzene. The tile based analysis (Table S-6) finds bromobenzene as the top hit, and has no false positives between the four spiked analytes. In the significantly more challenging 1.6 versus 0 ppm comparison, the tile based and pixel based analyses each find two of the four analytes at the top of their respective hit lists; however, the pixel based analysis (Table S-9) has approximately twice as many non-discriminating features (76) interspersed between the four spiked analytes, versus the tile based analysis (Table S-7) (34).

Table S-8. The hit list for the pixel based analysis of the 12.5 ppm versus 0 ppm comparison. The four spiked analytes are found as the first five entries in the hit list. The first hit of the analysis is a false positive.

F-ratio hit no.	Average F-ratio	^1t_R (s)	^2t_R (s)	Compound
1	896.7	1622	0.26	false positive
2	853.2	360	0.11	**bromobenzene**
3	715.5	534	0.73	**5-decyne**
4	568.7	441	0.91	**3-octanone**
5	322.4	255	0.94	**1-chlorohexane**
6	103.8	165	0.07	false positive
7-2428	…	…	…	false positives

Table S-9. The hit list for the pixel based analysis of the 1.6 ppm versus 0 ppm comparison. There are false positives interspersed with the true positives.

F-ratio hit no.	Average F-ratio	^1t_R (s)	^2t_R (s)	Compound
1	376.6	534	0.73	**5-decyne**
2	367.1	360	0.13	**bromobenzene**
3	133.4	2708	0.90	false positive
4	108.1	2415	0.68	false positive
5	102.1	255	0.93	**1-chlorohexane**
6	103.8	165	0.07	false positive
6-79	…	…	…	false positives
80	21.0	441	0.91	**3-octanone**
81-2459	…	…	…	false positives

As was observed in table S-6 through S-9, false positives were observed between true positives in both the pixel based and tile based analyses, though to a lesser degree in the latter. Tile based analysis consistently finds the four spiked analytes at the top of the hit list at all spike versus blank comparisons including and above the 6.2 ppm versus 0 ppm comparison. Conversely, pixel based analysis encounters false positives interspersed between true positives even at higher concentration comparisons. Tables S-10 and S-11 compare the results of the pixel based and tile based methods for the 25 ppm versus 0 ppm comparison. At this concentration level comparison, pixel based analysis finds two false positives between the hits for 3-octanone

and 1-chlorohexane. Analyzing the same data, tile based analysis finds no false positives between the four spiked analytes.

Table S-10. The hit list for the pixel based analysis of the 25 ppm versus 0 ppm comparison. Two false positives are interspersed with the true positives.

F-ratio hit no.	Average F-ratio	^1t_R (s)	^2t_R (s)	Compound
1	1102.7	360	0.14	**bromobenzene**
2	765.6	534	0.73	**5-decyne**
3	343.1	441	0.92	**3-octanone**
4	157.4	1003	0.50	false positive
5	143.6	2337	0.95	false positive
6	134.8	255	0.93	**1-chlorohexane**
7-2672	…	…	…	false positives

Table S-11. The hit list for the tile based analysis of the 25 ppm versus 0 ppm comparison. There are no false positives interspersed with the true positives.

F-ratio hit no.	Average F-ratio	^1t_R (s)	^2t_R (s)	Null classification	Compound
1	2167.2	360	0.13	hit	**1-chlorohexane**
2	1869.7	255	0.94	hit	**bromobenzene**
3	271.6	534	0.73	hit	**5-decyne**
4	131.2	441	0.91	hit	**3-octanone**
5-5123	…	…	…	potential hits and non-hits	

Overall, we found in our comparison of the pixel based and tile based methods that both successfully find analytes spiked into a complex matrix (diesel fuel) at low concentrations (substantially less than 100 ppm) relative to the matrix. Compared to pixel based analysis, tile based analysis demonstrated similar discovery rates for the true positives, with substantially lower rates for false positives. Whereas pixel based analysis demonstrated false positives interspersed with the four spiked analytes at spike versus blank comparisons of up to 25 ppm versus 0 ppm, tile based analysis applied to the same data did not encounter interspersed false positives until the 3.2 ppm versus 0 ppm concentration comparison.

2.8.4.2 Peak Table Based Comparison

To evaluate the feasibility of peak table based F-ratio analysis for the data analyzed by the tile based F-ratio software, we compiled peak tables using the instrument software (LECO ChromaTOF v 3.32). While we were unable to perform F-ratio analysis, which requires the LECO Statistical Compare add-on, we critically evaluated the peak table results to demonstrate for which analyte concentrations the F-ratio analysis of the peak tables would likely be viable. This critical evaluation allowed us to study both the advantages and disadvantages of peak table analysis and to predict the ultimate performance of a non-targeted analysis of the results. The peak table analysis software that is provided with the LECO Pegasus 4D is a powerful utility which integrates peak finding, deconvolution, mass spectral matching, and peaklet combination (for GC×GC–TOFMS) to generate a list of all peaks found in a chromatogram, along with metrics such as peak height, area, deconvolution purity, etc. Peak tables can be viewed in ChromaTOF or exported as .csv tables to other applications.

An important aspect of peak table analysis, as implemented in ChromaTOF, is the selection of appropriate parameters for the generation of the peak tables. These parameters include selections such as expected column 1 and column 2 peak widths, maximum number of peaks to find, *S/N* thresholds, matching thresholds, and others. Selection of these parameters greatly influences the success of peak finding and deconvolution, and consequently the discovery rates for true and false positives.[55] In order to best compare, in principle, peak table based methodology to our tile based software, the parameters were selected to balance the need for low detection limits with the preference for reducing false positives. Table S-12 summarizes the relevant data processing parameters selected for the peak table analysis.

Table S-12. The relevant parameters applied for peak table analysis (ChromaTOF v 3.32).

Baseline offset	1
Smoothing	Auto
Column 1 peak width (baseline to baseline)	0.2 s
Maximum number of unknown peaks to find	10000
Signal-to-noise threshold	10
Number of apexing masses	1
Match required to combine peaks	800
Column 2 peak width	4 s
Library search mode	Normal/forward
Masses to library search	All (m/z 41:340)
Maximum molecular weight allowed	300
Mass threshold	10
Minimum similarity for name assignment	800
Mass for area/height calculation	DA (deconvoluted analytical ion chromatogram)

After processing the individual chromatograms, the peak tables were exported to Excel, and the relevant entries (the four spiked analytes, and the internal standard) were manually selected and combined. The peak areas were normalized to the internal standard, 1-bromoheptane. Table S-13 summarizes the results of the peak table analysis. As found in the application of the pixel based and tile based methods, the peak table approach was sensitive to analyte concentration. Peaks were reliably found above the 12.5 ppm concentration level, more so for the less-interfered bromobenzene and 1-chlorohexane peaks. As evident by the relative standard deviations, the more-interfered 5-decyne and 3-octanone peaks were quantified with lesser precision. In the most lenient approach to an F-ratio analysis on the peak table data, the "discovery limit" (for this study, the nominal concentration level at which the analyte could feasibly be discovered in the course of F-ratio analysis) would be the 3.2 ppm and 12.5 ppm for 5-decyne and 3-octanone, respectively. Below the discovery limits, no peaks were found at the elution times of the respective analytes, as indicated in Table S-13 by "N.F."

Table S-13 Peak table results from the ChromaTOF processing of the chromatograms spanning the spiked analyte concentration levels from 1.6 ppm to 50 ppm. Given are the average peak areas for the four spiked analytes for which a peak was found, along with the relative standard deviation for the four injection replicates. N.F. indicates that no peak was found for the analyte at the given analyte-concentration pair. ([a]) indicates analyte-concentration pairs having fewer than 3 apexing *m/z*. ([b]) indicates analyte-concentration pairs having unidentified or misidentified analytes for at least one of the injection replicates.

	mean area (relative standard deviation) for spiked analyte			
Nominal concentration level	bromobenzene	1-chlorohexane	5-decyne	3-octanone
50 ppm	224767 (4%)	175228 (3%)	127339 (7%)	57834 (55%)
25 ppm	115272 (5%)	87680 (5%)	44211 (23%)	9991 (60%) [b]
12.5 ppm	56438 (7%)	45466 (5%)	15207 (47%)	2437 (35%) [a,b]
6.2 ppm	26239 (5%)	19356 (11%)	2044 (41%) [a,b]	N.F.
3.2 ppm	12623 (7%) [b]	9484 (14%)	842 (54%) [a,b]	N.F.
1.6 ppm	3814 (28%) [b]	2533 (23%) [b]	N.F.	N.F.

In a more stringent usage of peak table data for F-ratio analyses, additional metrics would be applied to the peak table data prior to an F-ratio calculation. An important parameter for ChromaTOF data processing is the number of apexing *m/z* for a given peak. Apexing *m/z* are important for spectral deconvolution; to reduce false positives, the ChromaTOF documentation recommends that 3 apexing *m/z* be required for peak inclusion; the default is 2 apexing *m/z*, which allows for detection of more peaks, but at the risk of more false positives and splitting of true positives. If at least 3 apexing *m/z* were required for inclusion in a peak table based F-ratio analysis, we find that the discovery limit would increase for 5-decyne and 3-octanone, to 12.5 ppm and 25 ppm, respectively. Analyte-concentration pairs having fewer than 3 apexing *m/z* are denoted by "[a]" in the Table S-13.

An additional constraint that may be applied in the course of an F-ratio analysis using peak table data would be the requirement of reliable mass spectral matching. Under ideal conditions, all analytes would be high *S/N*, free of chromatographic interference, and included in

mass spectral libraries. However, since these ideal conditions are not typical of most—if any—real-world analyses, the quality of mass spectral matching must be taken into account. To reduce false positives, a match value of at least 800 (out of 999) was required for name assignment for a given peak. Under this constraint, peaks with insufficient match value, or incorrect matches, would not be included in the F-ratio analysis. Analyte-concentration pairs having at least one replicate that was unidentified or misidentified are denoted by "[b]" in the Table S-13. Under this more stringent usage of peak tables, the discovery limit increases for all of the analytes, to 6.2 ppm (bromobenzene), 3.2 ppm (1-chlorohexane), 12.5 ppm (5-decyne), and 50 ppm (3-octanone). Because the tile based method is able to discover features even under conditions that are challenging for peak finding and deconvolution, its discovery limit for 3-octanone is much lower compared to peak table methods (found as a highly ranked hit even at the 6.2 versus 0 ppm comparison).

Overall, the peak table based F-ratio analysis performs well at higher *S/N*, and for analytes with little chromatographic interference. However, due to inherent limits in peak finding, deconvolution, and mass spectral matching, the peak table analysis was, for this data set, less reliable at lower *S/N*, especially for analyte peaks which are substantially interfered chromatographically, such as 3-octanone. Tile based F-ratio analysis significantly improved the "discovery limits" for the more challenging analytes and demonstrated that when performing discovery-based analysis on complicated chromatographic data sets, statistical analysis prior to deconvolution and careful quantification is both viable and beneficial. We also note that the tile based analysis workflow for discovery of class distinguishing features is substantially faster than peak table processing. A four chromatogram versus four chromatogram comparison using tile based analysis may be performed in less than 2 minutes (10 minutes including null distribution

analysis) on a mid-level desktop PC. Using the same PC to process the same eight GC×GC–TOFMS chromatograms for peak table analysis took approximately 80 minutes, which only includes generation of the peak tables; combination and statistical comparison of the peak tables would further add to the computational burden. The computational savings of the tile based analysis provide substantial advantages for rapid discovery, and additionally allows for rapid iteration of parameters when developing methods for a given experiment.

2.8.4.3 Summary of the Comparisons of the Tile, Pixel, and Peak Table Based Methods

Overall, the tile based analysis provides a reduced propensity for the discovery of false positives. Whereas the pixel based analysis encountered false positives interspersed with the four spiked analytes as high as the 25 ppm versus 0 ppm comparisons, the tile based analysis did not encounter interspersed false positives until the 3.2 ppm versus 0 ppm comparison. Compared to pixel based and tile based analyses, which perform minimal processing of the data prior to statistical analysis, peak table analysis performs peak finding, deconvolution, quantification, and matching prior to the statistical analysis of the processed data. Under typical use of peak table methods, this requires that the potentially class distinguishing peaks are properly located and identified in order to be included in the statistical analysis. In a stringent peak table F-ratio analysis where the parameters are chosen to reduce false positives, the lowest concentrations at which analytes are reliably discovered was be substantially higher than that of the pixel based or tile based methods. While the limit of discovery 3-octanone was ~56 ppm using the peak table method, this challenging analyte is easily discovered at the ~7 ppm when using the either the tile based or pixel based methods.

Chapter 3: Chemical Characterization of the Acid Alteration of Diesel Fuel: Non-targeted Analysis by GC × GC–TOFMS with Tile-Based Fisher Ratio and Combinatorial Threshold Determination[4]

3.1 Introduction

Petrochemical fuels are refined by a variety of methods that allow for inherently variable feedstocks to be better controlled in finished products to meet a range of quality metrics and other specifications, such as engine performance and longevity, storage stability, and emissions. Such processes and specifications ensure that the fuels are acceptable for distribution and end use by consumers. However, between the refinery and end user, intermediate parties may further alter the chemical composition of finished fuels, for the purpose of altering the fuel color [1]. Hence, there is substantial interest in the forensic detection of such alteration by law enforcement and regulatory agencies. An alteration that has been observed in the field is the reaction of petroleum fuels with concentrated sulfuric acid (H_2SO_4). Sulfuric acid is a prevalent and inexpensive reagent used in a wide variety of industrial, commercial, and household applications. Based on the chemical composition of petroleum fuels, one would expect reaction with sulfuric acid to cause a variety of chemical changes in fuel due to reactions between the sulfuric acid and native compounds in the fuel [2–4]. Gasoline fuel exhibits substantial chemical changes due to the presence of *tert*-butylating compounds, such as methyl *tert*-butyl ether (MTBE), while the changes to diesel fuel are more subtle, limited to the aromatic moiety of the fuel [2,4]. For the purposes of forensic classification of acid altered diesel fuel, it is necessary to better understand

[4] This chapter has been reproduced from B. A. Parsons, D. K. Pinkerton, B. W. Wright, R. E. Synovec. J. Chromatogr. A, 2016, 1440, 179-190.

the chemical compositional changes that occur and which may differentiate unaltered from altered fuels.

Reactions between sulfuric acid and aromatic compounds are well represented in the literature, particularly in the fields of surfactant and dye chemistry, in which electrophilic species in the sulfuric acid react with the aromatics to add sulfonic acid, altering the aqueous solubility of the aromatics [5]. Literature on sulfonation reactions using sulfuric acid indicate that various aromatic species have an intrinsically different reactivity with the electrophilic species in the concentrated acid, and thus will be chemically modified to different extents as the reaction proceeds [6–8]. An interesting aspect of aromatic sulfonation by sulfuric acid addition is that the reaction produces water, leading to a quenching of the reaction as concentrations of the electrophilic species decrease. Most studies on the reaction rates and extent of reactions for aromatic sulfonation using sulfuric acid involve simple reagent systems (i.e., neat reagent or reagent dissolved in a suitable solvent) and an excess of sulfuric acid (typically 3-4 molar equivalents). In the forensic study of acid altered diesel fuel, these ideal conditions are absent: first, the speciation of aromatics in diesel is highly complex, often ranging from benzene to pyrene with various degrees of alkylation and unsaturate substitution, as well as lesser amounts of aromatic heterocycles. Additionally, the sulfuric acid is probably not added stoichiometrically, and factors such as the water content of the diesel fuel may also impact the rates and extent of reaction. Further, industrial syntheses typically include temperature control and removal of water from the sulfuric acid to assist in driving the aromatic sulfonation to completion; such controls may not be present in illicit alterations.

Due to the substantial differences expected between the literature reaction conditions for synthesis of sulfonated aromatics versus the less-ideal conditions for illicit alteration of diesel

fuel, a non-targeted "discovery-based" analysis would be beneficial for characterizing the chemical changes that result from the alteration. In non-targeted analysis, the chemical features (i.e., analyte peaks) of interest are not presumed to be known prior to the experiment. Non-targeted approaches may be performed using supervised or unsupervised methods, where supervision refers to the prior classification of samples as they relate to the experimental design [9–11]. Overall, non-targeted methods aim to discover the key chemical features, i.e., the analyte peaks indicative of chemical marker compounds that robustly distinguish samples from each other. For the purpose of analyzing the chemical composition of diesel fuel, comprehensive two-dimensional (2D) gas chromatography coupled with time-of-flight mass spectrometry (GC × GC–TOFMS) provides the necessary analytical resolution, sensitivity, and sample throughput [12–19]. Recently, a comprehensive and informative review was reported, dealing with the application of GC × GC in forensics [20]. Indeed, GC × GC is increasingly being utilized in forensic studies, but it is acknowledged that the complexity of the data is a major factor in slowing the technology's implementation. To improve the utility of GC × GC for all users, and to increase its utilization in forensic applications, it is necessary to develop feature selection software to reduce the complex output to only the most significant chemical features.

We previously reported the development of tile-based Fisher ratio (F-ratio) analysis for the comprehensive discovery-based analysis of GC × GC–TOFMS data [21,22]. This methodology, herein referred to as tile-based F-ratio analysis, is a supervised non-targeted method that discovers features in a sample-class comparison (e.g., unaltered fuel versus acid altered fuel) that are class-distinguishing, i.e., peaks that are statistically different between sample classes. The tiling portion of the software utilizes a novel binning scheme which improves the discovery of class-distinguishing chemical features ("hits") while minimizing the

discovery of features which are not significantly different between sample classes ("non-hits"). Tile-based F-ratio analysis coupled with GC × GC–TOFMS is highly effective for the experimental determination of chemical changes in the highly complex matrix of diesel fuel.

In the process of feature selection using tile-based F-ratio analysis, the chromatograms for the sample-class comparison experiment are comprehensively analyzed, with only the most essential application of signal thresholds, enabling the discovery of class-distinguishing analytes, even at the trace concentration level. The F-ratio, which is the calculated value for the one-way analysis of variance (ANOVA) *F*-test [23] is used to rank chromatographic features in a hit list according to their class-distinguishing abilities, with a large F-ratio indicating that a given feature is highly class-distinguishing, and a small F-ratio indicating that a given feature is not class-distinguishing. In order to avoid false positives (type I errors) and to utilize analyst time most efficiently, only features with a sufficiently high F-ratio should be pursued in subsequent analyte deconvolution, identification and quantification steps; this may be accomplished by setting an F-ratio threshold for the hit list. However, determination of such a threshold is often a subjective matter that requires manual analyst intervention to decide the point at which the selected features become unreliable, and often leads to excessive, time-consuming manual data analysis steps [24,25].

As an alternative to manual threshold determination, statistics-based approaches should be considered and applied. One approach is to utilize the critical value for the *F*-test (F_{crit}) to determine a threshold for significance [26,27]. Another statistics-based approach is using a z-scores method [28]. An alternative approach for F-ratio threshold determination is to analyze the within-class variation for each sample class within the experiment, and utilize the maxima of these values as the cutoff, under the basis that any significant between-class variation will exceed

that of the within-class variation [29]. We recently reported a new approach, null distribution analysis, which is a permutation-based test [30] to establish the distribution of spurious F-ratio values for a given GC × GC–TOFMS experimental design analyzed using tile-based F-ratio analysis [22], which used a frequentist strategy to infer a threshold to differentiate hits from non-hits. Herein, we describe improvements to null distribution analysis to determine a statistically-appropriate F-ratio threshold aimed at minimizing false discoveries while simultaneously maximizing true discoveries. The improved null distribution analysis methodology is then applied to find class-distinguishing analytes, i.e., chemical marker compounds which discriminate acid altered from unaltered diesel fuel.

3.2 Theory

For robust determination of class-distinguishing analytes in non-targeted GC × GC–TOFMS F-ratio experiments, it is necessary to choose an appropriate threshold to cut off the analysis of the resulting hit list, in order to save analyst time and to avoid false discoveries. Most traditional statistical approaches would suggest simply using a critical value, in this case F_{crit}, which is determined for the degrees of freedom in the experiment and significance level desired, and which is provided in tables found in most quantitative analysis or statistics textbooks. However, the F_{crit} approach makes the assumption that the *F*-distribution arises from within-class and between-class variates that each follow a chi-squared distribution, and which are independent; the validity of the assumptions may vary. A more-pressing consideration is that the use of critical values is based on single hypothesis testing, and does not consider the overall error rate when testing multiple hypotheses. When testing multiple hypotheses, it is necessary to consider and control the false discovery rate (FDR) [31], the basis of which is described next.

In statistical hypothesis testing, the significance level, α, predicts the probability of a type I error (rejecting the null hypothesis when it is actually true, resulting in a false positive); in a sample-class comparison experiment, this would be "discovering" a feature that is not class-distinguishing and is instead caused by noise, baseline, or other spurious covariance. The significance level, α, provides a statistic for the type I error rate for testing a single hypothesis. However, in the application of the F-ratio method to a GC × GC–TOFMS sample-class comparison experiment, every feature in the chromatogram represents an individual hypothesis, i.e., each individual feature is tested to determine whether it is statistically class-distinguishing. In the traditional approach, hypothesis testing proceeds as follows: a significance level is chosen for a test statistic to calculate a critical value, for example, an analyst may choose $\alpha = 0.001$, which corresponds to a 1:1000 chance of a type I error. Statistics are calculated for the feature being tested and the generated *p*-value for the test is then compared against α to decide whether to reject the null hypothesis at that chosen significance level. Generally, if the *p*-value is less than α, the analyst considers the feature to be statistically different between classes. When this procedure is applied with $\alpha = 0.001$, an individual hypothesis may be expected to have a 0.1% chance of falsely failing, that is, producing a false positive. However, when testing multiple hypotheses, such as testing each peak in a chromatogram, the overall chance of at least one hypothesis test producing a false positive is actually greater than 1:1000, and is proportional to the number of hypotheses tested. This phenomenon is known as the multiplicity problem, which requires adjustment of the statistics according to the number of hypotheses tested [31,32]. Indeed, methods to control the FDR are an active area of contemporary statistics, particularly in the field of genetic microarray analysis and other biological analyses [33–35]. Herein, we now

introduce null distribution analysis as a method to control the FDR, while avoiding the assumptions of F_{crit} methods, concurrent with inherently addressing the multiplicity problem.

Null distribution analysis is a technique that leverages the large number of simultaneous hypotheses that may be tested in a GC × GC–TOFMS dataset to experimentally determine the distribution of potential false positives [22]. By rearranging the sample classes to test the null hypothesis (that there are no differences between the classes), the effects of non-meaningful variation in the dataset may be estimated for subsequent sample-class comparisons. The null distribution method is utilized for determining an F-ratio threshold which holds no assumptions about the underlying sources of variation that lead to non-significant F-ratios. Further, the method is applied to the results of the testing of multiple hypotheses, such that the results are inherently applicable to the multiple hypotheses testing in the sample-class comparison, and directly address the probabilities of false positives in context of the FDR. In our initial report for a spiked diesel study [22], the "null" sample classes were constructed by manually arranging six simple pairwise null combinations for a four versus four comparison (two sample classes, each comprised of four GC × GC–TOFMS chromatograms). Six pairwise arrangements were chosen to demonstrate proof-of-principle of the methodology, as the null arrangements for this case were simple to explain, and provided adequate sampling of all the possible null comparisons. However, to increase the extensibility of null distribution analysis, it is desirable to algorithmically determine all possible null comparisons in a rigorous and automated fashion.

Null distribution determination can be rigorously expanded, from a manual subset of arrangements, to include all possible null class arrangements through the use of combinatorial theory. In order to calculate the total number of unique null arrangements that can be generated from a given sample-class comparison experiment, the number of classes in the null

arrangements must be equal to the number of classes in the original data, and there must be an equal number of samples from each class in the null class; this means that the number of samples in each class of data must be a multiple of the number of classes. For example, in a 2 × 2 sample-class comparison (two samples in Class 1 and two samples in Class 2), a null arrangement is generated by creating two new classes: A and B, where Class A consists of one sample from Class 1 and one sample from Class 2, and Class B would then consist of the remaining samples from Classes 1 and 2. Because the order of the samples within a class does not affect the F-ratio calculation, we can determine the number of null arrangements by "counting" the number of unique combinations of a subset of *k* samples from a class of size *n*, a combinatorial method of sampling where order does not matter, often referred to as "*n* choose *k*"[36].

$$ {}_n\mathrm{C}_k = \frac{n!}{k!(n-k)!} \tag{1}$$

The value ${}_n\mathrm{C}_k$ in Eq. (1) is used to calculate the number of ways to select *k* samples from the set of *n* samples where *n* is the size of Class 1 and *k* is the number of samples from Class 1 to be included in each null class. For a two class system, $k = n/2$. This calculation must be performed for each class, and the total number of combinations is the product of these two values. However, there is no mathematical difference between Class A and Class B (i.e., Class A consisting of samples 1 and 2, Class B consisting of samples 3 and 4 is the same as Class A consisting of samples 3 and 4, Class B consisting of samples 1 and 2). Therefore, the number of unique null arrangements will be ½ the total number of combinations from Classes 1 and 2, utilizing Eq. (1),

$$ \#\ Unique\ Null\ Arrangements = \frac{1}{2} * {}_{n_1}\mathrm{C}_{k_1} * {}_{n_2}\mathrm{C}_{k_2} = \frac{1}{2} * \frac{n_1!}{k_1!(n_1-k_1)!} * \frac{n_2!}{k_2!(n_2-k_2)!} \tag{2}$$

With the above combinatorial method for creating null arrangements, we are now able to study the potential benefits of using more null distributions than previously reported, in which we explored the use of a small number of randomly selected null arrangements (i.e., 6 arrangements) [22]. Using Eq. (2), the number of possible unique null arrangements may be calculated; for common sizes of sample-class comparison experiments, 4 × 4, 6 × 6, and 8 × 8, there are 18, 200, and 2450 unique null arrangements, respectively. In the previous report, 6 null arrangements were selected from the 4 × 4 comparison that was performed. From a practical perspective a 6 × 6 sample-class size comparison, producing 200 unique null arrangements, is a sensible compromise between possibly having insufficient statistical coverage of the null distribution behavior (i.e., with only 18 unique null arrangements using a 4 × 4 comparison), and producing an overabundance of null arrangements which may begin to impact computational performance (i.e., using the 8 × 8 comparison that produces 2450 null arrangements). Thus, the 6 × 6 sample-class size comparison is utilized in the current study.

3.3 Experimental

3.3.1 Sample Preparation

Six diesel fuel samples were collected from separate fueling stations in the Seattle area, from various fuel brands, labeled herein as samples AR, FH, MB, SG, SS, and RC. Only samples SS and RC contained significant levels of biodiesel in the form of fatty acid methyl esters (FAMEs). The fuel samples were collected and stored in amber glass bottles. A spike solution was prepared to deliver two internal standards, bromoheptane (Aldrich, 99%) and bromobenzene (Aldrich, 99%), to each fuel at final nominal concentrations of 800 ppm for each of the internal standards. After thorough mixing, two 25.0 g aliquots of each of the six spiked fuels were added to individual glass sample jars (4 fl. oz. capacity with polypropylene-lined lids) along with

PTFE-coated magnetic stir bars. For each fuel, 5.0 g of concentrated sulfuric acid (Macron Fine Chemicals, ACS reagent grade) was added to one jar, while the other was a control (no acid added); control samples were handled similarly to avoid false discoveries due to sample handling. The samples were stirred using a magnetic stir plate at 1000 rpm for 10 min, which was sufficient time to produce the desired acid alteration chemical changes for the diesel samples in which acid was added. Upon completion of stirring, 1.5 ml of each sample was transferred to polypropylene 1.5 ml microcentrifuge tubes and centrifuged at 10,000 rpm (5,000 × g) for 5 min to separate the diesel and acid phases. The diesel phase of each centrifuged sample was then transferred to 1.5 ml autosampler vials for analysis by GC × GC–TOFMS.

3.3.2 Instrumental

The GC × GC–TOFMS instrument consisted of an Agilent 6890N gas chromatograph equipped with an Agilent 7683 autoinjector (Agilent Technologies, Palo Alto, CA) coupled with a LECO Pegasus III TOFMS equipped with a 4D thermal modulator upgrade (LECO, St. Joseph, MI). The primary column of the GC × GC (column 1) was a 20 m x 250 μm i.d. x 0.5 μm Rtx-5MS film (Restek, Bellefonte, PA) and the secondary column (column 2) was a 2 m x 180 μm i.d. x 0.2 μm Rtx-200 film (Restek, Bellefonte, PA). The GC instrument inlet was set to 275 °C and the transfer line was set to 290 °C. Column 1 was held at 40 °C for 1 min and then increased at 5 °C/min to 285 °C, where it was held for 5 min, for a total run time of 55 min. The column 2 oven and modulator block followed the same temperature program as column 1, with +5 °C and +20 °C offsets, respectively. The modulation period was 1 s and the hot and cold pulse times for each stage were 0.4 s and 0.1 s, respectively. A constant (ambient temperature and pressure corrected) flow rate of 2 ml/min at the outlet of column 2, with helium (Praxair, Grade 5.0) as the carrier gas. The ion source was set to 250 °C, the electron impact energy was 70 eV, and the

detector voltage was set to 1600 V. Mass channels, *m/z* 33-250, were collected at 100 spectra/s after a 10 s acquisition delay. A 1 μl injection of each diesel sample was made in split mode with a split ratio of 200:1. Each diesel sample was injected in duplicate.

3.3.3 Computational

To discover class-distinguishing chemical features for the acid alteration, a sample-class comparison experiment was constructed using three different diesel fuels collected from separate filling stations in the Seattle, WA area: samples AR, FH, and MB; the three fuels were analyzed prior to and following acid alteration. Two chromatograms from of each of the three fuels prior to acid alteration comprised the unaltered class, and two chromatograms of each of the three fuels after acid alteration comprised the altered class. Findings from the sample-class comparison experiment were validated using the remaining three samples: SG, SS, and RC. All chromatograms were normalized for injection variation using the sum of signals method (often referred to as TIC normalization) [9], which was validated against the bromoheptane and bromobenzene internal standards. The normalization values were used in the tile-based F-ratio analysis, as well as in plotting and quantification of selected class-distinguishing features.

GC × GC–TOFMS data from the 12 runs for the sample-class comparison (3 fuels × 2 replicates × 2 classes) were imported from the LECO ChromaTOF software v 3.32 (LECO, St. Joseph, MI) to Matlab R2014b (8.4.0.150421) (MathWorks, Inc., Natick, MA) via an in-house developed data converter [37]. The imported data were analyzed with in-house developed tile-based F-ratio software, performed on a mid-level personal computer, having an Intel Core i7-4770 processor (3.4 GHz), a 250 GB Samsung 840 solid state hard drive, and 16 GB dual-channel DDR3 RAM, with Windows 7 SP1 as the operating system. The tile-based F-ratio software was used to discover chemical features in the fuels that differentiated the unaltered and

altered classes [21,22]. The tile and cluster sizes, given as column 1 × column 2 (number of modulations × number of spectra) were 6 × 10 and 4 × 10, respectively. Selection of the tile size is a balance of two competing objectives. First, the tile aims to capture most of the 2D peak signal (using the ±2σ width) plus additional space to allow for minor retention time shifts in each dimension. Second, the tile size is kept sufficiently small to maintain selectivity for individual peaks (i.e., to minimize sampling neighboring peaks) and to minimize inclusion of noise [22]. The per-*m/z S/N* threshold was 3σ with ≥3 *m/z* required above the threshold for inclusion of the tile; all *m/z* collected were included in the analysis. The null probability limit was 0.1%.

Selected analyte features of interest were quantified using ChromaTOF. Briefly, all column 2 peaks (i.e., peaklets) that result from the modulation of the column 1 peak for selected analytes are individually detected and deconvoluted; unique *m/z* are then found for the chromatographic profiles present in the peaklets. Next, peaklets are combined to form a single 2D peak for each selected analyte, based on the mass spectra and column 2 retention times of the peaklets, as well as the expected peak widths in both dimensions. Finally, the combined 2D peak for each analyte was integrated using the unique *m/z* to calculate the quantified peak sum. The deconvoluted mass spectra, along with analyte retention times, were compared to the NIST11 mass spectral library and used to preliminarily identify discovered features.

Null distribution analysis was performed similarly to that described previously [22], with the distinction that in this report, we perform a 6 × 6 sample-class comparison, including the complete set of all 200 unique null arrangements. Furthermore, the 200 null distributions were combined by averaging and used to prepare a comprehensive null probability curve, which was used to determine the F-ratio threshold. The individual null distributions were then used to infer

the statistical confidence for the F-ratio threshold. Figure 1 is a flowchart summarizing the workflow performed in this study.

3.4 Results and Discussion

3.4.1 Tile-based F-ratio analysis

In this study, the analytical challenge was to discover changing analytes in a highly-complex sample with maximal discovery of significantly-changing analytes, even at very low relative concentrations, concurrent with minimal discovery of analytes that do not significantly change between sample classes. Further, we aimed to discover said changes without explicit prior knowledge of which chemicals, or even chemical classes, would be substantially modified by the alteration. GC × GC–TOFMS allows for the comprehensive analysis of diesel fuel with a far greater degree of chromatographic resolution than one-dimensional GC and additionally improves detection limits through the zone-focusing effects of the thermal modulator [16–19]. These benefits are of substantial value for the study of the acid alteration of diesel fuel, in which the affected compounds are at low abundances compared to the predominantly aliphatic content of diesel fuel (which is not affected by the alteration) and which may only be partially removed by the alteration. Figure 2 demonstrates the challenge: under visual comparison of the 2D total ion current (TIC) chromatograms, the visible differences between the fuels is more apparent than those prior to and following the acid alteration.

In cases where the differences between sample classes are subtle, algorithmic methods are critical for rapid and comprehensive discovery of class-distinguishing analytes. The tile-based F-ratio software enables analysis of GC × GC–TOFMS data with minimal user intervention, and is able to discover analytes even at low absolute concentration and a low concentration ratio. Further, the tile-based algorithm mitigates recognized challenges in the

analysis of GC × GC–TOFMS data, including the impacts of minor chromatographic retention time shifts and ensuring all of the column 2 peaklets for a given modulated analyte are accurately combined for 2D peak quantification [38–40]. By improving the signal-to-noise ratio (*S/N*) and reducing the impact of spurious chromatographic and detector variations prior to the F-ratio calculation, the tile-based algorithm maximizes the discovery of significant features while minimizing features of lesser value [21,22].

The analysis initially produces a hit list of features ranked in order of decreasing F-ratio values. The F-ratio is calculated for each feature in the sample-class comparison chromatograms that has sufficient signal, here, having three or more *m/z* above the *S/N* threshold of 3σ. Based on the number of pixels (data points) in the 2D chromatogram, there are 328,900 possible hits (3289 column 1 modulations × 100 column 2 mass spectra) for the sample-class comparison experiment. Tiling the 2D chromatogram reduces the data to 21,880 possible hits; applying the per-tile requirements for *S/N* further reduces this to 16,813 hits. Finally, redundant hit removal reduced the hit list to 3362 features prior to applying the F-ratio threshold determined by the combinatorial null distribution analysis.

In a sample-class comparison experiment such as the acid alteration of diesel fuel, only a relatively small fraction of the total number of chromatographic features are expected to be class-distinguishing. As a result, the preliminary hit list is dominated by small F-ratio values (features that are likely not class-distinguishing) with a lesser number of large F-ratio values (features that are likely class-distinguishing). Figure 3 is a histogram of all 3362 F-ratio values in the preliminary hit list for the sample-class comparison; the distribution is approximately centered on 1, with the vast majority of values below 10. The inset portion of Figure 3 is the tail of the distribution from 10 to 100; the tail of the described distribution contains the chromatographic

features that are the most class distinguishing for the acid alteration. However, Figure 3 shows that the distribution of F-ratio values is continuous, with no clear distinction between the lesser-value features in the main part of the distribution, and the greater-value features in the tail of the distribution. To distinguish class-distinguishing features from among all of the chromatographic features in the sample-class comparison, it is necessary to statistically define an F-ratio threshold using null distribution analysis.

3.4.2 Combinatorial null distribution and threshold determination

Combinatorial null distribution analysis comprehensively evaluates the possible null distributions that may occur in a given experiment. Performing multiple null distribution combinations allows us to predict the variability in the F-ratio distributions of non-hits for the sample-class comparison, allowing the inference of an F-ratio threshold that is robust to reasonable experimental variations in the sample-class comparison. Ultimately, our goal is to ensure that the chosen threshold applied to the preliminary hit list for the sample-class comparison provides the correct balance of avoiding false positives while also finding the lower-ranked features that may still be informative for the experimental study.

As described in the theory section, a 6 × 6 sample-class comparison allows for the computation of 200 unique null distributions. As noted, increasing the number of samples within each sample class rapidly increases the number of possible unique null combinations, e.g., 2450 for an 8 × 8 sample-class comparison. While increasing the number of samples within the sample classes may provide a more-comprehensive sampling of the possible ranges of diesel fuel composition, the calculation of the comprehensive null distributions quickly becomes computationally burdensome. Statistical subsampling methods such as Monte-Carlo sampling

may be an avenue to maintain a reasonable computational burden while realizing potential advantages to expanded sample sizes, and may be a fruitful area for future work.

For this study, sample injection replicates were treated as unique samples for the combinatorial null classes, as retention time and injection variation between injections of the same fuel may be similar in magnitude to differences between similar fuels, as was performed in previous studies [21,22]. Further, sample replicates reflect the nature of fuel station sampling: due to centralized refining and distribution, it is possible for different stations to dispense essentially the same fuel. In discovery-based analysis, there is also the risk of introducing too much sample variation, for example, two fuels (SS and RC) out of the six that were collected contained substantial amounts of FAME-based biodiesel and had lower contents of aromatics. Including these fuel samples in the sample-class comparison experiment would substantially increase the within-class variation and reduce the ability to find class-distinguishing features due to the acid alteration. Utilizing sample replicates strikes a balance between sampling the reasonable variation between fuels that may be encountered in the field, and introducing excessive within-class variation that may preclude the success of the F-ratio analysis.

Figure 4 illustrates a single null arrangement where the null classes are comprised of the switching of the replicates between the sample classes, such that Null Class A contains the first chromatogram (of the two replicates) of each fuel prior to (Class 1) and following acid alteration (Class 2), and Null Class B contains the remaining chromatograms. The null rearrangement eliminates the true source of variation in the sample-class comparison experiment (i.e., the reaction with sulfuric acid), such that the only sources of variation are those which are not germane to the class comparison, such as chromatographic and detector noise and variation. When the tile-based F-ratio software is applied to a null comparison, the resulting null hit list

represents the distribution of F-ratio values that one would expect to encounter had there been no meaningful class differences in the sample-class comparison experiment.

Figure 5A includes the null distributions from the 200 unique null combinations for the 6 × 6 sample-class comparison, per Eq. (2). Overall, nearly all of the null F-ratios are below 10, and most of the null distributions are centered on F-ratio values from about 1 to 2. The null distributions are transformed into null probability curves, which represent the proportion of the null features that would be included in the analysis at given F-ratio cutoffs. The null probabilities are calculated by dividing the number of null features above a given F-ratio by the total number of features in the null distribution, multiplied by 100 to yield a percentage. Figure 5B shows the resulting null probability curves; the dashed red line represents the 0.1% null probability limit, which is defined as the F-ratio that is exceeded by only 1 in 1000 values in the respective null distribution [22]. Most of the null distributions suggest a null probability limit of an F-ratio of approximately 6 to 10; however, there are curves that lie further to the right, e.g., the right-most null probability curve which has a 0.1% null probability limit with an F-ratio of 44. The suggested 0.1% null probability limits are more easily visualized in histogram form. Figure 5C shows the histogram (black trace) of the 0.1% null probability limits from all 200 null distributions overlaid with the average null distribution (blue) and the distribution of hits from the sample-class comparison from Fig. 3 (red). Figure 5D is a zoomed view of the overlapping distributions from F-ratios in the range of 10 to 100.

The distribution of 0.1% null probability limits provides insight to guide the analyst in selecting a suitable F-ratio threshold for the purpose of focusing on the true positive hits while minimizing analytical effort on hits that end up being false positives. For example, if the F-ratio threshold is set to 13.6, 90% of the 0.1% null probability limits are included. That is, in the

application of a threshold of 13.6, we would expect only a 10% chance of the FDR exceeding 1 in 1000 features (0.1%). At a threshold of 27.6, 99% of the 0.1% null probability limits are included, and we would expect only a 1% chance of the FDR exceeding 0.1%. Here, we chose the threshold by averaging all 200 null distributions and then determining the 0.1% null probability limit; this method suggests a threshold of 12.4 (indicated by the blue arrow in Figure 5C). In applying the threshold of 12.4 to the preliminary sample-class comparison hit list (Fig. 3), we cover 87% of the 0.1% null probability limits, such that there is only a 13% chance that the FDR will exceed 0.1%; thus we expect to encounter approximately 3 false positives above the threshold. At the threshold of 12.4, 107 out of the initial 3362 potential features were found to be class-distinguishing, the significance of which is discussed in the following section.

3.4.3 Acid alteration

Application of F-ratio analysis with combinatorial threshold determination found a total of 107 features that distinguish the altered fuels from the unaltered fuels. For purposes of concisely describing the chemical changes that occur from acid alteration of the diesel fuel, we will focus primarily on the top twenty hits found, which are summarized in an abbreviated hit list in Table 1. The hit list provides the F-ratio and 2D retention times for each discovered feature; additionally, the software determines whether the feature increases or decreases following the acid alteration. Features that were removed by the acid alteration are indicated by a minus sign (–), while features that are generated by the acid alteration are indicated by a plus sign (+). The null probability column indicates the overlap of each hit with the combined null distribution. All of the top twenty hits had an F-ratio exceeding that of the null distribution, and thus had a null probability of 0.00%. Indeed, the top 55 out of 107 hits above the threshold had a null probability

of 0.00%. Using the outputs of the software, analytes were tentatively identified by matching to the NIST11 mass spectral library.

The primary types of class-distinguishing features in the hit list were aromatic species, alkenes/alkynes, and compounds with both aromatic and alkene/alkyne moieties. The majority of discovered features were removed partially or entirely by the acid alteration. Only a small number of features were found to be generated by the acid alteration. The only feature which was generated by the acid alteration with adequate *S/N* and chromatographic resolution to be identified was sulfur dioxide, which was not present prior to acid alteration, but was consistently found following the acid alteration. To demonstrate the variety of chemical functional groups that were changing in response to the acid alteration, Figure 6A plots the top twenty hits as an overlay on a representative TIC chromatogram from the unaltered class; the blue circles are centered on the retention time for the class-distinguishing feature, and are sized according to their relative F-ratios (i.e., larger hits have bigger circles). The blue numbers next to the circles correspond to the hit numbers in Table 1. The presence of multiple hits for sulfur dioxide (Hits 2 and 14) was due to breakthrough during thermal modulation, resulting in double modulation and non-Gaussian column 2 chromatographic profiles for the volatile gas. Though we focus on the top twenty hits found for brevity, there were a total of 107 hits found above the F-ratio threshold of 12.4. Figure 6B shows all 107 hits, demonstrating that further class-distinguishing features show a similar pattern to the first twenty.

Overall, in agreement with literature on electrophilic aromatic sulfonation, the aromatic fractions of the diesel fuels were chemically altered by reaction with sulfuric acid resulting in substantial reduction of these compounds in the acid altered fuels. Compounds such as pyrene and alkyl-substituted pyrenes were removed by the acid alteration, most likely via electrophilic

aromatic sulfonation, and subsequent partitioning to the aqueous acid phase of the reaction mixture [2]. Overall, the relative changes in concentration agree with literature on reactivity of various aromatic species to sulfonation [8]. Literature on aromatic nitration, which also follows an electrophilic aromatic substitution mechanism, further support the relative relativities of the aromatics [41]. Figure 7 summarizes the relative peak sums for a series of aromatic species that were present in the diesel fuel samples, including benzene, naphthalene, phenanthrene, and pyrene. For the discovery of robust markers for the acid alteration of diesel fuel, it is preferable to utilize diverse fuels to comprise the sample classes; here we used fuels from three different sources to sample the variability of fuels. As shown in Figure 7, the amounts of aromatic species present in the diesel fuels prior to acid alteration were variable between samples; this is consistent with literature findings that the aromatic fraction of diesel fuel is the most important for chemometric discrimination of samples [42]. In comparing each fuel to itself prior to and following acid alteration, it is apparent that the degree of removal by the acid alteration for the aromatics is consistent with the expected reactivity. Benzene is less reactive and is removed to a small degree by acid alteration, while pyrene is more reactive and is removed to a much larger extent. Notably, though benzene exhibits a consistent pattern of slightly decreasing signal abundance after acid alteration, the amounts of benzene natively present in the unaltered fuels is relatively variable compared to the amount of benzene removed by the acid alteration. Though the alteration induces meaningful class-to-class differences in the relative amounts of benzene, the within-class variation is substantially larger, leading to a small F-ratio. As a result, benzene is not found as a hit in the analysis. In contrast, pyrene is extensively removed by the acid alteration and has substantial between-class variation, exceeding that of the within-class variation. As a result, pyrene has a substantial F-ratio of 53.7 and is found as Hit 22 in the final

hit list. Naphthalene is intermediate to benzene and pyrene; it is removed to a smaller degree than pyrene, but is relatively consistent prior to alteration, and is found as Hit 82 with an F-ratio of 15.5. We additionally examined other analytes present in the fuel that were expected to not change, such as decane; these analytes were quantified and confirmed to be unaffected by the alteration, and are not shown for brevity.

In addition to finding that aromatics with greater degrees of aromaticity were removed to a greater extent, the hit list revealed other aromatics with alkene and alkyne substituents were also removed by reaction with sulfuric acid. The top hit (Hit 1) was tentatively identified as 1-propynylbenzene; as shown in Figure 8, 1-propynylbenzene has relatively low within-class variation in the unaltered class, and was likely entirely removed by the acid alteration, as there was no detectable peak in the acid altered class. The peak's relatively low within-class variance coupled with its high between-class variance leads to a significant F-ratio of 410, placing it at the top of the hit list. Figure 8 includes similar plots of the next three top analytes, two of which are similar to Hit 1 in that they were detected only in the unaltered class, and in that they had both aromatic and alkene/alkyne moieties. As noted in the abbreviated hit list in Table 1, we also observed the unexpected removal of non-aromatic species from the fuel, particularly, alkenes; a subsequent review of literature suggests that the mechanism may be alkene sulfonation or sulfation [5]. A further interesting and unexpected observation was the presence of sulfur dioxide (SO_2) in the acid altered fuels. Sulfur dioxide was not found in any of the unaltered-fuels, but was founds at relatively high abundances in all of the acid altered fuels, as shown in Figure 8. It is unknown whether the sulfur dioxide was present as a pure compound in the acid altered fuels, as a product of residual sulfuric acid in the altered fuels, or whether it was produced by breakdown of other species during analysis in the hot (275 °C) inlet. Potential sources of sulfur

dioxide include sulfones that may be byproducts of aromatic sulfonation [5], which potentially could remain in the diesel phase. However, more study is needed to confirm this suggestion.

Six fuels were collected from separate fuel stations, with three fuels included in the F-ratio sample-class comparison, while the remaining three fuels were utilized as validation samples in this initial study. To demonstrate that the features discovered by the class-comparison experiment were useful for other acid altered fuels, the signals for the top four features from the analysis, as listed in Table 1, were quantified for all six fuels. Table 2 provides the mean integrated signals, with *N.D.* indicating that the analyte was not measured above the limit of detection. Overall, the class-distinguishing features discovered in the sample-class comparison using samples AR, FH, and MB could also be used to distinguish the acid altered validation samples SG, SS, and RC. The validation samples consistently exhibited the same pattern of hits 1, 3, and 4 being removed by the acid alteration, and hit 2 being created by the acid alteration. Compared to the samples used in the sample-class comparison, the validation samples had smaller signal intensities in the unaltered fuels for 1-propynylbenzene, and larger intensities for sulfur dioxide. For the aromatic species comprising hits 1, 3, and 4, sample SS had substantially lower signal intensities in the unaltered fuels, but was still distinguished from the altered class by the removal of these analytes by the acid alteration. While the results of this study are promising, further validation in future studies is warranted, with a larger set of samples.

The tile-based F-ratio software performed well in finding significant differences between the unaltered and altered classes, even with the variation between fuels within each class. Figure 9 demonstrates a key analytical challenge addressed by the software: many of the class-distinguishing features that were discovered were only present at very limited absolute signal abundance. Figure 9A-B are the TIC chromatograms for the 1D chromatographic region

corresponding to Hit 1 (1-propynylbenzene) and Hit 2 (sulfur dioxide), respectively. The blue traces correspond to the signals from the unaltered fuels, while the red traces correspond to the altered fuels. The black arrows indicate the 2D retention times of the discovered features. Notably, there is no apparent peak at the retention time of Hit 1 in the TIC chromatogram plotted in 9A. However, the *S/N* improvement via the tiling process and utilization of selective *m/z* made it possible to discover the feature, even with its relatively low signal abundance. Figures 9C-D are the extracted ion current (XIC) chromatograms for Hit 1 (*m/z* 116) and Hit 2 (*m/z* 64), respectively. Hit 1 is removed by the acid alteration, while Hit 2 is created by the acid alteration. Figure 9C shows that 1-propynylbenzene is not detected above the baseline in the acid altered samples. Conversely, Figure 9D shows that sulfur dioxide is not detected above the baseline in the unaltered samples. Figure 9D also illustrates that even non-Gaussian peak profiles can be successfully examined; as mentioned above, sulfur dioxide, a gas under standard conditions, is incompletely trapped during thermal modulation, resulting in non-standard peak shapes. These figures demonstrate the effectiveness with which the software finds class-distinguishing features, even for features with low *S/N* or non-Gaussian chromatographic peak profiles.

3.5 Conclusions

Overall, the tile-based F-ratio analysis of the acid altered diesel fuels revealed that the chemical changes induced by reaction with sulfuric acid are subtle yet of potential forensic significance, especially under the non-stoichiometric and short reaction time conditions utilized in this report. Further, the F-ratio analysis utilized three different fuels, each individually acid altered, adding to the challenge since differences between fuels may exceed the differences between classes. However, analytes were discovered that were both sufficiently consistent in the unaltered class, and significantly changed in relative concentration following the acid alteration.

The hypothesis that the relative reactivity of aromatic compounds toward electrophilic aromatic sulfonation was highly supported, as suggested in other literature. Furthermore, removal of alkenes and alkynes in the acid altered fuels was observed, suggesting additional mechanisms of reaction with sulfuric acid which may alter the chemical composition of the fuel. Finally, consistent generation of sulfur dioxide in acid altered fuels was observed. Further investigations are warranted to determine the origin, identities and analytical concentrations of the key species altered by reaction with sulfuric acid, all of which may potentially serve as chemical marker compounds for the forensic determination of diesel alteration.

In addition to the application of previously reported tile-based F-ratio software and methods to the acid alteration of diesel fuel, this report introduced an improved method for null distribution analysis for the determination of defensible thresholds specific to individual sample-class comparison experiments. Through evaluating the comprehensive set of 200 null distributions for a 6 × 6 sample-class comparison, we were able to observe the variability of the null distributions, and thus infer the reliability of a given null probability limit for use as a threshold to avoid (or certainly to minimize) false positives in the hit list. In this study, the combined null distribution suggested a 0.1% null probability threshold of 12.4; at this threshold value, 87% of the null probability limits are included, suggesting that there is only a 13% chance of the FDR exceeding 1 in 1000 for the sample-class comparison. Applying the F-ratio threshold of 12.4 to the acid alteration experiment, we found 107 features that should be class-distinguishing. Since the true positives in the experiment are not known *a priori*, it is not possible to explicitly determine the FDR, though we would expect it to be less than 1:1000 (about 3 false positives in this experiment), based on the combined 0.1% null probability limit of 12.4 having 87% coverage in the comprehensive null combinations. In the top 20 hits studied in

depth, no false positives were encountered. The major advantage of the combinatorial method presented here for F-ratio threshold determination is that it allows for a hit list cutoff to be selected that is statistically suitable for the sample-class comparison being studied. The cutoff is determined by the variability of the data, not by an *a priori* decision of how many hits should be chosen. If the analyst were to arbitrarily choose a number of hits to examine, many class-distinguishing features may be missed or an excessive number of non-hit features would be analyzed [22]. However, future work is underway to further characterize the robustness of the F-ratio cutoff determination in the context of the FDR in a controlled spike experiment in which true positives will be known *a priori* and with which the FDR predicted by null distribution analysis may be experimentally validated.

3.6 References

[1] B. Krakowska, I. Stanimirova, J. Orzel, M. Daszykowski, I. Grabowski, G. Zaleszczyk, et al., Detection of discoloration in diesel fuel based on gas chromatographic fingerprints, Anal. Bioanal. Chem. 407 (2014) 1159–1170. doi:10.1007/s00216-014-8332-4.

[2] C. Martín-Alberca, C. García-Ruiz, O. Delémont, Study of chemical modifications in acidified ignitable liquids analysed by GC–MS, Sci. Justice. 55 (2015) 446–455. doi:10.1016/j.scijus.2015.06.006.

[3] C. Martín-Alberca, C. García-Ruiz, O. Delémont, Study of acidified ignitable liquid residues in fire debris by solid-phase microextraction with gas chromatography and mass spectrometry, J. Sep. Sci. 38 (2015) 3218–3227. doi:10.1002/jssc.201500337.

[4] C. Martín-Alberca, M. López-López, C. García-Ruiz, Analysis of pre-ignited improvised incendiary devices using portable Raman, Talanta. 144 (2015) 612–618. doi:10.1016/j.talanta.2015.06.072.

[5] G.P. Dado, E.A. Knaggs, M.J. Nepras, Sulfonation and Sulfation, in: Kirk-Othmer Encycl. Chem. Technol., John Wiley & Sons, Inc., 2000. http://onlinelibrary.wiley.com/doi/10.1002/0471238961.1921120611140107.a01.pub2/abstract.

[6] H. Cerfontain, H.J.A. Lambrechts, Z.R.H. Schaasberg-Nienhuis, R.G. Coombes, P. Hadjigeorgiou, G.P. Tucker, Aromatic sulphonation. Part 91. The sulphonation of anisole, phenol, phenyl methanesulphonate, potassium phenyl sulphate, and a series of methyl-, bromo-, and chloro-substituted anisoles and phenols in concentrated aqueous sulphuric acid, J. Chem. Soc. Perkin Trans. 2. (1985) 659–667. doi:10.1039/P29850000659.

[7] R.A. Cox, Organic reactions in sulfuric acid. The excess acidity method, Acc. Chem. Res. 20 (1987) 27–31. doi:10.1021/ar00133a004.

[8] A.R. Katritzky, M.S. Kim, D. Fedoseyenko, K. Widyan, M. Siskin, M. Francisco, The sulfonation of aromatic and heteroaromatic polycyclic compounds, Tetrahedron. 65 (2009) 1111–1114. doi:10.1016/j.tet.2008.11.023.
[9] K.M. Pierce, B. Kehimkar, L.C. Marney, J.C. Hoggard, R.E. Synovec, Review of chemometric analysis techniques for comprehensive two dimensional separations data, J. Chromatogr. A. 1255 (2012) 3–11. doi:10.1016/j.chroma.2012.05.050.
[10] K.M. Pierce, J.S. Nadeau, R.E. Synovec, Chapter 17 - Data Analysis Methods, in: C.F. Poole (Ed.), Gas Chromatogr., Elsevier, Amsterdam, 2012: pp. 415–434. http://www.sciencedirect.com/science/article/pii/B9780123855404000171.
[11] S. Yang, J.C. Hoggard, M.E. Lidstrom, R.E. Synovec, Gas Chromatography and Comprehensive Two-Dimensional Gas Chromatography Hyphenated with Mass Spectrometry for Targeted and Nontargeted Metabolomics, in: M. Lämmerhofer, W. Weckwerth (Eds.), Metabolomics Pract., Wiley-VCH Verlag GmbH & Co. KGaA, 2013: pp. 69–92. http://onlinelibrary.wiley.com/doi/10.1002/9783527655861.ch4/summary.
[12] K.M. Pierce, S.P. Schale, Predicting percent composition of blends of biodiesel and conventional diesel using gas chromatography–mass spectrometry, comprehensive two-dimensional gas chromatography–mass spectrometry, and partial least squares analysis, Talanta. 83 (2011) 1254–1259. doi:10.1016/j.talanta.2010.07.084.
[13] R. van der Westhuizen, H. Potgieter, N. Prinsloo, A. de Villiers, P. Sandra, Fractionation by liquid chromatography combined with comprehensive two-dimensional gas chromatography–mass spectrometry for analysis of cyclics in oligomerisation products of Fischer–Tropsch derived light alkenes, J. Chromatogr. A. 1218 (2011) 3173–3179. doi:10.1016/j.chroma.2010.10.009.
[14] J.V. Seeley, S.K. Seeley, Multidimensional Gas Chromatography: Fundamental Advances and New Applications, Anal. Chem. 85 (2013) 557–578. doi:10.1021/ac303195u.
[15] M.K. Jennerwein, M. Eschner, T. Gröger, T. Wilharm, R. Zimmermann, Complete Group-Type Quantification of Petroleum Middle Distillates Based on Comprehensive Two-Dimensional Gas Chromatography Time-of-Flight Mass Spectrometry (GC×GC-TOFMS) and Visual Basic Scripting, Energy Fuels. 28 (2014) 5670–5681. doi:10.1021/ef501247h.
[16] A.L. Lee, K.D. Bartle, A.C. Lewis, A Model of Peak Amplitude Enhancement in Orthogonal Two-Dimensional Gas Chromatography, Anal. Chem. 73 (2001) 1330–1335. doi:10.1021/ac001120s.
[17] P. Marriott, R. Shellie, Principles and applications of comprehensive two-dimensional gas chromatography, TrAC Trends Anal. Chem. 21 (2002) 573–583. doi:10.1016/S0165-9936(02)00814-2.
[18] C. Vendeuvre, F. Bertoncini, L. Duval, J.-L. Duplan, D. Thiébaut, M.-C. Hennion, Comparison of conventional gas chromatography and comprehensive two-dimensional gas chromatography for the detailed analysis of petrochemical samples, J. Chromatogr. A. 1056 (2004) 155–162. doi:10.1016/j.chroma.2004.05.071.
[19] J. Krupčík, P. Májek, R. Gorovenko, J. Blaško, R. Kubinec, P. Sandra, Considerations on the determination of the limit of detection and the limit of quantification in one-dimensional and comprehensive two-dimensional gas chromatography, J. Chromatogr. A. 1396 (2015) 117–130. doi:10.1016/j.chroma.2015.03.084.
[20] A. Sampat, M. Lopatka, M. Sjerps, G. Vivo-Truyols, P. Schoenmakers, A. van Asten, The forensic potential of comprehensive two-dimensional gas chromatography, TrAC Trends Anal. Chem. (n.d.). doi:10.1016/j.trac.2015.10.011.

[21] L.C. Marney, W. Christopher Siegler, B.A. Parsons, J.C. Hoggard, B.W. Wright, R.E. Synovec, Tile-based Fisher-ratio software for improved feature selection analysis of comprehensive two-dimensional gas chromatography–time-of-flight mass spectrometry data, Talanta. 115 (2013) 887–895. doi:10.1016/j.talanta.2013.06.038.
[22] B.A. Parsons, L.C. Marney, W.C. Siegler, J.C. Hoggard, B.W. Wright, R.E. Synovec, Tile-Based Fisher Ratio Analysis of Comprehensive Two-Dimensional Gas Chromatography Time-of-Flight Mass Spectrometry (GC × GC–TOFMS) Data Using a Null Distribution Approach, Anal. Chem. 87 (2015) 3812–3819. doi:10.1021/ac504472s.
[23] K.J. Johnson, R.E. Synovec, Pattern recognition of jet fuels: comprehensive GC×GC with ANOVA-based feature selection and principal component analysis, Chemom. Intell. Lab. Syst. 60 (2002) 225–237. doi:10.1016/S0169-7439(01)00198-8.
[24] R.E. Mohler, K.M. Dombek, J.C. Hoggard, K.M. Pierce, E.T. Young, R.E. Synovec, Comprehensive analysis of yeast metabolite GC×GC–TOFMS data: combining discovery-mode and deconvolution chemometric software, Analyst. 132 (2007) 756–767. doi:10.1039/B700061H.
[25] J.E. Welke, V. Manfroi, M. Zanus, M. Lazzarotto, C. Alcaraz Zini, Differentiation of wines according to grape variety using multivariate analysis of comprehensive two-dimensional gas chromatography with time-of-flight mass spectrometric detection data, Food Chem. 141 (2013) 3897–3905. doi:10.1016/j.foodchem.2013.06.100.
[26] M. Brokl, L. Bishop, C.G. Wright, C. Liu, K. McAdam, J.-F. Focant, Multivariate analysis of mainstream tobacco smoke particulate phase by headspace solid-phase micro extraction coupled with comprehensive two-dimensional gas chromatography–time-of-flight mass spectrometry, J. Chromatogr. A. 1370 (2014) 216–229. doi:10.1016/j.chroma.2014.10.057.
[27] P.-H. Stefanuto, K.A. Perrault, R.M. Lloyd, B. Stuart, T. Rai, S.L. Forbes, et al., Exploring new dimensions in cadaveric decomposition odour analysis, Anal. Methods. 7 (2015) 2287–2294. doi:10.1039/C5AY00371G.
[28] P.-H. Stefanuto, K.A. Perrault, S. Stadler, R. Pesesse, H.N. LeBlanc, S.L. Forbes, et al., GC × GC–TOFMS and supervised multivariate approaches to study human cadaveric decomposition olfactive signatures, Anal. Bioanal. Chem. 407 (2015) 4767–4778. doi:10.1007/s00216-015-8683-5.
[29] H.P. Bailey, S.C. Rutan, Comparison of chemometric methods for the screening of comprehensive two-dimensional liquid chromatographic analysis of wine, Anal. Chim. Acta. 770 (2013) 18–28. doi:10.1016/j.aca.2013.01.062.
[30] D.J. Vis, J.A. Westerhuis, A.K. Smilde, J. van der Greef, Statistical validation of megavariate effects in ASCA, BMC Bioinformatics. 8 (2007) 322. doi:10.1186/1471-2105-8-322.
[31] Y. Benjamini, Y. Hochberg, Controlling the False Discovery Rate: A Practical and Powerful Approach to Multiple Testing, J. R. Stat. Soc. Ser. B Methodol. 57 (1995) 289–300. doi:10.2307/2346101.
[32] Y. Benjamini, D. Yekutieli, The Control of the False Discovery Rate in Multiple Testing under Dependency, Ann. Stat. 29 (2001) 1165–1188. doi:10.2307/2674075.
[33] B. Efron, R. Tibshirani, Empirical bayes methods and false discovery rates for microarrays, Genet. Epidemiol. 23 (2002) 70–86. doi:10.1002/gepi.1124.
[34] B. Efron, Bayesians, Frequentists, and Scientists, J. Am. Stat. Assoc. 100 (2005) 1–5. doi:10.1198/016214505000000033.

[35] S. Woo, J.T. Leek, J.D. Storey, A computationally efficient modular optimal discovery procedure, Bioinformatics. 27 (2011) 509–515. doi:10.1093/bioinformatics/btq701.
[36] H.J. RYSER, Combinatorial Mathematics, 1st ed., Mathematical Association of America, 1963. http://www.jstor.org/stable/10.4169/j.ctt5hh8v6 (accessed October 5, 2015).
[37] J.C. Hoggard, peg2mat3p8; http://depts.washington.edu/synlab/software/, (2011).
[38] G. Vivó-Truyols, H.-G. Janssen, Probability of failure of the watershed algorithm for peak detection in comprehensive two-dimensional chromatography, J. Chromatogr. A. 1217 (2010) 1375–1385. doi:10.1016/j.chroma.2009.12.063.
[39] S. Samanipour, P. Dimitriou-Christidis, J. Gros, A. Grange, J. Samuel Arey, Analyte quantification with comprehensive two-dimensional gas chromatography: Assessment of methods for baseline correction, peak delineation, and matrix effect elimination for real samples, J. Chromatogr. A. 1375 (2015) 123–139. doi:10.1016/j.chroma.2014.11.049.
[40] H.D. Bean, J.E. Hill, J.-M.D. Dimandja, Improving the quality of biomarker candidates in untargeted metabolomics via peak table-based alignment of comprehensive two-dimensional gas chromatography–mass spectrometry data, J. Chromatogr. A. 1394 (2015) 111–117. doi:10.1016/j.chroma.2015.03.001.
[41] W.A. Pryor, G.J. Gleicher, J.P. Cosgrove, D.F. Church, Reaction of polycyclic aromatic hydrocarbons (PAH) with nitrogen dioxide in solution. Support for an electron-transfer mechanism of aromatic nitration based on correlations using simple molecular orbital theory, J. Org. Chem. 49 (1984) 5189–5194. doi:10.1021/jo00200a035.
[42] A.M. Hupp, L.J. Marshall, D.I. Campbell, R.W. Smith, V.L. McGuffin, Chemometric analysis of diesel fuel for forensic and environmental applications, Anal. Chim. Acta. 606 (2008) 159–171. doi:10.1016/j.aca.2007.11.007.

3.7 Tables

Table 3-1 The top twenty hits from the tile-based F-ratio analysis of the acid alteration experiment. There were a total of 3362 analyte peak features, 107 of which were above the 0.1% null probability limit. 55 hits were found with 0.00% null probability. A 0.00% null probability implies the given hit has an F-ratio that exceeds the largest F-ratio found in all of the 200 null probability distributions. The class change metric indicates whether the analyte is decreasing as a result of acid alteration (-) or increasing as a result of acid alteration (+). The analytes were identified based on 2D retention times and matching to the NIST11 mass spectral library.

Hit no.	Avg F-ratio	Class Change	Null Prob	^1t_R (s)	^2t_R (s)	Preliminary ID
1	410.4	-	0.00%	733	0.61	1-propynylbenzene
2	153.2	+	0.00%	60	0.10	sulfur dioxide
3	122.4	-	0.00%	1115	0.56	1,1-dimethyl-1H-indene
4	122.4	-	0.00%	933	0.66	1-methyl-1H-indene
5	94.6	-	0.00%	638	0.54	2-propenylbenzene
6	93.5	-	0.00%	1132	0.59	1,2-dimethyl-1H-indene
7	92.1	-	0.00%	2427	0.95	2-methylpyrene
8	86.6	-	0.00%	2402	0.98	1-methylpyrene
9	83.6	-	0.00%	2549	0.93	1,3-dimethylpyrene
10	81.1	-	0.00%	1132	0.49	1,3-dimethyl-1H-indene
11	79.8	-	0.00%	671	0.14	1-decene
12	77.5	-	0.00%	1474	0.67	acenaphthene
13	75.3	-	0.00%	475	0.10	cis-2-nonene
14	74.0	+	0.00%	60	0.61	sulfur dioxide
15	73.4	-	0.00%	644	0.55	(Z)-1-propenylbenzene
16	73.1	-	0.00%	1782	0.61	4,4'-dimethylbiphenyl
17	65.2	-	0.00%	1104	0.51	1,3-dimethyl-1H-indene
18	61.7	-	0.00%	845	0.17	5-methyl-1-decene
19	61.6	-	0.00%	589	0.41	1,2,3-trimethylbenzene
20	60.8	-	0.00%	2434	0.96	3-methylpyrene

Table 3-2. The mean integrated signals for the top four analytes from the F-ratio analysis, for each of the six fuels that were analyzed, for both the unaltered (U) and altered (A) classes. *N.D.* indicates that the analyte was not detected. Samples AR, FH, and MB were analyzed to discover class-distinguishing analytes. Samples SG, SS, and RC were independent samples that serve to validate the findings of the F-ratio analysis.

Sample	Class	1-propynylbenzene (Hit 1)	Sulfur dioxide (Hit 2)	1,1-dimethyl-1H-indene (Hit 3)	1-methyl-1H-indene (Hit 4)
AR	U	1700	*N.D.*	2110	2180
	A	*N.D.*	47600	*N.D.*	*N.D.*
FH	U	1850	*N.D.*	2220	2230
	A	*N.D.*	37300	*N.D.*	*N.D.*
MB	U	1740	*N.D.*	2220	2380
	A	*N.D.*	19500	*N.D.*	*N.D.*
SG	U	700	*N.D.*	2410	2090
	A	*N.D.*	171000	*N.D.*	*N.D.*
SS	U	410	*N.D.*	1290	1110
	A	*N.D.*	90900	*N.D.*	*N.D.*
RC	U	840	N.D.	2430	2440
	A	*N.D.*	152000	*N.D.*	*N.D.*

3.8 Figures

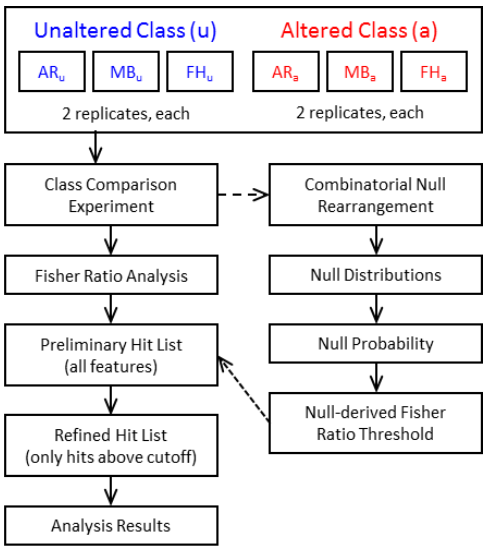

Figure 3-1. Flowchart of the experimental design with three fuels: AR, MB, FH.

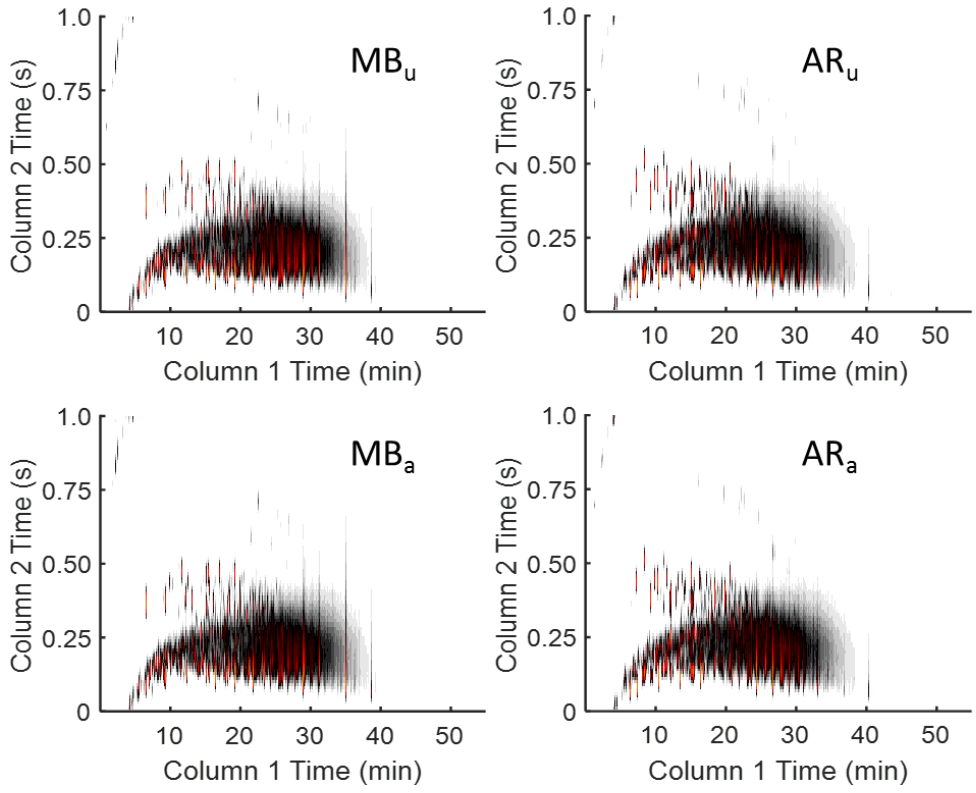

Figure 3-2. Example total ion count (TIC) chromatograms for representative chromatograms from two unaltered fuels (MB_u and AR_u) and those same fuels after acid alteration (MB_a and AR_a). Visible differences in the TIC chromatograms are more obvious between fuel samples than between their unaltered and altered states.

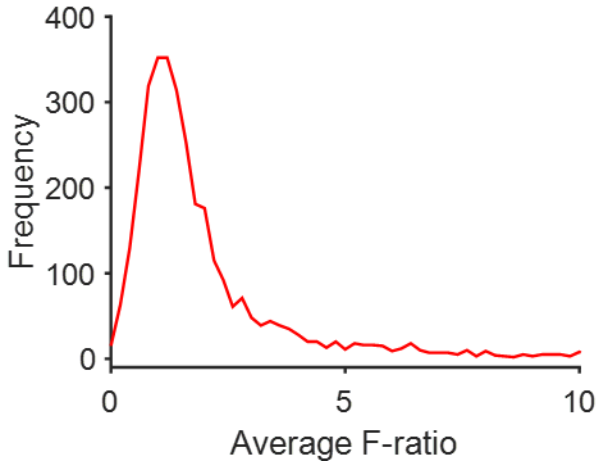

Figure 3-3. The distribution of average F-ratios for the features in the preliminary hit list for the sample-class comparison of unaltered and acid altered fuels. The distribution is approximately centered on an F-ratio of 1 to 2. The inset plot is the histogram of the tail from 10 to 100, which shows the features which are most likely to be class-distinguishing. There were four features with average F-ratios greater than 100 which are not shown in the inset for clarity.

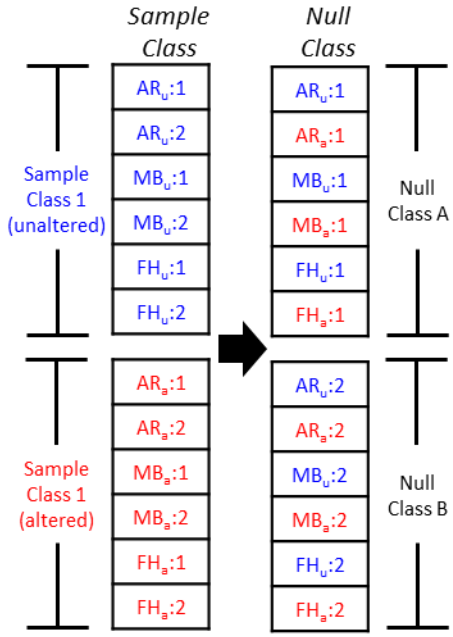

Figure 3-4. Illustration of combinatorial rearrangement for 1 of the 200 unique null combinations. The original unaltered class (Sample Class 1) and original altered class (Sample Class 2) are rearranged to create a null distribution from the analysis of the null classes (Null Class A and Null Class B). In this null arrangement, the first injection replicates of all samples are compared against the second injection replicates, for example, AR_u:1 is the first injection replicate for unaltered AR fuel, and AR_u:2 is the second injection replicate. This rearrangement mitigates the between-class variance that was present in the original sample-class comparison, such that the null hypothesis may instead be tested.

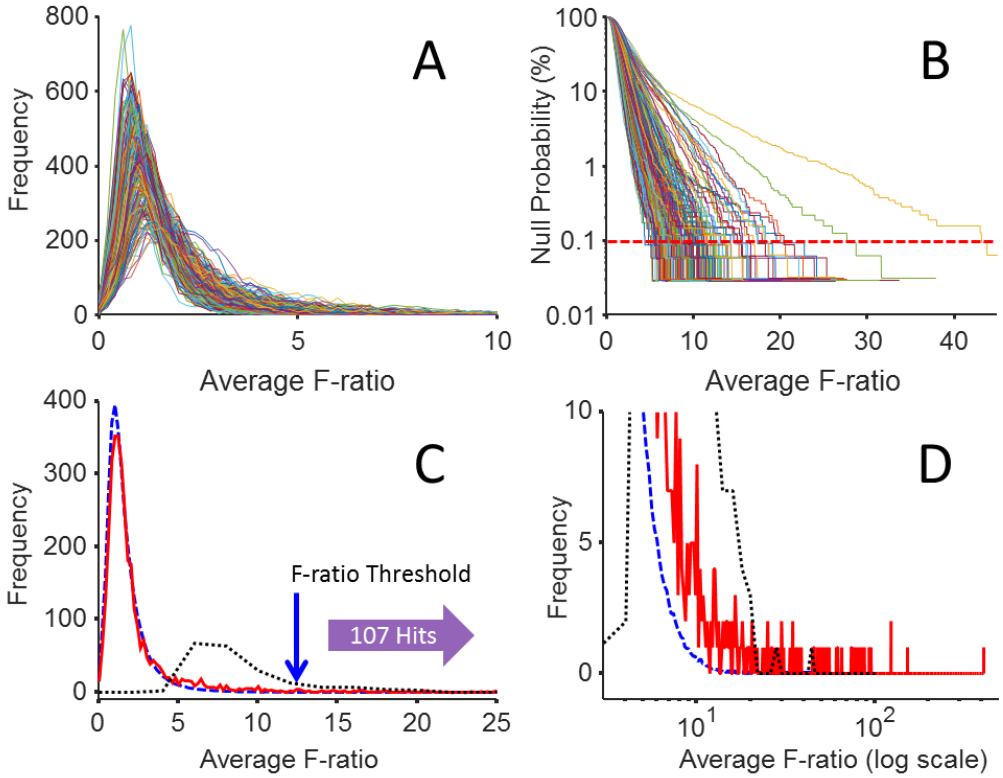

Figure 3-5. (A) The comprehensive null distributions (200 total) for the 6 × 6 sample-class comparison of unaltered and altered diesel fuel. Most null F-ratio values were less than 10, with most distributions centered around 1 to 2. (B) All null probability curves; the dashed red line corresponds to a 0.1% null probability limit. (C) The combined null distribution (blue, long-dashed line), sample-class comparison distribution (red, solid line), from Fig. 3 for comparison, and distribution of 0.1% null probability limits (black, short-dashed line). The 0.1% null probability limit from the combined null distribution is 12.4, and is indicated by the arrow. (D) The tail of the distribution in (C), which shows the relative abundance of higher F-ratio features in the sample-class comparison.

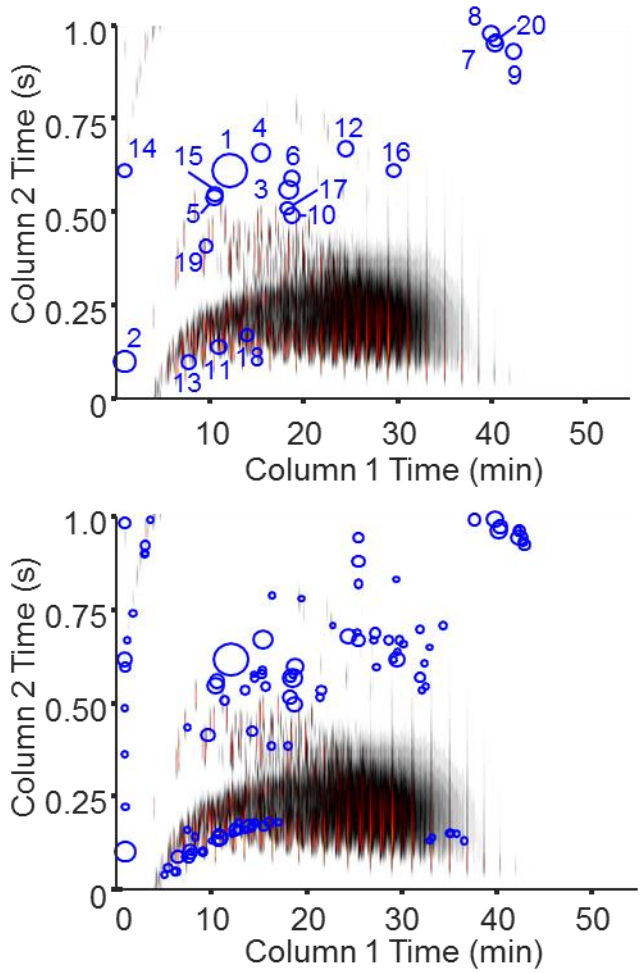

Figure 3-6. (Top) The top twenty hits from the tile-based F-ratio analysis of the acid alteration experiment overlaid on a representative 2D TIC chromatogram from the unaltered fuel class. The blue circles are centered on each hit, and the size of the circle corresponds to the average F-ratio for the hit. The hit numbers for each feature correspond to those in Table 1. (Bottom) The top 107 hits (i.e., all hits above the 0.1% null probability limit of 12.4) from the tile-based F-ratio analysis of the acid alteration experiment.

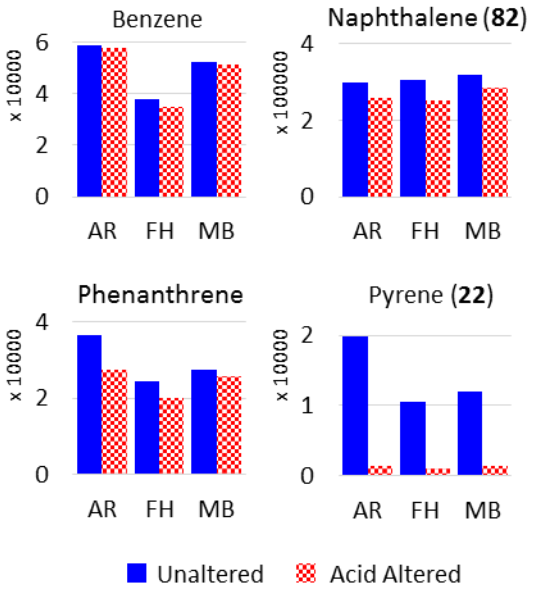

Figure 3-7. The quantified peak sums for unique *m/z* for selected species in the diesel fuel samples. The solid blue bars correspond to the average peak sum of the two injection replicates for the fuel prior to acid alteration, while the patterned red bars represent the peak sum after acid alteration. The numbers in parentheses in the analyte names are the hit numbers if they were found by the tile-based F-ratio analysis.

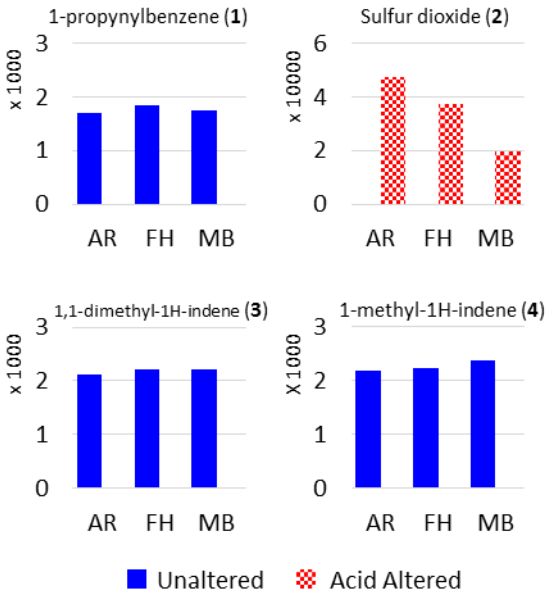

Figure 3-8. The quantified peak sums for unique ions for the first four hits from the F-ratio analysis of the diesel fuel samples. The solid blue bars correspond to the average peak sum of the two injection replicates for the fuel prior to acid alteration, while the patterned red bars represent the peak sum after acid alteration. Missing bars indicate that the analytes was not detected in that sample. The numbers in parentheses in the analyte names are the hit numbers from the tile-based F-ratio analysis.

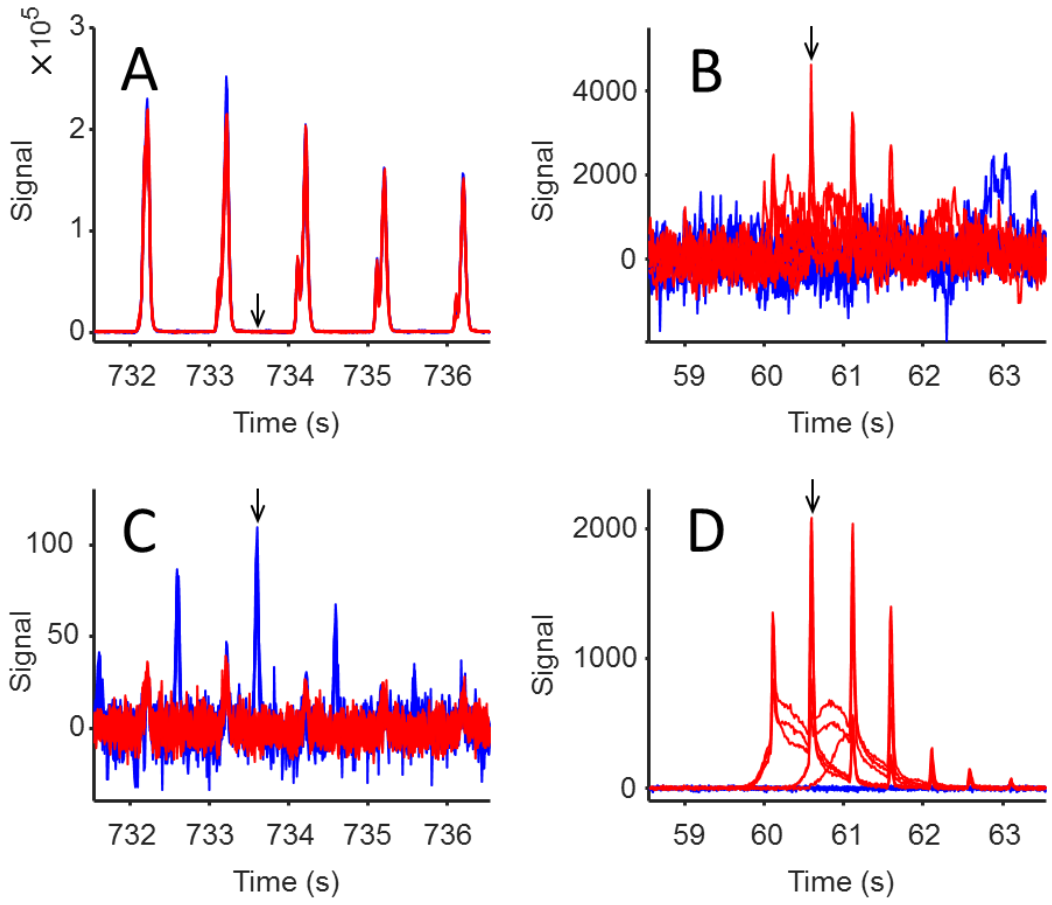

Figure 3-9. The top two hits (Hits 1 and 2, tentatively identified as 1-propynylbenzene and sulfur dioxide, respectively) from the tile-based F-ratio analysis of the acid alteration experiment. Blue lines correspond to the unaltered fuel samples while the red lines correspond to the acid altered fuels. (A-B) The total ion current (TIC) chromatograms for the 1D chromatographic regions centered on the analyte features for hits 1 and 2, respectively. (C-D) The extracted ion current (XIC) chromatograms for selective mass channels for the 1D regions for hits 1 (*m/z* 116) and 2 (*m/z* 64), respectively. Arrows indicate the 2D peak apices as identified by the pinning and clustering step of the software. Quantitative information for the peaks is provided in Figure 8.

Chapter 4: Implications of Phase Ratio (β) for Maximizing Peak Capacity in Comprehensive Two-Dimensional Gas Chromatography Time-of-Flight Mass Spectrometry

4.1 Introduction

Comprehensive two-dimensional (2D) gas chromatography coupled with time-of-flight mass spectrometry (GC×GC–TOFMS) is a powerful instrumental platform for the qualitative and quantitative analysis of complex samples, especially those which are otherwise challenging to analyze by conventional one-dimensional gas chromatography (GC). By providing additional separation efficiency with similar run times to that of one-dimensional gas chromatography (1D-GC), GC×GC improves the capability of the instrument for resolving critical peaks in complex samples. The benefits of GC×GC for complex samples has been highlighted in recent applications, including fuel forensics [1], environmental samples [2,3], and metabolomics [4], as well as more broadly in recent reviews of GC×GC applications [5–7]. An important figure-of-merit for chromatographic separations is peak capacity, n_c, which is generally defined as the time of the separation window divided by the average peak width at base (4σ width) [8]. Broadly, n_c describes the number of peaks that will fit into a given separation at a chromatographic resolution, R_s, of 1. Overall, n_c provides a performance-oriented metric to allow for comparisons of chromatographic systems, and allow for approximation of predicted chromatographic resolution of analytes, for example, through statistical overlap theory [9–11].

As a rule, chromatographic systems aim to maximize n_c, or to maintain adequate n_c while reducing separation run time. Compared to 1D-GC, GC×GC should in principle provide approximately an order of magnitude increase in n_c with comparable run times, provided the instrument parameters are carefully selected [3]. For the analysis of complex samples, such as

with metabolomics, environmental chemistry, petroleum products, and chemical forensics, the two-dimensional peak capacity ($n_{c,2D}$) attainable by GC×GC provides an advantage in successful classification of samples, followed by the identification and quantification of the analytes that comprise them. Recent work has focused on improving n_c by means of both theoretical modeling [3,12,13] and instrumental improvements, both in terms of introducing new instrument technologies [14,15] and by optimizing instrument parameters [3]. There are many factors to be considered in the selection of parameters for GC×GC [16]. Recently, it has been recognized that high $n_{c,2D}$ separations may be achieved through careful selection of the dimensions of the primary and secondary capillary columns [3,14,15,17]. Column dimensions have also been considered recently for control of the pressures and flows of the primary and secondary columns in the context of $n_{c,2D}$ [18,19].

While capillary dimensions and associated carrier gas flows have been closely studied in the context of impacting $n_{c,2D}$, another critical parameter for chromatographic columns, phase ratio (β), has received comparatively little attention in GC×GC method development. Phase ratio (β), for a wall-coated open tubular (WCOT) capillary column, is the ratio of the volume of mobile phase (V_m) to volume of stationary phase (V_s), and is calculated as $\beta = d_c/4d_f$, where d_c is the inside diameter (i.d.) of the capillary and d_f is the thickness of the stationary phase film. Phase ratio relates an analyte's retention factor (k, also referred to in some literature as k') to its distribution constant (K_D) as $k = K_D/\beta$. Phase ratio is an important term for the practice of gas chromatography, as it allows for manipulation of k through selection of column film thickness relative to the diameter of the capillary. In practice, β allows for method considerations such as phase ratio focusing [20] and control of elution temperatures [21], while holding the chemical selectivity of the stationary phase constant. Further, by influencing k, in certain situations β may

influence R_s [22]. Notably, compared to parameters such as column length or oven temperature, the variety of β available in method development is much more limited, particularly if the chromatographer is limited to commercially available columns. Arguably, the most common β is 250; an example of which for the primary column of GC×GC is a column of 250 μm inner diameter (i.d.) with a 0.25 μm film thickness. Columns are generally available with smaller β (having a relatively thicker film) for volatiles applications, where phase ratio focusing helps to provide narrow peaks even at ambient or near-ambient GC oven temperatures [20]. Columns with larger β (having a relatively thin film) are also available for applications having higher molecular weight analytes, such as in polyaromatic hydrocarbon (PAH) analyses, in which the larger β is necessary to elute very high boiling point analytes within the temperature limits of the column and/or the instrument [21].

Herein, we examine the relationship of β between the first and second separation dimensions of GC×GC separations, and the implications of β on realization of maximal $n_{c,2D}$. In this study, the modulation period, P_M, and the phase ratios of the two analytical columns were the conditions that were changed to assess cause and effect. All other chromatographic conditions were held constant. Aside from application-specific columns, commercially-available columns are relatively limited in choice of β for a given column dimension and stationary phase composition. We utilized two column types: 250 μm i.d. primary columns with -5MS (diphenyl dimethyl polysiloxane) films and 180 μm i.d. secondary columns with -200 (trifluoropropylmethyl polysiloxane) films. From the selected vendor for the chosen column dimensions, -5MS columns are available in 0.1, 0.25, 0.5, and 1.0 μm film thicknesses (with β of 625, 250, 125, and 62.5, respectively), while the -200 columns are limited to 0.2 and 0.4 μm films (with β of 225 and 112.5, respectively). Taking into account the limited β commercially

available, this report aims to examine the implications of a series of six GC×GC configurations chosen from the aforementioned columns. Whereas many GC×GC methods utilize primary and secondary columns both having β of 250, we have historically used an alternative configuration with a primary column having β of 125 and secondary column having β of 225, as well as other configurations utilizing a primary column with smaller β than that of the secondary column.

Here we study the effects of β in GC×GC using a complex sample test mixture comprised of 115 analytes of various molecular masses and functional groups, while adjusting only the modulation period as required by the degree of analyte retention on the secondary column in order to assess and maximize the use of the 2D separation space. Other instrument parameters such as the carrier gas flow rate, oven temperature program, and inlet and detector settings were held constant. To compare the relative performance of the six GC×GC configurations, we will focus on the effects of β on n_c for both the primary and secondary columns, and subsequently the two-dimensional peak capacity ($n_{c,2D}$) that was realized for each configuration.

4.2 Theory

The fundamental chromatographic theory relating β, particularly in the context of film thickness (d_f), to other chromatographic parameters is well represented in the literature [13,22,23]. Briefly, β is a critical chromatographic parameter as it relates the distribution constant (K_D) to the retention factor (k) according to

$$k = \frac{K_D}{\beta} \qquad (1)$$

where k may be determined from the retention time (t_R) and dead time (t_0) as

$$k = \frac{t_R - t_0}{t_0} \qquad (2)$$

and β may be calculated for a WCOT column from the column inner diameter (d_c) and film thickness (d_f) as

$$\beta = \frac{d_c}{4 \cdot d_f} \qquad (3)$$

Modifications to β, considering the impact to k while holding other chromatographic parameters constant, will affect the secondary column peak width (${}^2w_b$) according to the approximation [13,24,25]

$${}^2w_{\mathrm{b}} \approx {}^2w_{\mathrm{b,k}} + {}^2w_{\mathrm{b,0}} = 4 \cdot {}^2k \left(\frac{11 d_c^2 f \cdot {}^2t_0}{96 D_{g,0} j} \right)^{1/2} + {}^2w_{\mathrm{b,0}} \qquad (4)$$

where ${}^2w_{\mathrm{b,k}}$ is the ${}^2k$ dependent width for ${}^2k > 0$ due to on-column band broadening, and ${}^2\mathrm{w}_{\mathrm{b,0}}$ is the minimum peak width of the analyte, at ${}^2k = 0$, primarily due to modulator-dominated "extra-column" band broadening.

The effects of changes in ${}^2w_b$ from changes in β are principally of concern for their impact to peak capacity (n_c), which considers the number of peaks that can fit into a given separation at a defined resolution. Peak capacity may be defined for separation having constant peak widths as

$$n_c = \frac{\Delta t_R}{w_b} \qquad (5)$$

where Δt_R is the difference in retention time between the first and last eluting peak. For isothermal separations, or pseudo-isothermal separations such as those involving the secondary column in GC×GC, w_b is not constant and in fact increases with k according to equation 2. The variable w_b with k requires that the 2nc be determined iteratively, as described in the experimental section. For the purpose of describing the overall performance of a GC×GC system, especially relative to that of another GC×GC system, two-dimensional peak capacity

($n_{c,2D}$) is a useful metric. The Giddings definition of 2D peak capacity multiplies the peak capacity of each dimension at unit resolution [8] as

$$n_{c,2D} = {}^{1}n_c \times {}^{2}n_c \quad (6)$$

Several authors have discussed improvements to equation 6 to account for considerations of statistical overlap theory and/or the geometry inherent to multidimensional separations [11,15,26]. These considerations are highly useful for comparisons of GC×GC to 1D-GC, or for comparisons of substantially-different GC×GC systems; however, for the purpose of understanding the impact of β in terms of $n_{c,2D}$ equation 6 is sufficient.

4.3 Experimental

4.3.1 GC×GC Column Sets

Capillary GC columns were obtained from Restek (Bellefonte, PA). A total of five columns were used, three primary columns (column 1) and two secondary columns (column 2). The primary columns were 20.0 m long × 250 µm internal diameter and were 0.25 µm (Rtx®-5MS), 0.5 µm (Rtx®-5MS), and 1.0 µm (Rtx®-5) films; both Rtx®-5 and Rtx®-5MS films are Crossbond® diphenyl dimethyl polysiloxane. The secondary columns were 2.0 m long × 180 µm and were 0.2 µm and 0.4 µm Rtx®-200 films, which are Crossbond® trifluoropropylmethyl polysiloxane. The five columns were combined to make six unique column combinations, summarized in Table 1. In addition to the aforementioned columns, three additional columns were cut for isothermal data collection: a 10.0 m × 250 µm × 0.25 µm Rtx®-5MS, a 10.0 m × 180 µm × 0.2 µm Rtx®-200, and a 10.0 m × 180 µm × 0.5 µm Rtx®-200.

4.3.2 GC×GC–TOFMS Data Collection and Analysis

The six column sets were installed into a Pegasus 4D system (LECO, St. Joseph, MI), consisting an Agilent 6890N gas chromatograph with 7683 autosampler (Agilent Technologies, Palo Alto, CA) coupled to a Pegasus III time-of-flight mass spectrometer (TOFMS) with a quad-jet thermal modulator and secondary oven. For the purposes of avoiding variation in the column 2 length and installation between column sets, all column sets using the 0.2 µm film primary column were run together, changing only the primary columns between runs. After the data collection for the first 3 column sets was completed, the TOFMS was vented and the 0.2 µm film secondary column exchanged for the 0.4 µm film. The acquisitions for the column sets using the 0.4 µm film secondary column were then completed, changing only the primary column between column sets. The secondary column installation was carefully performed to ensure that the column lengths were consistent between the 0.2 µm and 0.4 µm film columns.

The instrumental parameters were set based on prior published work by our group, to place the findings of this work in context of previous results. The GC inlet was set to 275 °C and the transfer line was set to 285 °C. The primary oven was held at 40 °C for 1 min and then increased at 5 °C/min to end of the temperature program (see Table 2), where it was held for 1 min, for a total run time of 47-52 min. The secondary oven and modulator block followed the same temperature program as the primary oven, with +5 °C and +40 °C offsets, respectively. The modulation period and hot and cold pulse times are provided in Table 2. The GC instrument was set to maintain a constant (ambient temperature and pressure corrected) flow rate of 2 ml/min at the outlet of the secondary column, with helium (Praxair, Grade 5.0) as the carrier gas. The ion source was set to 225 °C, the electron impact energy was 70 eV, and the detector voltage was set to 1690 V. Mass channels, *m/z* 33-300, were collected at 500 spectra/s after a 10 s acquisition

delay. A 0.1 µl injection was made with a 0.5 µl autosampler syringe (Hamilton, Reno, NV) of the neat 115 component mixture was made in split mode with a split ratio of 200:1. For each column set, the sample was injected in quadruplicate.

Data from the GC×GC–TOFMS data collection with the six column sets were principally analyzed using ChromaTOF v3.32 (LECO, St. Joseph, MI). Peak processing methods were built to find 2D peaks in the chromatograms, and subject them to deconvolution, peaklet assignment, and mass spectral library matching, along with measurement of primary column retention time (^1t_R), secondary retention time (^2t_R), and secondary column width at half height ($^2w_{1/2}$). The peak assignments were manually inspected and corrected, as needed. The peak tables were then further processed in Microsoft Excel 2013 to correct ^2t_R for wrap-around, as well as to calculate secondary column width at base (^2w_b) and retention factor (^2k). The secondary column dead time ($^2t_0$) was calculated for each column set using the ChromaTOF flow calculator, and was estimated to be 1.00 s at a primary oven temperature of 150 °C. A total of 70 peaks were selected for in-depth analysis and were measured for each of the six column combinations. GC×GC–TOFMS data were also imported into MATLAB 2015b (The MathWorks, Natick, MA) using an in-house data converter, peg2mat3p8 [27], for the purposes of plotting and to measure primary column width at base (^1w_b).

4.3.3 GC×GC–TOFMS Column 1 Peak Capacity Determination

^1w_b was measured for each analyte based on a method described by Adcock *et al.* and Siegler *et al.* [28,29], which utilizes curve fitting to a Gaussian profile to determine the parameters of the primary column peak profile represented by the profile of the peaklets in the unfolded chromatographic data. While the method described by Adcock *et al.* [28] was developed for accurate measurement of ^1t_R, our approach here was to accurately measure ^1w_b. It

is important to note that the peak widths measured here have been broadened by modulation, as described theoretically and experimentally by several authors [14,15,29–31], and do not require additional correction for peak width, such as the undersampling correction factor [31]. Note that the peak widths measured in this manner take into account only the effective width of the peak, and do not account for concepts of statistical overlap [31] that may reduce the calculated theoretical peak capacities in practice. Briefly, Curve Fitting Toolbox (The MathWorks, Natick, MA) was used to fit Gaussian profiles to each of the secondary column peaks, herein referred to as peaklets, belonging to the 2D peak. The amplitude (*a*) and position (*b*) terms of the equation for each peaklet were then used to fit a primary column peak profile to modulated peaklets. The standard deviation (*c*) term from this second fitting step was then used to calculate ${}^{1}w_b$.

The technique described above was applied to tetradecane using *m/z* 57, which was free of interferences from neighboring peaks, and which eluted near the middle of the primary column separation. To determine the peak capacity on the primary column (${}^{1}n_c$), the observed separation window was calculated by subtracting the retention time of the first eluting analyte (2-propanol) from that of the last eluting analyte (1-eicosanol) in the 115 component mixture. For each column set, the separation window was divided by the ${}^{1}w_b$ for tetradecane, according to equation 5 which is derived for ${}^{1}R_s$ of 1 and which assumes constant ${}^{1}w_b$ throughout the primary column separation. This method allows for reasonable comparison of ${}^{1}n_c$ between column sets.

4.3.4 GC×GC–TOFMS Column 2 Peak Capacity Determination

The determination of the secondary column peak capacity (${}^{2}n_c$) is somewhat more complicated than that of ${}^{1}n_c$, as the pseudo-isothermal nature of the secondary column separation precludes the assumption that the peak width is constant, such that we cannot use the average peak width on the secondary column. Instead, it is necessary to iteratively model the secondary

column separation, as previously reported [13,25], using a function describing the dependence of ${}^2w_b$ on ${}^2k$, as determined by the linear best fit equation obtained from the measurements of ${}^2k$ and ${}^2w_b$ for the 70 analytes that were included in the study, as described in Section 4.3.2. Briefly, an equation can be described for the retention times and widths of a series of Gaussian peaks at ${}^2R_s$ of 1. By setting the retention time of the first peak commensurate with that observed in the data, and allowing for partial wrap around such that the measured ${}^2t_R$ of the most retained peak does not overlap with that of the measured ${}^2t_R$ of the least retained peak, the number of peaks that fit in the separation window may be determined.

4.3.5 GC–FID Data Collection and Analysis

The 20.0 m × 250 µm × 0.5 µm Rtx®-5MS and 20.0 m × 250 µm × 1.0 µm Rtx®-5 primary columns, and the three additional 10.0 m columns described in 3.1, were individually installed into an Agilent 6890N gas chromatograph with a 7683 autosampler (Agilent Technologies, Palo Alto, CA), equipped with a flame ionization detector (FID). Eleven selected analytes from the 115 component mixture were each diluted to 1 ppth (w/w) in hexane and injected. The GC inlet was set to 250 °C and the split ratio was set to 200:1 with a column flow of 2.5 ml/min of hydrogen. The oven was held isothermal at the desired temperature until the given analyte eluted. A 5 µl autosampler syringe (Hamilton, Reno, NV) was used to inject 1 µl of sample for the 250 µm i.d. columns and 0.1 µl for the 180 µm i.d. columns. Column dead times (t_0) were determined at each oven temperature by an injection of 1 µl of methane. Syringe rinses using acetone (2 rinses) and hexane (1 rinse) were performed after each analyte injection to prevent carry-over between analytes. The FID was operated at a temperature of 250 °C, with flows of 40.0 ml/min hydrogen, 450.0 ml/min air, and 45.0 ml/min nitrogen makeup gas. The detector reported data to the instrument at 200 Hz.

Data from the isothermal injections for the eleven selected analytes and methane, at temperatures incremented by 10 °C, were exported as a .csv from MSD Chemstation D.03.00.611. (Agilent Technologies, Palo Alto, CA). Because Chemstation records time only to the nearest 0.001 minute (0.06 s), it was necessary to write in-house software in MATLAB 2015b to find analyte peak apices in the raw data and calculate accurate retention times to the nearest 0.005 s. *k* was calculated for each analyte using the retention time of methane at the given column/temperature combination to determine the column dead time (t_0). Run temperatures were converted to Kelvin and used to generate van 't Hoff plots, which plot the natural log of *k* versus inverse Kelvin to determine thermodynamic parameters for the analyte. Linear best fits were applied to each analyte's van 't Hoff curve to allow for interpolation of *k* at the secondary column elution temperature (^2T_e) for that analyte from each GC×GC column set.

4.4 Results and Discussion

4.4.1 Primary Column Phase Ratio and Retention on the Secondary Column

The initial motivation for this study was to understand the effect of GC×GC parameters on ^2t_R. Surveying the literature, we found that the chromatograms collected by our group tended to have reduced ranges of ^2t_R compared to those published by other authors in the field. Initially, we speculated that the differences were likely due to the range of functional groups in samples that were being analyzed, the stationary phases being applied, or the column dimensions chosen. Though these considerations are likely influence ^2t_R, we discovered another parameter that, for GC×GC, has received scant attention: phase ratio (β). β is defined as the ratio of the volume of mobile phase to that of the stationary phase; in a wall coated open tubular capillary column, this is defined as equation 3. Overall, larger numbers of β indicate relatively larger volumes of mobile phase to stationary phase; when holding the inner diameter of the column constant, larger

β corresponds to thinner stationary phase films. As shown in equation 1, β is an important term in the calculation of k along with the thermodynamic terms.

In a temperature programmed separation, the general rule of thumb is that for every factor of two change in β, the elution temperature changes by approximately 10 ˚C. For example, suppose a given analyte elutes in a temperature programmed separation at 100 ˚C on a column with a β of 250. Holding all other parameters constant, if a thicker film column with a β of 125 were substituted, we would expect the elution temperature to increase to approximately 110 ˚C. In 1D GC, the change in elution temperature with β has little impact; however, in GC×GC the effect of β on the temperature-programmed primary column separation has a much greater significance. The critical consideration is that in GC×GC, the temperatures of the primary and secondary columns are closely linked by the temperature programming of the oven. If the secondary column separation is pseudo-isothermal, as discussed in detail in Section 4.4.3, the elution temperature (T_e) of an analyte from the primary column determines the temperature of that analyte's separation on the secondary column. Table 3 includes the calculated ${}^1T_e$ for a series of 11 analytes (as described in Section 4.4.3) that span the 2D chromatograms for each ${}^1\beta$ studied in this work. As expected, decreasing ${}^1\beta$ by increasing the primary column film thickness significantly increases the ${}^1T_e$.

Since changes in ${}^1\beta$ alter ${}^1T_e$, the choice of ${}^1\beta$ may substantially impact the temperature of the secondary column separation for each analyte, and thus alter ${}^2k$. This effect is particularly significant for GC×GC instruments in which the secondary column temperature is equal to that of the primary column, in which the temperature of the secondary column cannot be controlled independently of the primary column. For this work, the Pegasus 4D has a secondary column oven, which was set to the minimum temperature offset of +5 ˚C versus the primary oven. The

column sets selected for this experiment test the range of common ${}^{1}\beta$, and provide insight into the implications of this parameter for the practice of high peak capacity GC×GC.

4.4.2 Secondary Column Retention Time Range and Implications for Modulation Period

A critical parameter in method development for GC×GC separations is the modulation period (P_M), which defines the timing interval for trapping eluent from the primary column and reinjecting it onto the secondary column. Figure 1A is a representative total ion current (TIC) chromatogram from column set 3 collected with a P_M of 6 s. Analytes eluting before ~5 minutes have less retention on column 2, likely due to differences in the degree of solute interaction levels with the stationary phase on the primary column as a function of T_e and the oven temperature program [32]. For this reason, most of the analysis is this work is based on the portion of the chromatogram after the secondary column retention times of the n-alkanes begin to plateau, after ~5 minutes; this region spans cyclohexanol to 1-eicosanol, and includes 70 analytes. The band of peaks from ~5-32 minutes on the primary column and ~1.9 s on the secondary column includes most of the n-alkanes in the 115 component mixture, from nonane to eicosane. This band represents the least retained analytes on the secondary column. The peak at ${}^{2}t_R$ of ~23 minutes and ${}^{2}t_R$ of ~4.6 s is the most retained analyte on the secondary column, diethyl phthalate.

For column set 3, using a P_M of 6 s, there is excessive separation space that is unutilized. A more appropriate P_M would be shorter, such that the secondary column separation time does not exceed that of the most retained analyte, diethyl phthalate; this would suggest a P_M of approximately 5 s. However, while the P_M of 5 s would eliminate excessive "white space" in the upper portion of the 2D chromatogram, there would still be substantial unused separation space in the lower portion of the 2D chromatogram. The most appropriate P_M would be based on the

difference in retention time between the most and least retained analytes; subtracting the ${}^2t_R$ for the n-alkane band (~1.9 s) from that of diethyl phthalate (~4.6 s), and allowing for the ${}^2w_b$ of those peaks (~0.12 s and ~0.24 s, respectively), suggests a P_M of 3 s. Under these conditions, secondary column wraparound is allowed: the most retained analytes on the secondary column have retention times exceeding that of the P_M. Figure 1B is a representative TIC chromatogram from column set 3 using a P_M of 3 s. Under these conditions, the 2D separation space is completely utilized. However, due to secondary column wraparound, the observed elution order is misleading; the n-alkane band is still at ${}^2t_R$ of ~1.9 s, but diethyl phthalate now appears below the n-alkane band, at ${}^2t_R$ of ~1.5 s. However, since the separation is continuous, it is possible to reregister the 2D chromatogram so that the observed elution order is consistent with that of the true elution order. Figure 1C shows the reregistered TIC chromatogram for column set 3 with P_M of 3 s; note that the n-alkane band is once again at the bottom of the 2D chromatogram and diethyl phthalate is once again at the top of the chromatogram. For the purpose of easier visual interpretation, all further 2D chromatograms are presented in the reregistered form of Figure 1C; however, all data was collected in the form of Figure 1B, with the appropriate P_M chosen based on the relative retention times of the n-alkane band and diethyl phthalate. Figure 2 shows the reregistered TIC chromatograms for column sets 1, 2, 3, and 6. Using knowledge of ${}^2t_0$ and P_M, along with each peak's observed ${}^2t_R$, it is possible to calculate the true ${}^2t_R$ for all 70 peaks included in the subsequent analysis.

4.4.3 Pseudo-isothermal Conditions of the Secondary Column Separation

In typical comprehensive GC×GC, the nature of the primary column separation is distinct from that of the secondary column separation. Broadly, the former can be considered slow (tens of minutes) with a high peak capacity (hundreds of peaks), while the latter is fast (usually less

than ten seconds) with a more moderate peak capacity (tens of peaks). This general style of GC×GC separations is predicated by the need to maintain appropriate modulation ratio (M_R) to avoid sampling-based band broadening on the primary column, while maintaining reasonable overall run times. Longer secondary column run times, and consequently longer P_M, may be utilized; however, this may require inadequate M_R, inefficient primary column performance, and/or excessively long method run times. The solution that many GC×GC practitioners have adopted is to operate the primary column as efficiently as possible to maximize ${}^1n_c$, and to utilize a short P_M to maintain the maximized ${}^1n_c$, and to operate the secondary column to provide moderate ${}^2n_c$ with minimal harm to ${}^1n_c$ [3,14,15].

The short secondary column separation relative to that of the primary column, combined with moderate oven temperature programming rates, implies that relative to the primary column, the secondary column separation may be considered as a series of pseudo-isothermal separations [13]. The temperature change between modulations (ΔT) may be calculated from the programmed temperature ramp for the primary and secondary oven (T_{ramp}) and modulation period as $\Delta T = T_{ramp} \cdot P_M$. For column set 3 under optimal conditions, there is only a differential in temperature of 0.25 ˚C within the span of each secondary column separation (i.e., each modulation). The most impactful consequence of the pseudo-isothermal nature of the secondary column separation is that the general elution problem applies, causing ${}^2w_b$ to increase linearly with ${}^2k$ [13,24,25], as noted in the theory section.

The linear relationship between the ${}^2k$ of an analyte and its subsequent ${}^2w_b$ is readily observed in the data. Figure 3A is a section of the reregistered 2D TIC chromatogram from the column set 3 separation, from which 2D peaks for six analytes having different ${}^2t_R$ were selected. To cover the range of ${}^2k$ observed in the experiment, it was necessary to combine peaks from a

range of primary column times, as there were insufficient primary column coelutions at any given ${}^{1}t_R$. The six selected analytes, numbered in order of increasing ${}^{2}t_R$ were hexadecane, 1-tetradecanol, methyl dodecanoate, 2-pentadecanone, benzophenone, and diethyl phthalate. The combined secondary column chromatogram was generated by selecting the most abundant modulation for the six 2D peaks and extracting the secondary column chromatographic profile using a selective *m/z* for each analyte. The six extracted chromatographic profiles were then summed together to generate a combined secondary column profile, which was smoothed using a Savitzsky-Golay filter with a window of 7 data points (mass spectra) and a polynomial degree of 2. These parameters were selected manually to balance noise reduction against smoothing-induced broadening, determined by comparison of the raw and smoothed data. This combined secondary column profile, plotted in Figure 3B, represents the secondary column chromatogram that would be expected had all six analytes co-eluted on the primary column and then been separated on the secondary column.

The series of peaks in Figure 3B were evaluated using in-house developed software to determine ${}^{2}k$ and ${}^{2}w_b$, as summarized in the inset of Figure 3B, which plots ${}^{2}k$ versus ${}^{2}w_b$, showing a clear linear trend. Because peak width is also a function of chemical constants for a given analyte, such as $D_{g,0}$, [33] some scatter around the line of best fit is expected; however, the overall observation of linear increase of ${}^{2}w_b$ with ${}^{2}k$ is consistent throughout the 2D chromatogram. To comprehensively demonstrate this effect, a total of 70 analytes were measured, as described in Section 4.3.2. The measured analytes spanned the range of cyclohexanol to 1-eicosanol, which was a range of 277 to 2185 s on the primary column for column set 3. Figure 4A is a plot of ${}^{2}w_b$ versus ${}^{2}k$ for the 70 measured analytes, as separated on column set 3. The markers for each ${}^{2}w_b$ and ${}^{2}k$ pair have been assigned according to the

represented analytes' $^{1}t_R$; in order of $^{1}t_R$, analytes 1-23, 24-46, and 47-70 are represented by circles, triangles, and squares, respectively. This figure demonstrates the consistently linear trend between ^{2}k and the resulting $^{2}w_b$, as well as the independence of this phenomenon from $^{1}t_R$. An interesting implication of the $^{2}w_b$ versus ^{2}k curve fitting is that it allows for estimation of $^{2}w_b$ for an unretained peak, according to the y-intercept of the best fit line. For column set 3, we estimate that an unretained peak would have a $^{2}w_b$ of only 55 ms, which highlights the impressive performance of the thermal modulator for generating very narrow injection pulses [34].

The measurement of ^{2}k from the GC×GC chromatograms was validated by analyzing a subset of the 70 measured analytes by isothermal GC–FID. 11 analytes were selected comprising a total of 4 groups of closely eluting compounds from the primary column. Within each selected group, all analytes eluted within ~1-2 ˚C of each other, and included coelutions on the primary that are resolved by secondary column. Each of these analytes was analyzed by isothermal GC–FID using longer segment (10.0 m) of the secondary columns, cut from the same column spool, at a series of temperatures with 10 ˚C increments to determine *k* as a function of temperature, and to allow interpolation of the *k* for each analyte at the temperature corresponding to $^{2}T_e$. Figure 4B plots ^{2}k for each of the 11 analytes, as determined from the column set 3 GC×GC separation versus those determined from the isothermal GC–FID separations. The plot shows strong agreement between the ^{2}k calculated by each experiment. One of the assumptions made in the calculation of ^{2}k from the GC×GC separations was that $^{2}t_0$ could be accurately calculated using the column flow calculator included with the ChromaTOF instrument software. Traditionally, t_0 determinations are performed by injection of an unretained analyte, such as methane [35]; however, this is not possible in thermally modulated GC×GC, though it has been demonstrated in flow-modulated GC×GC [36].

Figure 5 includes the comparisons of ${}^{2}k$ from the GC×GC experiment versus that of the isothermal GC–FID analysis all six column sets. Overall, we see that ${}^{2}k$ is predicted with reasonable accuracy between experiments, with deviations from unity likely due to systematic bias in the determination of ${}^{2}t_0$ in the GC×GC experiment and/or flow deviations during its temperature programmed separation. Briefly, we find that bias in slope is consistent within column sets 1-3, and within column sets 4-6, which utilize secondary columns with 0.2 µm and 0.4 µm films, respectively. This provides further evidence that the bias is due to systematic error in the calculated ${}^{2}t_0$. Figure 6 shows the differences in the ${}^{2}w_b$ versus ${}^{2}k$ plots between column sets 1, 2, and 3. Overall, we observe a similar linear relationship between ${}^{2}w_b$ and ${}^{2}k$ for each column set, with similar slopes and y-intercepts. The major difference between column sets is the range of ${}^{2}k$ present in each column set, which increases with β_R. Further, we observe that the starting ${}^{2}k$ increases with as β_R well, shifting the best fit lines to the right.

4.4.4 Column 2 Peak Capacity

Peak capacity is defined as the number of chromatographic peaks that fit within a given time at a given resolution, and is representative of the separation ability of a system. Peak capacity describes the "resolving power" of a chromatograph for a hypothetical mixture of analytes that cover the separation space. One of the more-prominent implications of peak capacity is as it pertains to statistical overlap theory, which estimates the theoretical peak capacity required for a given system to sufficiently resolve a mixture of analytes. For example, to resolve to single peaks 98% of the components in a mixture having uniform random retention times, the peak capacity of a separation must exceed the number of components separated by a factor of approximately 100 [8]. For reasonably complex mixtures, it thus follows that a separation's peak capacity must be large. However, using conventional 1D GC, the requirements

to achieve an order of magnitude increase in peak capacity (e.g., by using a longer column) are impractical, and may only be reasonable achieved via GC×GC, provided the system is optimized for that objective [3]. In an optimized GC×GC, the peak capacity advantage over 1D GC [3,12,14] is largely realized by the peak capacity provided by the secondary column in a relatively short separation time, and which combines with the peak capacity of the primary column to provide the two-dimensional peak capacity of the GC×GC.

As described in Section 4.4.3 the secondary column separation may be considered as a pseudo-isothermal process which is impacted by the general elution problem, and subject to a linear dependence of ${}^{2}w_b$ on ${}^{2}k$. For the measurement of ${}^{2}n_c$, this is critically important; rather than simply dividing the separation window by the average peak width, as is applied for ${}^{1}n_c$, we must take into account the effect of ${}^{2}k$ dependent band broadening. For an isothermal separation, the retention time of a series of peaks at *Rs* of 1 may be defined [13]. Utilizing the equation of best fit described in Section 4.3.4 to define ${}^{2}w_b$ as a function of ${}^{2}k$, and the range of ${}^{2}k$ encountered in the data, it is possible to iteratively simulate the number of peaks that may fit within the defined retention window. Figure 7 is a series of peaks simulated using the parameters obtained from linear best fits of ${}^{2}w_b$ versus ${}^{2}k$ for column sets 1, 2, and 3, as summarized in Figure 6. Each peak has a width defined by the best fit equation, and is at R_s of 1 relative to its neighbors. The first interesting finding of this effort is that the least retained analytes, in this experiment represented by the n-alkane band, have non-negligible retention and that their retention increase with β_R. For the purposes of determining ${}^{2}n_c$, the retention time window should not be defined by P_M, rather, it should be defined by the differences of retention times between the most and least retained analytes. While it may be possible to squeeze more peaks between ${}^{2}k$

of zero and the minimum ${}^2k$ observed, doing so would require the improbable occurrence of compounds which are less retained than n-alkanes on a polar column.

Under the specified conditions, it is found that there are diminishing returns from experimentally extending the ${}^2k$ range though manipulation of β. In the case of column set 1, which has the smallest ${}^2k$ range, ${}^2n_c$ is 12 with a P_M of 1 s; in column set 3, P_M is tripled to 3 s, but ${}^2n_c$ is not quite doubled at 21. The band broadening with ${}^2k$ results in progressively smaller gains in ${}^2n_c$ as the ${}^2k$ range is increased. The gains to ${}^2n_c$ are further decreased since the ${}^2k$ range is not just extending, it is also shifting such that the minimum ${}^2k$ is increasing, as observed for the ${}^2w_b$ versus ${}^2k$ plots in Figure 6, in which the lines of best fit both extend and shift to higher ${}^2k$ as β_R increases. This further deprecates the ${}^2n_c$ gained at higher β_R as the minimum ${}^2k$ increases for the least-retained n-alkanes.

4.4.5 Column 1 Peak Capacity

While the change ${}^2n_c$ is the most obvious impact of the effect of β on the ${}^2k$ range, there is also a meaningful effect on ${}^1n_c$ by the influence of ${}^2k$ range on M_R. As described in the Section 4.4.2, the optimal P_M should be set according to the observed ${}^2k$ range, such as to allow wraparound as needed for utilizing the 2D separation space, without so much as to have overlap between analytes with minimal versus maximal ${}^2k$. It is well know that the chosen P_M affects ${}^1n_c$ by way of broadening primary peaks as a function of M_R [3,12,13]. Briefly, at high M_R the width of a modulated peak approaches that of the peak prior to modulation; that is, at sufficiently high M_R, there is no band broadening due to modulation. However, under typical GC×GC operational parameters, M_R tends to be smaller, with impacts to ${}^1n_c$. Using statistical overlap theory, one may predict the impact to ${}^1n_c$, provided knowledge of P_M and ${}^1w_b$ prior to modulation [31]. In common practice of GC×GC, however, ${}^1w_b$ prior to modulation is not known, since all we can

observe is the signal after the modulation and subsequent secondary column separations have occurred. Instead, we may measure ${}^{1}w_b$ following modulation, and use this "effective" width for all subsequent analysis. It is of note that the measured ${}^{1}w_b$ following modulation only takes into account the band broadening that results from modulation, and does not consider other matters which are addressed by statistical overlap approaches. However, the methods applied here are adequate for estimation of ${}^{1}w_b$ and ${}^{1}n_c$ and allow for comparison of these metrics between column sets.

Using the method described in Section 4.3.3, ${}^{1}w_b$ was calculated for tetradecane in each column set. The data were collected with the optimal P_M for the particular column set. Additionally, the data was collected with longer P_M to eliminate analyte wraparound, which simplifies the interpretation of GC×GC chromatograms, but has notable impacts on ${}^{1}w_b$ and ${}^{1}n_c$. At a P_M of 3 s, the ${}^{1}w_b$ was 5.496 s, while at a P_M of 6 s, the ${}^{1}w_b$ was 7.452 s. It is worth emphasizing that, between these conditions, only P_M was changed. Similar degrees of modulator-induced band broadening were observed for column sets 1 and 2 when the longer P_M were used; these results are summarized in Table 4.

Comparing between column sets is more difficult, as the primary column film thickness is expected to influence ${}^{1}w_b$ prior to modulation. Specifically, column set 1 utilizes a 1.0 µm film on the primary column, while that of column set 3 is 0.25 µm. Prior to modulation, column set 1 would be expected to produce peaks with wider ${}^{1}w_b$, all other things equal, than column set 3. Further, we see that under the same experimental conditions, the primary column retention range between the most and least retained analytes is larger with thicker films. Typically, we would expect the peak capacity to be comparable between the primary columns used, as the shorter retention time range the column with the thinner film would be made up for by its narrower

peaks. After considering modulator-induced band broadening, however, the longer P_M required for column set 3 eliminates any ${}^1w_b$ advantages it thinner film may have provided. Between column sets 1 and 3, the measured M_R is substantially reduced from 5.485 to 1.832, respectively. Ultimately, the combination of primary column film thickness and modulator-induced band broadening result in measured ${}^1w_b$ which are approximately the same between column sets 1, 2, and 3. When M_R drops more substantially, such as in the experiments using longer P_M than optimal, the increase in ${}^1w_b$ is more significant.

4.4.6 2D Peak Capacity

Two-dimensional peak capacity ($n_{c,2D}$) is defined as the product of ${}^1n_c$ and ${}^2n_c$, according to equation 6. $n_{c,2D}$ is useful for comparing the ability of GC×GC systems to separate complex mixtures. It may also be expressed as a rate in the form of peak capacity production, which is the $n_{c,2D}$ per unit time [14]. In the work described here, $n_{c,2D}$ is the principal metric by which the column sets are compared, as it takes into account the performance of both the primary and secondary column separations. Table 4 summarizes the performance of all of the column sets at their optimal P_M, the performance of column sets 1-3 under conditions of longer P_M, as well as the expected performance of sets 2 and 3 under hypothetical conditions.

Under optimal conditions, we find that column set 3 provides the best $n_{c,2D}$ for the sample studied. This column set provides a large ${}^2n_c$ of 21, and has a ${}^2k$ range that is amenable to a short P_M of 3 s that provides for a reasonable M_R for tetradecane of 1.832. This column set utilizes a thin film of 0.25 µm on the primary column, which provides narrower peaks that are somewhat broadened by the modulator. It should be mentioned that the M_R was determined for an analyte eluting near the middle of the primary column separation and that the M_R may be smaller for peaks which having narrower ${}^1w_b$. Additionally, the measured ${}^1w_b$ is may be less precise at lower

M_R due to the impacts of sampling phase, which significantly affects the number of high *S/N* peaklets when M_R is small.

Column set 2 has a smaller ${}^2k$ range and a subsequently smaller ${}^2n_c$ of 14 compared to column set 3. However, the optimum P_M for column set 2 is also shorter at 1.5 s, which allows for an improved M_R of 3.657 for tetradecane. At this M_R, we expect negligible modulator-based band broadening for peaks of equivalent ${}^1w_b$ to tetradecane; additionally, ${}^1w_b$ can be more precisely measured due to the improved data density across the primary column peak. While the limited ${}^2k$ range of column sets 1 and 2 provides for a short P_M and enhanced M_R relative to column set 3, the M_R is perhaps larger than needed. In simulation work recently published by Pinkerton et. al., peak capacities were studied using M_R of 2 or 4 as a function of P_M; briefly, it was found that $n_{c,2D}$ could be improved by moving from M_R of 4 to 2 by means of narrowing ${}^1w_b$ prior to modulation. Entry 2-b in Table 4 is a hypothetical condition, whereby the M_R of 3.657 from column set 2 has been decreased to that of column set 3 by decreasing ${}^1w_b$ to 2.8 s; under this condition, ${}^2n_c$ remains constant, while ${}^1n_c$ substantially improves for an overall improvement in $n_{c,2D}$ from ~5850 to ~11450. This decrease in ${}^1w_b$ while maintaining method run time could be accomplished by reductions in primary column inner diameter, though there are tradeoffs in terms of working concentration ranges and column backpressure, as well as impacts to flow on the secondary column [3,12,37]. Improvements to ${}^1w_b$ may also be accomplished by minimizing off-column band broadening by the injector [14,15]. Entry 2-c considers a more realistic improvement to ${}^1n_c$ by reducing ${}^1w_b$ to 4.0 s. Under these conditions, the M_R would be ~2.67, and the $n_{c,2D}$ would be ~8020, which is equivalent to that obtained in column set 3. In previously reported metabolomics studies by our group [38,39], we observed exceptional peak capacity though applying instrument operating parameters similar to those in 2-c.

Another hypothetical example that is covered in Table 4 is entry 3-b, which considers the ${}^{1}w_b$ needed to achieve a M_R on column set 3, when operated under no wraparound conditions (P_M of 6 s), which is equivalent to that of column set 2 operated under optimal conditions. Under these conditions, ${}^{1}w_b$ would need to be experimentally broadened, such as by reducing the carrier gas flow to below optimal, to 22 s in order to match the M_R achieved with column set 2. While this hypothetical separation would have the higher ${}^{2}n_c$ of 21, ${}^{1}n_c$ would be significantly diminished to ~100, and the resulting $n_{c,2D}$ would be only ~2030.

In summary, we find that for the test mixture studied here, column set 3 provides the maximum $n_{c,2D}$ under optimal P_M. Operating at extensive P_M so as to avoid wraparound has dramatic implications, as the realized ${}^{2}n_c$ stays constant, with substantial decreases in ${}^{1}n_c$ due to modulator-based band broadening. The effect is particularly apparent if attempts are made to improve M_R by means of increasing ${}^{1}w_b$. The differences in M_R and $n_{c,2D}$ between column sets 1, 2, and 3 demonstrate that there are inherent tradeoffs between these metrics; depending on what is planned for the data following collection, analysts may prefer the M_R provided by column sets 1 and 2, or the $n_{c,2D}$ provided by column set 3. For example, separations having a higher M_R may be preferred to avoid under sampling narrower peaks that elute in earlier portions of the chromatogram, or to enable more accurate and precise measurement of ${}^{1}t_R$ needed for some experiments. Another case for higher M_R could be where any lost resolution on the primary column is unlikely to be made up for on the secondary column, such as in the example of chiral-GC×GC [40], where a high M_R may be needed to maintain quantitative accuracy for critical peak pairs.

4.4.7 Impacts of Increasing Film Thickness on the Secondary Column

The aforementioned data were collected with column sets 1-3, which utilized a thin film of 0.2 µm on the secondary column (β of 225), which is representative of most GC×GC configurations. In contrast, column sets 4-6 used a 0.4 µm film on the secondary column (β of 112.5), which is less commonly utilized in GC×GC. The data was collected on column sets 4-6 to allow for the study of more extensive ${}^{2}k$ ranges, and their implications for P_M, M_R, and n_c. As summarized in Table 4, the observed ${}^{2}k$ ranges in column sets 4-6 were substantially increased by the thicker secondary column stationary phase, compared to the thinner film counterpart in column sets 1-3. Using the 0.2 µm film, ${}^{2}k$ ranged from 0.269 to 3.541; using the 0.4 µm film, ${}^{2}k$ ranged from 0.965 to 9.870. Commensurate with the increase in the range of ${}^{2}k$, P_M was also increased as described earlier. In contrast to findings that ${}^{2}n_c$ increased with ${}^{2}k$ range within column 1-3—albeit with diminishing returns—when comparing between column sets using the same primary column (e.g. comparing sets 1 and 4), we see subdued benefits to ${}^{2}n_c$. Though using the thicker film on the secondary column significantly increases $2k$, ${}^{2}n_c$ is only slightly improved.

The restrained gains in ${}^{2}n_c$ for column sets 4-6 relative to set 1-3 may be attributed to two causes. First, with the thicker film, the starting ${}^{2}k$ is higher, which results in the ${}^{2}w_b$ of the first eluting peak in the series starting relatively wider, and increasing from there. Second, retained peaks on thicker films have non-negligible broadening from inhibited mass transfer in the stationary phase. Additionally, holding other parameters constant, thicker films increase H_{min} and reduce the overall efficiency of a separation [22]. The increased on-column band-broadening reduces the impact of increased ${}^{2}k$ range in increasing ${}^{2}n_c$, especially in light of reductions to ${}^{1}n_c$ due to modulator-induced band broadening that at occurs at the longer optimal P_M required by

column set 4-6. As is demonstrated in Table 4, column sets 4-6 achieve similar ${}^{2}n_c$ to the sets 1-3, but with longer P_M; as a result, column sets 4-6 have lower M_R, wider ${}^{1}w_b$, and ultimately, reduced $n_{c,2D}$. If the data were collected with longer than optimal P_M to avoid secondary column wraparound, the reductions in $n_{c,2D}$ would be even more substantial.

4.4.8 Implications of Phase Ratio for the Practice of High Peak Capacity GC×GC

As thoroughly discussed in the preceding sections, β has a meaningful impact on the experimental operation of GC×GC, and should be considered during method development. Consistent with theoretical studies of $n_{c,2D}$ in GC×GC, we observed that $n_{c,2D}$ was maximized by utilizing a limited ${}^{2}k$ range with a moderate P_M. While improvements to M_R and ${}^{1}n_c$ were possible by reducing the ${}^{2}k$ range, the loss to ${}^{2}n_c$ was more substantial than the gain to ${}^{1}n_c$, resulting in an overall slight decrease to $n_{c,2D}$. Considering each column individually, we found that β has a relatively small effect on ${}^{1}n_c$ and a much more substantial effect on ${}^{2}n_c$. Due to the loss of ${}^{2}n_c$ when using a relatively thick film on the secondary column, such columns are generally best avoided, unless temperature considerations necessitate the use of the lower ${}^{2}\beta$ to increase retention. Considered separately from the impacts to P_M and M_R, the changes in ${}^{1}\beta$ resulted in only small changes in ${}^{1}n_c$, with the trend that smaller ${}^{1}\beta$ resulted in somewhat broader ${}^{1}w_b$. The more important consequence of ${}^{1}\beta$ was the effect it had on ${}^{1}T_e$ for analytes in the temperature-programmed separation. Since the temperature of the pseudo-isothermal secondary column separation depends on ${}^{1}T_e$ for each analyte, significant changes to ${}^{1}T_e$ will substantially alter ${}^{2}k$ and associated metrics, such as ${}^{2}w_b$ and ${}^{2}n_c$. When subsequent considerations such as P_M are accounted for, ${}^{1}\beta$ may have broad effects on ${}^{1}n_c$ and $n_{c,2D}$ beyond its direct effects on the primary column efficiency.

It should be noted that this work was performed under the presumed limitation of not having independent temperature control of the primary and secondary columns. As noted in Section 4.3.2, the secondary column tracked the primary oven temperature program with a constant offset of +5 °C; this temperature offset is the minimum allowed by the instrument control software. Utilizing different secondary column temperature offsets was not considered in this work for two reasons. First, many GC×GC instruments implement designs in which the secondary column resides in the primary oven and cannot be temperature controlled independently of the primary column. Second, in the most common implementation of secondary column ovens, such as that used in the LECO Pegasus 4D, the secondary column oven is only partially independent of the primary oven; while the secondary oven may be set to a higher temperature than that of the primary oven, it cannot be set to a lower temperature. In the context of this work, if the chromatographer had a separation with insufficient ${}^{2}k$ range using a +5 °C offset, retention on the secondary column could not be further improved by means of the secondary column temperature settings available on that instrument. Within common instrument limitations, this work shows that β can be used as a parameter to control ${}^{2}k$ and, with proper considerations, maximize $n_{c,2D}$ in commercially-available GC×GC instruments.

4.5 Conclusions

For the practice of high peak capacity GC×GC, a variety of instrument factors, including both fixed hardware design and variable instrument parameters, must be carefully chosen to maximize $n_{c,2D}$. Many of these factors have received previous attention in the context of $n_{c,2D}$ with the exception of the phase ratio (β) selected for both the primary and secondary columns. In this work, we studied the effects of changes in β while holding instrument parameters other than the modulation period (P_M) constant. Overall, we found that β substantially affected $n_{c,2D}$ by

influencing retention factors on the secondary column (^2k), and thereby changing the P_M necessary for proper secondary column separations. The necessary changes to P_M modify the modulation ratio (M_R), which affects the primary column peak widths and ^1n_c. Through changes to $^1\beta$, the range of ^2k may be controlled, with subsequent effects to both ^2n_c and ^1n_c. These effects were opposite in direction, such that improvements to ^2n_c may result in declines in ^1n_c. Due to the pseudo-isothermal nature of the secondary column separation, there are diminishing returns to extending the ^2n_c at the cost of ^1n_c.

In this particular experiment, we found that column set 3 with an optimal P_M provided the highest theoretical $n_{c,2D}$ of ~8100, though this was at a relatively low M_R of ~1.8. Column set 2 provided a high theoretical $n_{c,2D}$ of ~5800, at a much higher M_R of ~3.7. Though column set 2 had a lesser total peak capacity than column set 3, its higher M_R suggests that further improvements are possible by improving the primary column efficiency (i.e., narrowing the primary column peak widths) to improve ^1n_c. Similar efforts with column set 3 would result in primary column peaks that are severely under-modulated with subsequent deleterious effects. Overall, manipulating β, particularly for the primary column, is a useful method for controlling secondary column retention and consequent effects on P_M, M_R, and $n_{c,2D}$.

4.6 References

[1] B.A. Parsons, D.K. Pinkerton, B.W. Wright, R.E. Synovec, Chemical characterization of the acid alteration of diesel fuel: Non-targeted analysis by two-dimensional gas chromatography coupled with time-of-flight mass spectrometry with tile-based Fisher ratio and combinatorial threshold determination, J. Chromatogr. A. 1440 (2016) 179–190. doi:10.1016/j.chroma.2016.02.067.

[2] S. Prebihalo, A. Brockman, J. Cochran, F.L. Dorman, Determination of emerging contaminants in wastewater utilizing comprehensive two-dimensional gas-chromatography coupled with time-of-flight mass spectrometry, J. Chromatogr. A. 1419 (2015) 109–115. doi:10.1016/j.chroma.2015.09.080.

[3] M.S. Klee, J. Cochran, M. Merrick, L.M. Blumberg, Evaluation of conditions of comprehensive two-dimensional gas chromatography that yield a near-theoretical maximum in peak capacity gain, J. Chromatogr. A. 1383 (2015) 151–159. doi:10.1016/j.chroma.2015.01.031.

[4] N.P. Vasquez, M. Crosnier de bellaistre-Bonose, N. Lévêque, E. Thioulouse, D. Doummar, T. Billette de Villemeur, D. Rodriguez, R. Couderc, S. Robin, C. Courderot-Masuyer, F. Moussa, Advances in the metabolic profiling of acidic compounds in children's urines achieved by comprehensive two-dimensional gas chromatography, J. Chromatogr. B. 1002 (2015) 130–138. doi:10.1016/j.jchromb.2015.08.006.

[5] P.Q. Tranchida, P. Donato, F. Cacciola, M. Beccaria, P. Dugo, L. Mondello, Potential of comprehensive chromatography in food analysis, TrAC Trends Anal. Chem. 52 (2013) 186–205. doi:10.1016/j.trac.2013.07.008.

[6] J.V. Seeley, S.K. Seeley, Multidimensional Gas Chromatography: Fundamental Advances and New Applications, Anal. Chem. 85 (2013) 557–578. doi:10.1021/ac303195u.

[7] A. Sampat, M. Lopatka, M. Sjerps, G. Vivo-Truyols, P. Schoenmakers, A. van Asten, Forensic potential of comprehensive two-dimensional gas chromatography, TrAC Trends Anal. Chem. 80 (2016) 345–363. doi:10.1016/j.trac.2015.10.011.

[8] J.C. Giddings, Unified separation science, Wiley, New York, 1991. http://catalog.hathitrust.org/api/volumes/oclc/21764363.html (accessed June 8, 2016).

[9] J.M. Davis, J.C. Giddings, Statistical method for estimation of number of components from single complex chromatograms: theory, computer-based testing, and analysis of errors, Anal. Chem. 57 (1985) 2168–2177. doi:10.1021/ac00289a002.

[10] J.M. Davis, J.C. Giddings, Statistical method for estimation of number of components from single complex chromatograms: application to experimental chromatograms, Anal. Chem. 57 (1985) 2178–2182. doi:10.1021/ac00289a003.

[11] J.M. Davis, Statistical theory of spot overlap in two-dimensional separations, Anal. Chem. 63 (1991) 2141–2152.

[12] L.M. Blumberg, F. David, M.S. Klee, P. Sandra, Comparison of one-dimensional and comprehensive two-dimensional separations by gas chromatography, J. Chromatogr. A. 1188 (2008) 2–16. doi:10.1016/j.chroma.2008.02.044.

[13] D.K. Pinkerton, B.A. Parsons, T.J. Anderson, R.E. Synovec, Trilinearity deviation ratio: A new metric for chemometric analysis of comprehensive two-dimensional gas chromatography time-of-flight mass spectrometry data, Anal. Chim. Acta. 871 (2015) 66–76. doi:10.1016/j.aca.2015.02.040.

[14] R.B. Wilson, W.C. Siegler, J.C. Hoggard, B.D. Fitz, J.S. Nadeau, R.E. Synovec, Achieving high peak capacity production for gas chromatography and comprehensive two-dimensional gas chromatography by minimizing off-column peak broadening, J. Chromatogr. A. 1218 (2011) 3130–3139. doi:10.1016/j.chroma.2010.12.108.
[15] B.D. Fitz, R.B. Wilson, B.A. Parsons, J.C. Hoggard, R.E. Synovec, Fast, high peak capacity separations in comprehensive two-dimensional gas chromatography with time-of-flight mass spectrometry, J. Chromatogr. A. 1266 (2012) 116–123. doi:10.1016/j.chroma.2012.09.096.
[16] A. Mostafa, M. Edwards, T. Górecki, Optimization aspects of comprehensive two-dimensional gas chromatography, J. Chromatogr. A. 1255 (2012) 38–55. doi:10.1016/j.chroma.2012.02.064.
[17] M.M. Koek, B. Muilwijk, L.L.P. van Stee, T. Hankemeier, Higher mass loadability in comprehensive two-dimensional gas chromatography–mass spectrometry for improved analytical performance in metabolomics analysis, J. Chromatogr. A. 1186 (2008) 420–429. doi:10.1016/j.chroma.2007.11.107.
[18] D. Peroni, H.-G. Janssen, Comprehensive two-dimensional gas chromatography under high outlet pressure conditions: A new approach to correct the flow-mismatch issue in the two dimensions, J. Chromatogr. A. 1332 (2014) 57–63. doi:10.1016/j.chroma.2014.01.051.
[19] P.Q. Tranchida, M. Maimone, F.A. Franchina, T.R. Bjerk, C.A. Zini, G. Purcaro, L. Mondello, Four-stage (low-)flow modulation comprehensive gas chromatography–quadrupole mass spectrometry for the determination of recently-highlighted cosmetic allergens, J. Chromatogr. A. 1439 (2016) 144–151. doi:10.1016/j.chroma.2015.12.002.
[20] M.S. Klee, GC Inlets An Introduction, Second, Agilent Technogies, Inc., Wilmington, DE USA, 2005. http://www.agilent.com/cs/library/usermanuals/public/5958-9468_041007.pdf.
[21] L. Mahé, M. Courtiade, C. Dartiguelongue, J. Ponthus, V. Souchon, D. Thiébaut, Overcoming the high-temperature two-dimensional gas chromatography limits to elute heavy compounds, J. Chromatogr. A. 1229 (2012) 298–301. doi:10.1016/j.chroma.2012.01.030.
[22] L.M. Blumberg, Theory of Fast Capillary Gas Chromatography Part 4: Column Performance vs.Liquid Film Thickness, J. High Resolut. Chromatogr. 22 (1999) 501–508. doi:10.1002/(SICI)1521-4168(19990901)22:9<501::AID-JHRC501>3.0.CO;2-N.
[23] V.R. Reid, R.E. Synovec, High-speed gas chromatography: The importance of instrumentation optimization and the elimination of extra-column band broadening, Talanta. 76 (2008) 703–717. doi:10.1016/j.talanta.2008.05.012.
[24] G.M. Gross, B.J. Prazen, J.W. Grate, R.E. Synovec, High-Speed Gas Chromatography Using Synchronized Dual-Valve Injection, Anal. Chem. 76 (2004) 3517–3524. doi:10.1021/ac049909g.
[25] R.B. Wilson, J.C. Hoggard, R.E. Synovec, High throughput analysis of atmospheric volatile organic compounds by thermal injection – isothermal gas chromatography – time-of-flight mass spectrometry, Talanta. 103 (2013) 95–102. doi:10.1016/j.talanta.2012.10.013.
[26] L.M. Blumberg, Accumulating resampling (modulation) in comprehensive two-dimensional capillary GC (GC×GC), J. Sep. Sci. 31 (2008) 3358–3365. doi:10.1002/jssc.200800424.

[27] J.C. Hoggard, peg2mat3p8; http://depts.washington.edu/synlab/software/, (2011).
[28] J.L. Adcock, M. Adams, B.S. Mitrevski, P.J. Marriott, Peak Modeling Approach to Accurate Assignment of First-Dimension Retention Times in Comprehensive Two-Dimensional Chromatography, Anal. Chem. 81 (2009) 6797–6804. doi:10.1021/ac900960n.
[29] W.C. Siegler, B.D. Fitz, J.C. Hoggard, R.E. Synovec, Experimental Study of the Quantitative Precision for Valve-Based Comprehensive Two-Dimensional Gas Chromatography, Anal. Chem. 83 (2011) 5190–5196. doi:10.1021/ac200302b.
[30] W. Khummueng, J. Harynuk, P.J. Marriott, Modulation Ratio in Comprehensive Two-dimensional Gas Chromatography, Anal. Chem. 78 (2006) 4578–4587. doi:10.1021/ac052270b.
[31] J.M. Davis, D.R. Stoll, P.W. Carr, Effect of First-Dimension Undersampling on Effective Peak Capacity in Comprehensive Two-Dimensional Separations, Anal. Chem. 80 (2008) 461–473. doi:10.1021/ac071504j.
[32] L.M. Blumberg, M.S. Klee, Elution parameters in constant-pressure, single-ramp temperature-programmed gas chromatography, J. Chromatogr. A. 918 (2001) 113–120. doi:10.1016/S0021-9673(01)00659-8.
[33] B.D. Fitz, B.C. Reaser, D.K. Pinkerton, J.C. Hoggard, K.J. Skogerboe, R.E. Synovec, Enhancing Gas Chromatography–Time of Flight Mass Spectrometry Data Analysis Using Two-Dimensional Mass Channel Cluster Plots, Anal. Chem. 86 (2014) 3973–3979. doi:10.1021/ac5004344.
[34] R.B. Wilson, J.C. Hoggard, R.E. Synovec, Fast, high peak capacity separations in gas chromatography-time-of-flight mass spectrometry, Anal. Chem. 84 (2012) 4167–4173. doi:10.1021/ac300481k.
[35] S. Vezzani, G. Castello, D. Pierani, Measurement and prediction of dead times and column diameter in capillary gas chromatography by using air, methane and some solvents, J. Chromatogr. A. 811 (1998) 85–96. doi:10.1016/S0021-9673(98)00215-5.
[36] M.S. Klee, L.M. Blumberg, Measurement of retention in comprehensive two-dimensional gas chromatography using flow modulation with methane dopant, J. Chromatogr. A. 1217 (2010) 1830–1837. doi:10.1016/j.chroma.2010.01.027.
[37] D. Peroni, A.A.S. Sampat, W. van Egmond, S. de Koning, J. Cochran, R. Lautamo, H.-G. Janssen, Comprehensive two-dimensional gas chromatography with a multi-capillary second dimension: A new column-set format for simultaneous optimum linear velocity operation, J. Chromatogr. A. (2013). doi:10.1016/j.chroma.2013.07.097.
[38] R.E. Mohler, K.M. Dombek, J.C. Hoggard, E.T. Young, R.E. Synovec, Comprehensive Two-Dimensional Gas Chromatography Time-of-Flight Mass Spectrometry Analysis of Metabolites in Fermenting and Respiring Yeast Cells, Anal. Chem. 78 (2006) 2700–2709. doi:10.1021/ac052106o.
[39] R.E. Mohler, K.M. Dombek, J.C. Hoggard, K.M. Pierce, E.T. Young, R.E. Synovec, Comprehensive analysis of yeast metabolite GC×GC–TOFMS data: combining discovery-mode and deconvolution chemometric software, Analyst. 132 (2007) 756–767. doi:10.1039/B700061H.
[40] Y.F. Wong, R.N. West, S.-T. Chin, P.J. Marriott, Evaluation of fast enantioselective multidimensional gas chromatography methods for monoterpenic compounds: Authenticity control of Australian tea tree oil, J. Chromatogr. A. 1406 (2015) 307–315. doi:10.1016/j.chroma.2015.06.036.

4.7 Tables

Table 4-1. The column sets utilized in this report, with film thicknesses and corresponding beta ratio (β_R).

Column Set	Primary column film (µm)	Secondary column film (µm)	β_R
1	1.0	0.2	0.28
2	0.5	0.2	0.56
3	0.25	0.2	1.11
4	1.0	0.4	0.56
5	0.5	0.4	1.11
6	0.25	0.4	2.22

Table 4-2. The modulator and oven parameters used for each column set. The hot and cold pulse times are listed for each stage in the dual-stage thermal modulator. The maximum temperature of the primary oven program ($^1T_{max}$) and the thermal offset applied to the modulator block ($T_{mod,offset}$) are also provided.

Column Set	β_R	P_M (s)	Hot Pulse (s)	Cold Pulse (s)	$^1T_{max}$ (°C)	$T_{mod,offset}$ (°C)
1	0.28	1	0.40	0.10	250	20
2	0.56	1.5	0.40	0.35	240	20
3	1.11	3	0.60	0.90	230	40
4	0.56	3	0.60	0.90	250	40
5	1.11	5	1.25	1.25	240	40
6	2.22	8	2.00	2.00	230	40

Table 4-3. The calculated primary column elution temperatures (°C) for the 11 selected analytes, provided for each of the three primary column film thicknesses applied.

	0.25 µm film	0.5 µm film	1.0 µm film
2-heptanone	59.3	67.1	81.7
nonane	59.8	68.3	83.0
methyl hexanoate	63.1	72.0	87.1
2,6-dimethyloctane	63.8	73.1	88.5
bromobenzene	63.3	72.8	88.9
1-bromohexane	64.1	73.5	89.2
1-undecene	85.6	96.6	113.8
2-nonanone	86.1	96.8	114.0
adamantane	83.6	95.6	114.3
hexadecane	150.8	163.6	182.5
diethyl phthalate	150.8	163.7	183.4

Table 4-4 Summary of results. 1-6 are results using the optimal P_M. –a (e.g., 1-a) indicates results from the alternative P_M which does not allow for analyte wraparound. –b and –c indicate hypothetical results predicted for changes to peak widths to meet targeted M_R.

Column Set	^{2}k' range	P_M (s)	^1w_b (s)	M_R	^1n_c	^2n_c	$n_{c,2D}$	^1t_R range (min)	PCP (min^{-1})
1	0.269 - 1.090	1	5.485	5.485	458	12	5491	41.83	131
2	0.506 - 2.123	1.5	5.486	3.657	418	14	5846	38.18	153
3	0.736 - 3.541	3	5.496	1.832	387	21	8127	35.45	229
4	0.965 - 3.197	3	6.4674	2.156	388	13	5047	41.85	121
5	1.467 - 5.851	5	7.2483	1.450	317	17	5394	38.33	141
6	2.059 - 9.870	8	9.5459	1.193	224	21	4699	35.60	132
1-a	0.269 - 1.090	3	6.523	2.174	385	12	4618	41.83	110
2-a	0.506 - 2.123	3	6.938	2.313	330	14	4622	38.18	121
3-a	0.736 - 3.541	6	7.452	1.242	285	21	5994	35.45	169
2-b	0.506 - 2.123	1.5	*2.8*	1.867	818	14	*11453*	38.18	300
2-c	0.506 - 2.123	1.5	*4.0*	2.667	573	14	*8017*	38.18	210
3-b	0.736 - 3.541	6	*22*	3.667	97	21	*2030*	35.45	57

4.8 Figures

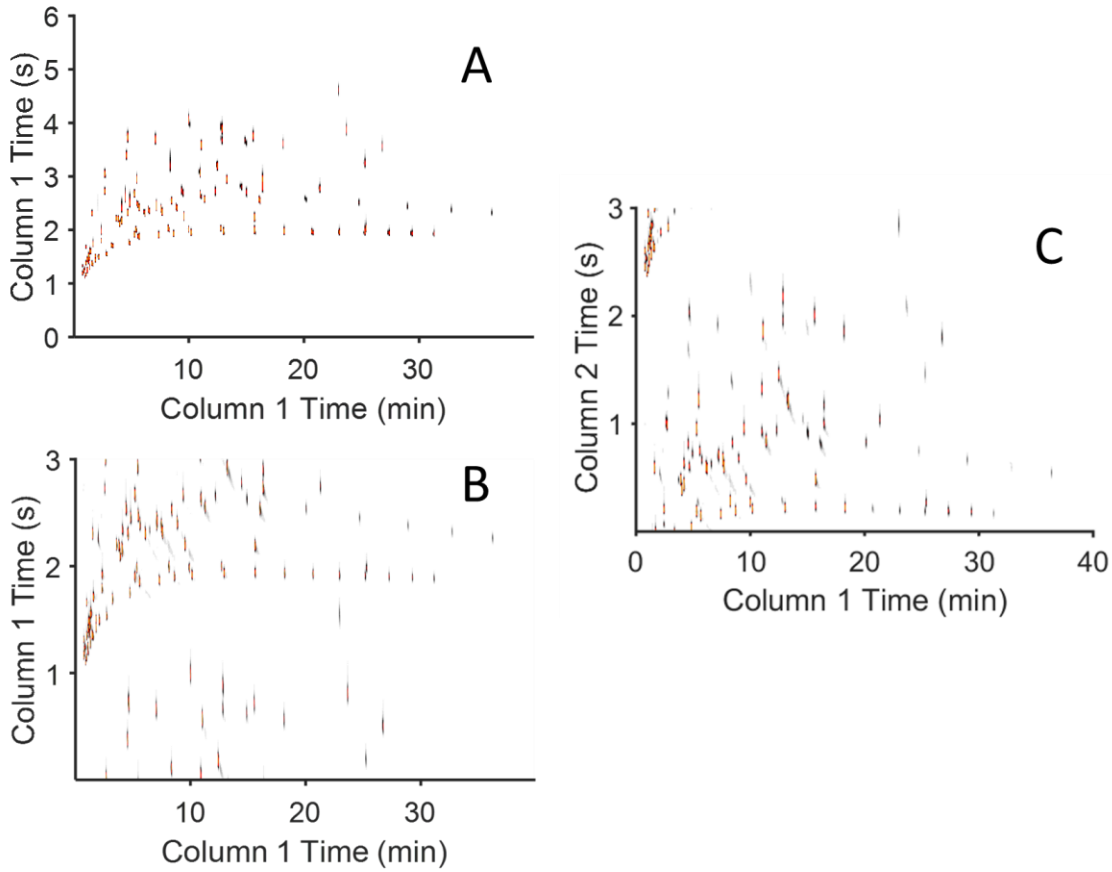

Figure 4-1. Representative total ion current (TIC) chromatograms from the separation of the 115 component mixture on column set 3. (A) using a P_M of 6 s, which allows for no wraparound of analytes. (B) using an optimal P_M of 3 s, which allows for partial wraparound to better utilize the 2D separation space. (C) reregistered chromatogram in which (B) has been replotted such that the least retained analytes appear at the bottom of the chromatogram.

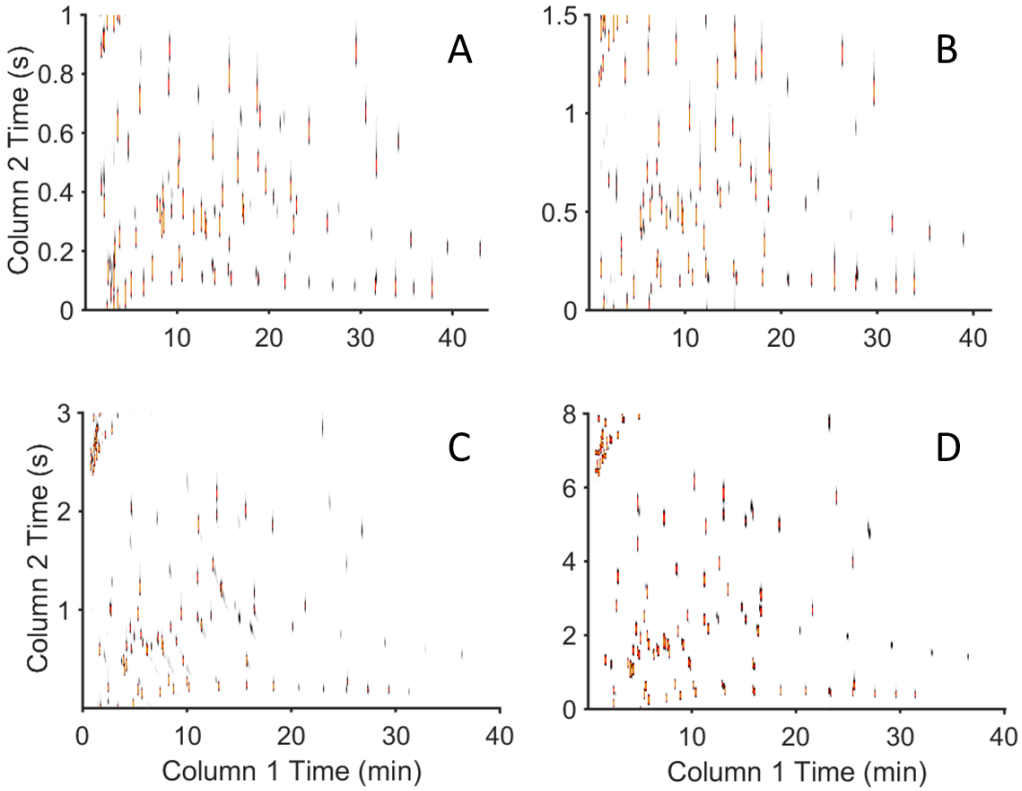

Figure 4-2. Representative reregistered TIC chromatograms for four column sets used in the report, including (A) column set 1 (B) column set 2, (C) column set 3, and (D) column set 6.

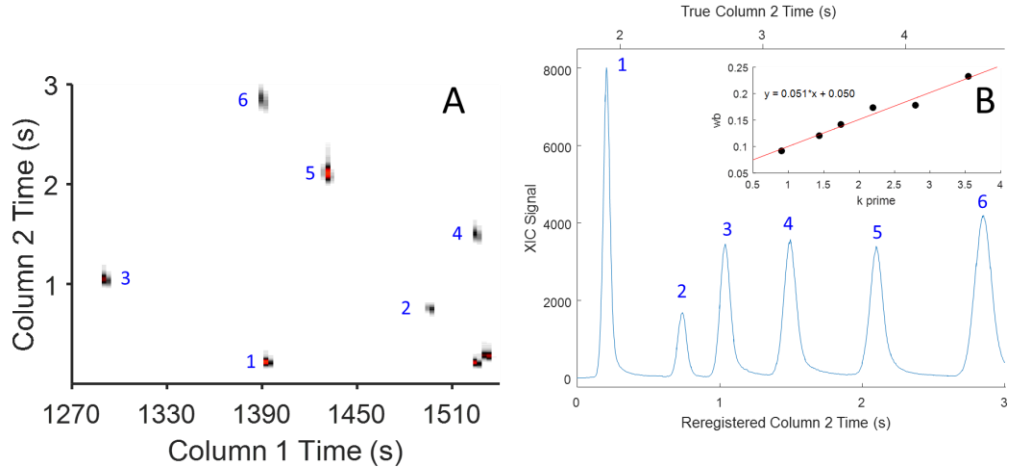

Figure 4-3. (A) a section of the reregistered separation using column set 3, from which six peaks were selected to demonstrate the relationship between ${}^2t_R$ and ${}^2w_b$. The six analytes in order of increasing ${}^2t_R$ are: hexadecane, 1-tetradecanol, methyl dodecanoate, 2-pentadecanone, benzophenone, and diethyl phthalate. (B) the combined secondary column profile from the most intense modulations of the six 2D peaks. The inset figure plots the ${}^2w_b$ versus ${}^2k$ for the six peaks with a linear best fit line (red).

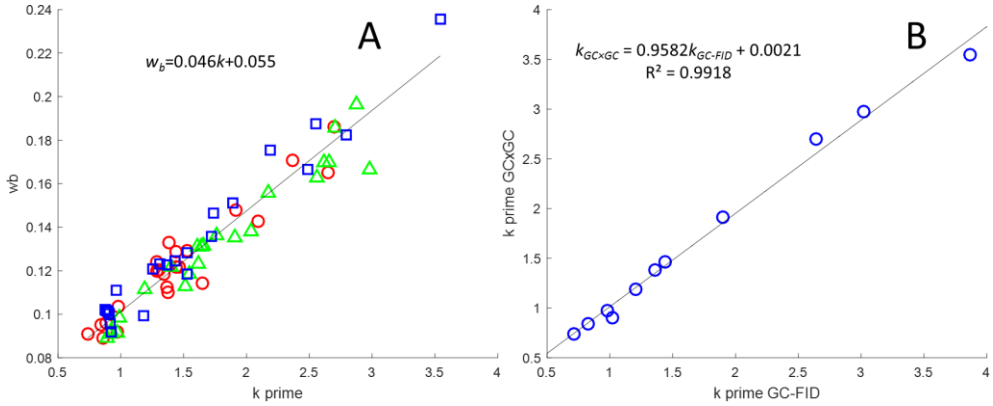

Figure 4-4. (A) is a plot of ${}^{2}w_b$ versus ${}^{2}k$ for the 70 measured analytes, as separated on column set 3. The markers for each ${}^{2}w_b$ and ${}^{2}k$ pair have been assigned according to the represented analytes' ${}^{1}t_R$; in order of ${}^{1}t_R$, analytes 1-23, 24-46, and 47-70 are represented by circles, triangles, and squares, respectively. (B) is a plot of ${}^{2}k$ for each of the 11 analytes, as determined from the column set 3 GC×GC separation versus those determined from the isothermal GC–FID separations.

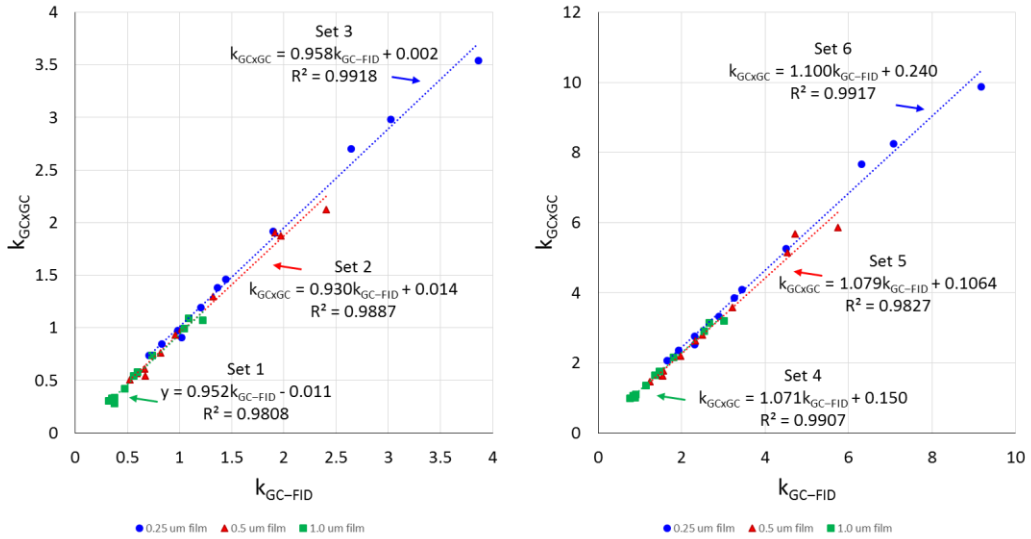

Figure 4-5. Plots of ${}^{2}k$ for each of the 11 analytes, as determined from the GC×GC separations for each column set versus those determined from the isothermal GC–FID separations.

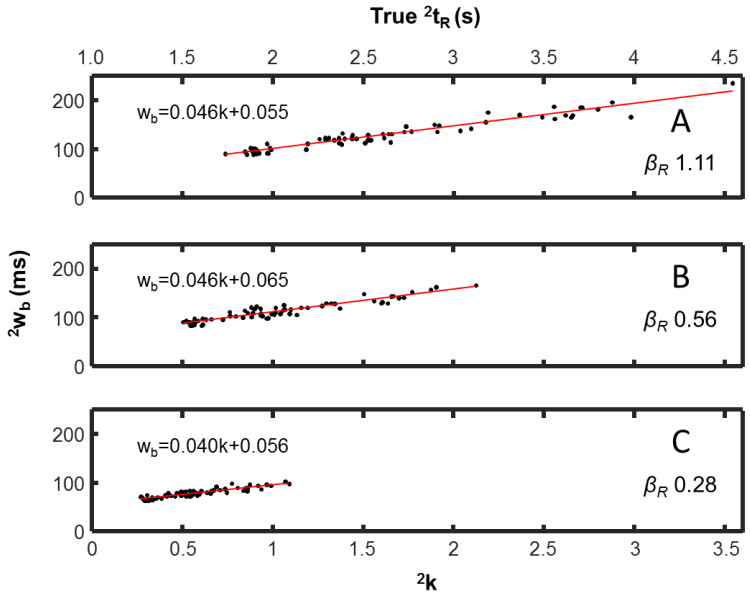

Figure 4-6. The ^2w_b versus ^2k plots for (A) column set 3, (B) column set 2, and (C) column set 1.

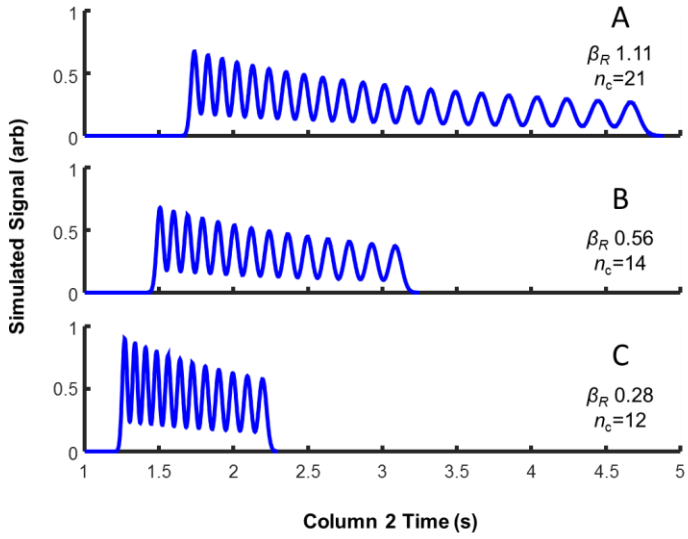

Figure 4-7. Simulated isothermal secondary column chromatograms used to determine ^2n_c for (A) column set 3, (B) column set 2, and (C) column set 1.

Chapter 5: Conclusions

5.1 Summary of Presented Work

The development and implementation of GC×GC–TOFMS is likely the most significant advance in gas chromatography over the last two decades, and arguably has enabled the largest advance in the peak capacity capabilities of gas chromatographs since the introduction of WCOT capillary columns in 1979. However, alongside the advances in capabilities introduced by GC×GC–TOFMS has been new challenges in instrument design, operation, optimization, and data processing and analysis. An abundance of authors have addressed these challenges and made substantial improvements to increase the usability of the platform, including its commercially-available implementation as the LECO Pegasus 4D. One of the major challenges remaining in GC×GC–TOFMS is strategies and methods for data processing, quantification, and interpretation. Historically, data has been analyzed on the following three levels: pixel, peak table, or peak region. While all of these three levels of data are utilized, the peak table and peak region methods approaches are firmly provided by the instrument manufacturers, and hence the analyst must apply such software in the commercially available state. Hence, there is generally little room for independent development of data processing software at these two data levels, whereas at the pixel-level, there has been relative bounty of opportunity for both improvements in existing methods and entirely new ideas.

The tile-based F-ratio software builds on previous work in pixel-based methods, while additionally encompassing ideas and advantages of peak table and peak region approaches. By inherently mitigating minor misalignment and spurious pixel-level covariance, the tile-based method improves on the pixel-based method, simultaneously improving the discovery of class-distinguishing analytes while reducing the occurrence of false positives. The tile-based method

also retains the advantages of its pixel-based roots: robust to chromatographic interference and non-Gaussian peak shapes, and making minimal assumptions about peak widths, shifts, and abundances. Further, the tile-based F-ratio software is designed around class-comparison experiments, unlike most commercial software which is designed around a chromatogram-by-chromatogram workflow, with export to other software for class-comparison efforts.

Chapter 2 presented work to determine the performance of the tile-based F-ratio method in a spiked analyte study in a complicated matrix: diesel fuel. The tile-based method was found to outperform both pixel-based and peak table methods for non-targeted analyses of complex mixtures, for both the spike versus blank comparisons and the concentration ratio of two comparisons. To objectively limit the tile based F-ratio results to only features which are statistically likely to be true positives, we developed a combinatorial technique using null class comparisons, called null distribution analysis, by which we determined a statistically defensible F-ratio cutoff for the analysis of the hit list. After applying null distribution analysis, spiked analytes were reliably discovered at ~ 1 to ~ 10 ppm (~ 5 to ~ 50 pg using a 200:1 split), depending upon the degree of mass spectral selectivity and 2D chromatographic resolution, with minimal occurrence of false positives. Compared to the pixel-based method, the tile-based method performed similarly at concentrations at and above 50 ppm; below 50 ppm, the tile-based method had superior performance with fewer false positives interspersed between hits, even at the lowest concentration comparisons. Compared to the peak table method, both pixel-based and tile-based methods performed better at concentrations below 50 ppm, as the peak table method encountered trouble with reliable peak detection and quantification at lower *S/N*.

Chapter 3 presented work which improved on the combinatorial null distribution method described in Chapter 2. The expanded null distribution analysis algorithmically determined an F-

ratio threshold to confidently select only the features which are sufficiently class-distinguishing. When applied to the acid alteration of diesel fuel, the suggested per-hit F-ratio threshold was 12.4, which predicted a false discovery rate (FDR) below 0.1%. Using this F-ratio threshold, 107 of the 3362 preliminary hits were deemed significantly changing due to the acid alteration, with the number of false positives estimated to be about 3. The use of diverse fuel samples within the sample classes focused the results of the class comparison experiment to discover features which were sufficiently consistent within the sample class, deprioritizing analytes which were too variable compared to the chemical changes induced by the fuel alteration procedure. Validation of the F-ratio analysis was performed using an additional three fuel samples. The subsequent analysis of the discovered class-distinguishing features confirmed that aromatic species are removed by the acid alteration, with the degree of removal consistent with predicted reactivity toward electrophilic aromatic sulfonation. Additionally, we observed that alkenes and alkynes were also removed from the fuel, and that sulfur dioxide or compounds that degrade to sulfur dioxide are generated by the acid alteration

Chapter 4 presented work to study the effects of phase ratio (β) on peak capacity (n_c) for GC×GC–TOFMS, and to determine the conditions under which $n_{c,2D}$ is maximized. Overall, β substantially affected $n_{c,2D}$ by influencing retention factors on the secondary column (^2k), and thereby changing the P_M necessary for proper secondary column separations. The necessary changes to P_M modify the modulation ratio (M_R), which affects the primary column peak widths and ^1n_c. Through changes to $^1\beta$, the range of ^2k may be controlled, with subsequent effects to both ^2n_c and ^1n_c. These effects were opposite in direction, such that improvements to ^2n_c may result in declines in ^1n_c. Due to the pseudo-isothermal nature of the secondary column separation, there are diminishing returns to extending the ^2n_c at the cost of ^1n_c. In this particular experiment,

we found that column set 3 with an optimal P_M provided the highest theoretical $n_{c,2D}$ of ~8100, though this was at a relatively low M_R of ~1.8. Column set 2 provided a high theoretical $n_{c,2D}$ of ~5800, at a much higher M_R of ~3.7. Though column set 2 had a lesser total peak capacity than column set 3, its higher M_R suggests that further improvements are possible by improving the primary column efficiency (i.e., narrowing the primary column peak widths) to improve ${}^1n_c$. Overall, manipulating β, particularly for the primary column, is a useful method for controlling secondary column retention and consequent effects on P_M, M_R, and $n_{c,2D}$.

5.2 Future Directions

There remain several future directions for the research presented in each chapter of this document. The results from each project suggest ways in which methods could be improved, fundamentals better understood, and mechanisms explored. This section will expand on ideas suggested by the results of the tile-based F-ratio development, the study of diesel fuel alteration, and investigations into the role of phase ratio in GC×GC.

5.2.1 Tile-based F-ratio software development and characterization

In the development of the tile-based F-ratio software, I made extensive comparisons to pixel and peak table methods to demonstrate the advantages provided by the tile-based approach. I believe that the issue of comparison to other approaches is now resolved, such that focus can instead be directed at optimization of the tile-based method itself. There are several parameters that are known to affect the performance of the method in terms of false positive and false negative rates: tile size, signal-to-noise thresholds, and number of mass channels averaged for ranking of features in the hit list. However, to adequately characterize this performance requires an experimental comparison having a larger number of controlled class-distinguishing analytes than the four that were utilized in the study described in Chapter 2. Fortunately, data have been

collected utilizing an expanded spike study, as was originally proposed in my candidacy exam, and are currently being analyzed by Brooke C. Reaser, who was one of the group member to inherit the tile-based F-ratio project. An upcoming publication will describe the performance of the tile-based F-ratio software in context of signal-to-noise threshold and number of mass channels averaged for ranking, using receiver operating characteristic (ROC) curves to quantitatively describe the performance under various parameters.

The effects of tile size on performance have only been preliminarily explored. At this point it is known that too large of a tile size leads to false negatives as the summation of noise and signal from interfering peaks dilutes the selectivity of the tile-based quantification. Further, too small of a tile size is unable to mitigate retention time shifting and may additionally lose sensitivity through under-summation of the 2D peaks. The study of tile size implications would be warranted to better understand these effects, and could potentially be performed using the expanded spike study mentioned in the previous paragraph. In the current implementation of tiling, substantial constraints apply to the size of the tile, due to the unique grid scheme. For the secondary column tile size, the tile must be even (to allow for shifting the grid upwards by a half tile), and must evenly divide into the length of the secondary column separation. For example, if the secondary column separation is 1.5 s at 100 Hz, there would be 150 mass spectra comprising the second dimension. Under the aforementioned constraints, the tile size along the secondary column must be 10, 30, or 50. These limitations substantially reduce the flexibility of the analysis in selecting a tile size that is optimal for the peaks in the GC×GC chromatogram. One way by which this limitation could be resolved would be by performing interpolation on the secondary separation in order to “fit” with other tile sizes. Such interpolation must be carefully

studied, however, as distortions to the data may occur that could lead to false negative and false positive issues.

Another area of opportunity in the study of tile size is in relation to the results of the phase ratio study presented in Chapter 4. I found that the phase ratio used on each column substantially affected the retention factor range, and subsequently the range of widths, observed on the secondary column. The development of the tile-based F-ratio software was performed under conditions that led to only minor difference in ${}^{2}w_b$ between the most and least retained analytes on the secondary column. However, under other plausible GC×GC conditions, there may be substantial difference in ${}^{2}w_b$ between analytes with high ${}^{2}k$ versus those with low ${}^{2}k$. Ideally, based on what is known about optimal tile size based on peak widths, the tiles which sample the high ${}^{2}k$ peaks should be larger than the tiles which sample the low ${}^{2}k$ peaks. Doing so would require a complete revision of the tiling scheme, but could improve the performance of the software, particularly when it is applied to GC×GC chromatograms having longer P_M.

Lastly, a principal focus of the acid alteration study presented in Chapter 3 was the development of a combinatorial method for threshold determination in F-ratio analysis. The idea of the work was that the false discovery rate (FDR) could be controlled at the data analysis stage by study of the null hypothesis by computational means. Using the statistical approaches I developed, a maximum of three false positives out of the 107 features above the F-ratio threshold of 12.4 would be expected, for that experiment. However, since the application of the study does not allow for known knowns and known unknowns—unlike that of a spiked analyte study—the true number of false positives in the study remains elusive. Natanial E. Watson, another group member to inherit the F-ratio project, has submitted a manuscript which applies the statistical

methods to a previously characterized GC×GC metabolomics data set, in order to verify that the method described in Chapter 3 is able to control the FDR.

5.2.2 Acid alteration non-targeted analysis and mechanism exploration

Prior to inheriting the acid alteration of diesel fuel project, there were limited hypotheses about the fate of the fuel dye that was removed by the alteration process. Previously, most efforts had involved a more-or-less targeted analysis of hypothesized dye breakdown products that may be found in the altered fuel and serve as a "smoking gun" that the fuel was previously dye-containing and had been illicitly altered. It was not until I undertook non-targeted F-ratio analysis of the acid alteration project that alternative hypotheses began to form. Early on, the results of the tile-based F-ratio analysis—at the onset of that software's development—there was evidence that in addition to the dye being removed, other aromatic species were removed as well, and further, that very little was being "created" in the fuel following the alteration. The observation of these results guided a study of relevant organic chemistry literature, which suggested that electrophilic aromatic substitution was a likely mechanism by which the aromatic fuel dye and other aromatic species may be removed by the sulfuric acid alteration of the fuel. As discussed in Chapter 3, the results of an expanded alteration experiment lend support to that mechanism.

Interestingly, the results of the analysis also suggest that trace-level alkene and alkynes are being removed by the acid alteration, as well, suggesting that a concurrent mechanism may also be at play. A review of the pertinent literature reveals that an alkene to carbocation alkylation mechanism may also be possible. Such a reaction is widely used in the petroleum refining industry in so-called "alkylate plant" which react small alkenes and branched alkanes to produce larger branched alkanes for formulation into gasoline to improve its octane (anti-

knocking) index. These plants often utilize concentrated sulfuric acid in the reaction, under temperature and pressure conditions similar to that of the diesel fuel alteration. Future studies could utilize simple "model diesel" samples so that concentrations of key analytes could be controlled and tracked over the course of the reaction to better examine the likelihood of both the electrophilic aromatic sulfonation and alkylation mechanisms.

5.2.3 Further study of retention factor and peak capacity in GC×GC

The work described in Chapter 4 reports a complete investigation of the effects of phase ratio on retention factors and peak capacities in GC×GC–TOFMS. I found that there are substantial tradeoffs between pursuing enhanced peak capacity on the secondary column versus the primary column, due primarily to the effect of modulator-induced band broadening. Surprisingly, I found that the instrument parameters under which our research typically collected GC×GC–TOFMS data provided a higher modulation ratio and subsequently less peak capacity than what might be realized through minor adjustments. Based on the conclusions of the project, it may be useful to further test the instrument configurations using a real sample and evaluate performance not just using the somewhat abstract concept of peak capacity, but instead on the application-oriented metric of chromatographic resolution of critical peak pairs. This study would help to answer the question of whether losing resolution on the primary column due to collecting at a lower modulation ratio is made up for by gaining resolution on the secondary column.

Bibliography

Adahchour, Mohamed, Leo L.P van Stee, Jan Beens, René J.J Vreuls, Max A Batenburg, and Udo A.Th Brinkman. 2003. "Comprehensive Two-Dimensional Gas Chromatography with Time-of-Flight Mass Spectrometric Detection for the Trace Analysis of Flavour Compounds in Food." Journal of Chromatography A 1019 (1–2): 157–72. doi:10.1016/S0021-9673(03)01131-2.

Adcock, Jacqui L., Mike Adams, Blagoj S. Mitrevski, and Philip J. Marriott. 2009. "Peak Modeling Approach to Accurate Assignment of First-Dimension Retention Times in Comprehensive Two-Dimensional Chromatography." *Analytical Chemistry* 81 (16): 6797–6804. doi:10.1021/ac900960n.

Allen, Robert C., and Sarah C. Rutan. 2011. "Investigation of Interpolation Techniques for the Reconstruction of the First Dimension of Comprehensive Two-Dimensional Liquid Chromatography–diode Array Detector Data." *Analytica Chimica Acta*, A selection of papers presented at the 12th International Conference on Chemometrics in Analytical Chemistry, 705 (1–2): 253–60. doi:10.1016/j.aca.2011.06.022.

Almstetter, Martin F., Inka J. Appel, Katja Dettmer, Michael A. Gruber, and Peter J. Oefner. 2011. "Comparison of Two Algorithmic Data Processing Strategies for Metabolic Fingerprinting by Comprehensive Two-Dimensional Gas Chromatography–time-of-Flight Mass Spectrometry." *Journal of Chromatography A* 1218 (39): 7031–38. doi:10.1016/j.chroma.2011.08.006.

Amador-Muñoz, Omar, and Philip J. Marriott. 2008. "Quantification in Comprehensive Two-Dimensional Gas Chromatography and a Model of Quantification Based on Selected Summed Modulated Peaks." *Journal of Chromatography A*, 50 Years Journal of Chromatography, 1184 (1–2): 323–40. doi:10.1016/j.chroma.2007.10.041.

Bailey, Hope P., and Sarah C. Rutan. 2013. "Comparison of Chemometric Methods for the Screening of Comprehensive Two-Dimensional Liquid Chromatographic Analysis of Wine." *Analytica Chimica Acta* 770 (April): 18–28. doi:10.1016/j.aca.2013.01.062.

Bailey, Hope P., Sarah C. Rutan, and Peter W. Carr. 2011. "Factors That Affect Quantification of Diode Array Data in Comprehensive Two-Dimensional Liquid Chromatography Using Chemometric Data Analysis." *Journal of Chromatography A* 1218 (46): 8411–22. doi:10.1016/j.chroma.2011.09.057.

Bean, Heather D., Jane E. Hill, and Jean-Marie D. Dimandja. 2015. "Improving the Quality of Biomarker Candidates in Untargeted Metabolomics via Peak Table-Based Alignment of Comprehensive Two-Dimensional Gas Chromatography–mass Spectrometry Data." *Journal of Chromatography A* 1394 (May): 111–17. doi:10.1016/j.chroma.2015.03.001.

Beckstrom, Andrew C., Elizabeth M. Humston, Laura R. Snyder, Robert E. Synovec, and Sandra E. Juul. 2011. "Application of Comprehensive Two-Dimensional Gas Chromatography with Time-of-Flight Mass Spectrometry Method to Identify Potential Biomarkers of Perinatal Asphyxia in a Non-Human Primate Model." *Journal of Chromatography A* 1218 (14): 1899–1906. doi:10.1016/j.chroma.2011.01.086.

Beens, Jan, Mohamed Adahchour, René J.J. Vreuls, Klaas van Altena, and Udo A. Th. Brinkman. 2001. “Simple, Non-Moving Modulation Interface for Comprehensive Two-Dimensional Gas Chromatography.” *Journal of Chromatography A* 919 (1): 127–32. doi:10.1016/S0021-9673(01)00785-3.

Benjamini, Yoav, and Yosef Hochberg. 1995. “Controlling the False Discovery Rate: A Practical and Powerful Approach to Multiple Testing.” *Journal of the Royal Statistical Society. Series B (Methodological)* 57 (1): 289–300. doi:10.2307/2346101.

Benjamini, Yoav, and Daniel Yekutieli. 2001. “The Control of the False Discovery Rate in Multiple Testing under Dependency.” *The Annals of Statistics* 29 (4): 1165–88. doi:10.2307/2674075.

Blumberg, Leonid M. 1999. “Theory of Fast Capillary Gas Chromatography Part 4: Column Performance vs.Liquid Film Thickness.” *Journal of High Resolution Chromatography* 22 (9): 501–8. doi:10.1002/(SICI)1521-4168(19990901)22:9<501::AID-JHRC501>3.0.CO;2-N.

Blumberg, Leonid M. 2008. “Accumulating Resampling (Modulation) in Comprehensive Two-Dimensional Capillary GC (GC×GC).” *Journal of Separation Science* 31 (19): 3358–65. doi:10.1002/jssc.200800424.

Blumberg, Leonid M., Frank David, Matthew S. Klee, and Pat Sandra. 2008. “Comparison of One-Dimensional and Comprehensive Two-Dimensional Separations by Gas Chromatography.” *Journal of Chromatography A*, 30th International Symposium on Capillary Chromatography and Electrophoresis and 4th Comprehensive Two-Dimensional Gas Chromatography Symposium, 1188 (1): 2–16. doi:10.1016/j.chroma.2008.02.044.

Blumberg, Leonid M., and Matthew S. Klee. 2001. “Elution Parameters in Constant-Pressure, Single-Ramp Temperature-Programmed Gas Chromatography.” *Journal of Chromatography A* 918 (1): 113–20. doi:10.1016/S0021-9673(01)00659-8.

Brokl, Michał, Louise Bishop, Christopher G. Wright, Chuan Liu, Kevin McAdam, and Jean-François Focant. 2014. “Multivariate Analysis of Mainstream Tobacco Smoke Particulate Phase by Headspace Solid-Phase Micro Extraction Coupled with Comprehensive Two-Dimensional Gas Chromatography–time-of-Flight Mass Spectrometry.” *Journal of Chromatography A* 1370 (November): 216–29. doi:10.1016/j.chroma.2014.10.057.

Bruckner, Carsten A., Bryan J. Prazen, and Robert E. Synovec. 1998. “Comprehensive Two-Dimensional High-Speed Gas Chromatography with Chemometric Analysis.” *Analytical Chemistry* 70 (14): 2796–2804. doi:10.1021/ac980164m.

Castillo, Sandra, Ismo Mattila, Jarkko Miettinen, Matej Orešič, and Tuulia Hyötyläinen. 2011. “Data Analysis Tool for Comprehensive Two-Dimensional Gas Chromatography/Time-of-Flight Mass Spectrometry.” *Analytical Chemistry* 83 (8): 3058–67. doi:10.1021/ac103308x.

Centner, Vítězslav, Désiré-Luc Massart, Onno E. de Noord, Sijmen de Jong, Bernard M. Vandeginste, and Cécile Sterna. 1996. “Elimination of Uninformative Variables for

Multivariate Calibration." *Analytical Chemistry* 68 (21): 3851–58. doi:10.1021/ac960321m.

Cerfontain, Hans, Hans J. A. Lambrechts, Zwaan R. H. Schaasberg-Nienhuis, Robert G. Coombes, Panicos Hadjigeorgiou, and Geoffrey P. Tucker. 1985. "Aromatic Sulphonation. Part 91. The Sulphonation of Anisole, Phenol, Phenyl Methanesulphonate, Potassium Phenyl Sulphate, and a Series of Methyl-, Bromo-, and Chloro-Substituted Anisoles and Phenols in Concentrated Aqueous Sulphuric Acid." *Journal of the Chemical Society, Perkin Transactions 2*, no. 5(January): 659–67. doi:10.1039/P29850000659.

Cordero, Chiara, Carlo Bicchi, Mario Galli, Stefano Galli, and Patrizia Rubiolo. 2008. "Evaluation of Different Internal-Diameter Column Combinations in Comprehensive Two-Dimensional Gas Chromatography in Flavour and Fragrance Analysis." *Journal of Separation Science* 31 (19): 3437–50. doi:10.1002/jssc.200800280.

Cortes, Hernan J., Bill Winniford, Jim Luong, and Matthias Pursch. 2009. "Comprehensive Two Dimensional Gas Chromatography Review." *Journal of Separation Science* 32 (5–6): 883–904. doi:10.1002/jssc.200800654.

Cox, Robin A. 1987. "Organic Reactions in Sulfuric Acid. The Excess Acidity Method." *Accounts of Chemical Research* 20 (1): 27–31. doi:10.1021/ar00133a004.

Dado, Gregory P., Edward A. Knaggs, and Marshall J. Nepras. 2000. "Sulfonation and Sulfation." In *Kirk-Othmer Encyclopedia of Chemical Technology*. John Wiley & Sons, Inc. http://onlinelibrary.wiley.com/doi/10.1002/0471238961.1921120611140107.a01.pub2/abstract.

Dallüge, Jens, Martijn van Rijn, Jan Beens, René J.J Vreuls, and Udo A.Th Brinkman. 2002. "Comprehensive Two-Dimensional Gas Chromatography with Time-of-Flight Mass Spectrometric Detection Applied to the Determination of Pesticides in Food Extracts." *Journal of Chromatography A* 965 (1–2): 207–17. doi:10.1016/S0021-9673(01)01324-3.

Dandeneau, Raymond D., and E. H. Zerenner. 1979. "An Investigation of Glasses for Capillary Chromatography." *Journal of High Resolution Chromatography* 2 (6): 351–56. doi:10.1002/jhrc.1240020617.

Daszykowski, M., M. S. Wróbel, A. Bierczynska-Krzysik, J. Silberring, G. Lubec, and B. Walczak. 2009. "Automatic Preprocessing of Electrophoretic Images." *Chemometrics and Intelligent Laboratory Systems* 97 (2): 132–40. doi:10.1016/j.chemolab.2009.03.002.

Davis, J.M. 1991. "Statistical Theory of Spot Overlap in Two-Dimensional Separations." *Analytical Chemistry* 63 (19): 2141–52.

Davis, Joe M., and J. Calvin Giddings. 1985. "Statistical Method for Estimation of Number of Components from Single Complex Chromatograms: Application to Experimental Chromatograms." *Analytical Chemistry* 57 (12): 2178–82. doi:10.1021/ac00289a003.

Davis, Joe M., and J. Calvin Giddings. 1985. "Statistical Method for Estimation of Number of Components from Single Complex Chromatograms: Theory, Computer-Based Testing,

and Analysis of Errors." *Analytical Chemistry* 57 (12): 2168–77. doi:10.1021/ac00289a002.

Davis, Joe M., Dwight R. Stoll, and Peter W. Carr. 2008. "Effect of First-Dimension Undersampling on Effective Peak Capacity in Comprehensive Two-Dimensional Separations." *Analytical Chemistry* 80 (2): 461–73. doi:10.1021/ac071504j.

Duda, Richard O., Peter E. Hart, and David G. Stork. 2012. *Pattern Classification*. John Wiley & Sons.

Efron, Bradley. 2005. "Bayesians, Frequentists, and Scientists." *Journal of the American Statistical Association* 100 (469): 1–5. doi:10.1198/016214505000000033.

Efron, Bradley. 2007. "Correlation and Large-Scale Simultaneous Significance Testing." *Journal of the American Statistical Association* 102 (477): 93–103. doi:10.1198/016214506000001211.

Efron, Bradley. 2010. "Correlated Z-Values and the Accuracy of Large-Scale Statistical Estimates." *Journal of the American Statistical Association* 105 (491): 1042–55. doi:10.1198/jasa.2010.tm09129.

Efron, Bradley, and Robert Tibshirani. 2002. "Empirical Bayes Methods and False Discovery Rates for Microarrays." *Genetic Epidemiology* 23 (1): 70–86. doi:10.1002/gepi.1124.

Fitz, Brian D., Brooke C. Reaser, David K. Pinkerton, Jamin C. Hoggard, Kristen J. Skogerboe, and Robert E. Synovec. 2014. "Enhancing Gas Chromatography–Time of Flight Mass Spectrometry Data Analysis Using Two-Dimensional Mass Channel Cluster Plots." *Analytical Chemistry* 86 (8): 3973–79. doi:10.1021/ac5004344.

Fitz, Brian D., Ryan B. Wilson, Brendon A. Parsons, Jamin C. Hoggard, and Robert E. Synovec. 2012. "Fast, High Peak Capacity Separations in Comprehensive Two-Dimensional Gas Chromatography with Time-of-Flight Mass Spectrometry." *Journal of Chromatography A* 1266 (November): 116–23. doi:10.1016/j.chroma.2012.09.096.

Fraga, Carlos G., Bryan J. Prazen, and Robert E. Synovec. 2000. "Comprehensive Two-Dimensional Gas Chromatography and Chemometrics for the High-Speed Quantitative Analysis of Aromatic Isomers in a Jet Fuel Using the Standard Addition Method and an Objective Retention Time Alignment Algorithm." *Analytical Chemistry* 72 (17): 4154–62. doi:10.1021/ac000303b.

Fraga, C.G., B.J. Prazen, and R.E. Synovec. 2001. "Objective Data Alignment and Chemometric Analysis of Comprehensive Two-Dimensional Separations with Run-to-Run Peak Shifting on Both Dimensions." *Analytical Chemistry* 73 (24): 5833–40. doi:10.1021/ac010656q.

François, Isabelle, Koen Sandra, and Pat Sandra. 2009. "Comprehensive Liquid Chromatography: Fundamental Aspects and Practical considerations—A Review." *Analytica Chimica Acta* 641 (1–2): 14–31. doi:10.1016/j.aca.2009.03.041.

Giddings, J. Calvin. 1991. *Unified Separation Science*. New York: Wiley. http://catalog.hathitrust.org/api/volumes/oclc/21764363.html.

Gröger, Th., M. Schäffer, M. Pütz, B. Ahrens, K. Drew, M. Eschner, and R. Zimmermann. 2008. "Application of Two-Dimensional Gas Chromatography Combined with Pixel-Based Chemometric Processing for the Chemical Profiling of Illicit Drug Samples." *Journal of Chromatography A* 1200 (1): 8–16. doi:10.1016/j.chroma.2008.05.028.

Gröger, Thomas, and Ralf Zimmermann. 2011. "Application of Parallel Computing to Speed up Chemometrics for GC × GC–TOFMS Based Metabolic Fingerprinting." *Talanta*, Enhancing Chemical Separations with Chemometric Data Analysis, 83 (4): 1289–94. doi:10.1016/j.talanta.2010.09.015.

Gros, Jonas, Deedar Nabi, Petros Dimitriou-Christidis, Rebecca Rutler, and J. Samuel Arey. 2012. "Robust Algorithm for Aligning Two-Dimensional Chromatograms." *Analytical Chemistry* 84 (21): 9033–40. doi:10.1021/ac301367s.

Gross, Gwen M., Bryan J. Prazen, Jay W. Grate, and Robert E. Synovec. 2004. "High-Speed Gas Chromatography Using Synchronized Dual-Valve Injection." *Analytical Chemistry* 76 (13): 3517–24. doi:10.1021/ac049909g.

Hantao, Leandro Wang, Bruna Regina Toledo, Fabiana Alves de Lima Ribeiro, Marilia Pizetta, Caroline Geraldi Pierozzi, Edson Luiz Furtado, and Fabio Augusto. 2013. "Comprehensive Two-Dimensional Gas Chromatography Combined to Multivariate Data Analysis for Detection of Disease-Resistant Clones of Eucalyptus." *Talanta* 116 (November): 1079–84. doi:10.1016/j.talanta.2013.08.033.

Harvey, Paul McA., and Robert A. Shellie. 2012. "Data Reduction in Comprehensive Two-Dimensional Gas Chromatography for Rapid and Repeatable Automated Data Analysis." *Analytical Chemistry* 84 (15): 6501–7. doi:10.1021/ac300664h.

Heim, John. 2010. "Utilization of Statistical Compare Software and Fisher Ratios Prior to Multivariate Analysis for Complex GCxGC-TOFMS Data in Order to Define Statistical Variation Between the Small Molecule Metabolite Profiles of Different Fish Species." LECO Corporation.

Hoggard, Jamin C. 2011. peg2mat3p8; Http://depts.washington.edu/synlab/software/." http://depts.washington.edu/synlab/software/.

Hoggard, Jamin C., and Robert E. Synovec. 2007. "Parallel Factor Analysis (PARAFAC) of Target Analytes in GC × GC−TOFMS Data: Automated Selection of a Model with an Appropriate Number of Factors." *Analytical Chemistry* 79 (4): 1611–19. doi:10.1021/ac061710b.

Hoggard, Jamin C., Jon H. Wahl, Robert E. Synovec, Gary M. Mong, and Carlos G. Fraga. 2010. "Impurity Profiling of a Chemical Weapon Precursor for Possible Forensic Signatures by Comprehensive Two-Dimensional Gas Chromatography/Mass Spectrometry and Chemometrics." *Analytical Chemistry* 82 (2): 689–98. doi:10.1021/ac902247x.

Humston, Elizabeth M., Kenneth M. Dombek, Benjamin P. Tu, Elton T. Young, and Robert E. Synovec. 2011. "Toward a Global Analysis of Metabolites in Regulatory Mutants of Yeast." *Analytical and Bioanalytical Chemistry* 401 (8): 2387–2402. doi:10.1007/s00216-011-4800-2.

Humston, Elizabeth M., Jamin C. Hoggard, and Robert E. Synovec. 2010. “Utilizing the Third Order Advantage with Isotope Dilution Mass Spectrometry.” *Analytical Chemistry* 82 (1): 41–43. doi:10.1021/ac902184b.

Hupp, Amber M., Lucas J. Marshall, Dahlia I. Campbell, Ruth Waddell Smith, and Victoria L. McGuffin. 2008. “Chemometric Analysis of Diesel Fuel for Forensic and Environmental Applications.” *Analytica Chimica Acta* 606 (2): 159–71. doi:10.1016/j.aca.2007.11.007.

Jennerwein, Maximilian K., Markus Eschner, Thomas Gröger, Thomas Wilharm, and Ralf Zimmermann. 2014. “Complete Group-Type Quantification of Petroleum Middle Distillates Based on Comprehensive Two-Dimensional Gas Chromatography Time-of-Flight Mass Spectrometry (GC×GC-TOFMS) and Visual Basic Scripting.” *Energy & Fuels* 28 (9): 5670–81. doi:10.1021/ef501247h.

Johnson, Kevin J, and Robert E Synovec. 2002a. “Pattern Recognition of Jet Fuels: Comprehensive GC×GC with ANOVA-Based Feature Selection and Principal Component Analysis.” *Chemometrics and Intelligent Laboratory Systems* 60 (1–2): 225–37. doi:10.1016/S0169-7439(01)00198-8.

Johnson, Kevin J., Bob W. Wright, Kristin H. Jarman, and Robert E. Synovec. 2003. “High-Speed Peak Matching Algorithm for Retention Time Alignment of Gas Chromatographic Data for Chemometric Analysis.” *Journal of Chromatography A* 996 (1–2): 141–55. doi:10.1016/S0021-9673(03)00616-2.

K. (Kevin) Robards. 2004. *Principles and Practice of Modern Chromatographic Methods*. London ; Boston: Elsevier Academic Press.

Kallio, Minna, Maarit Kivilompolo, Sami Varjo, Matti Jussila, and Tuulia Hyötyläinen. 2009. “Data Analysis Programs for Comprehensive Two-Dimensional Chromatography.” *Journal of Chromatography A*, 32nd International Symposium on Capillary Chromatography and 5th GCxGC Symposium, 1216 (14): 2923–27. doi:10.1016/j.chroma.2008.11.037.

Katritzky, Alan R., Myong Sang Kim, Dmytro Fedoseyenko, Khalid Widyan, Mike Siskin, and Manuel Francisco. 2009. “The Sulfonation of Aromatic and Heteroaromatic Polycyclic Compounds.” *Tetrahedron* 65 (6): 1111–14. doi:10.1016/j.tet.2008.11.023.

Kempa, Stefan, Jan Hummel, Thorsten Schwemmer, Matthias Pietzke, Nadine Strehmel, Stefanie Wienkoop, Joachim Kopka, and Wolfram Weckwerth. 2009. “An Automated GCxGC-TOF-MS Protocol for Batch-Wise Extraction and Alignment of Mass Isotopomer Matrixes from Differential 13C-Labelling Experiments: A Case Study for Photoautotrophic-Mixotrophic Grown Chlamydomonas Reinhardtii Cells.” *Journal of Basic Microbiology* 49 (1): 82–91. doi:10.1002/jobm.200800337.

Khummueng, Weeraya, James Harynuk, and Philip J. Marriott. 2006. “Modulation Ratio in Comprehensive Two-Dimensional Gas Chromatography.” *Analytical Chemistry* 78 (13): 4578–87. doi:10.1021/ac052270b.

Kinghorn, Russell M., and Philip J. Marriott. 1998. “Comprehensive Two-Dimensional Gas Chromatography Using a Modulating Cryogenic Trap.” *Journal of High Resolution*

Chromatography 21 (11): 620–622. doi:10.1002/(SICI)1521-4168(19981101)21:11<620::AID-JHRC620>3.0.CO;2-#.

Klee, Matthew S. 2005. *GC Inlets An Introduction*. Second. Wilmington, DE USA: Agilent Technogies, Inc. http://www.agilent.com/cs/library/usermanuals/public/5958-9468_041007.pdf.

Klee, Matthew S., and Leonid M. Blumberg. 2010. "Measurement of Retention in Comprehensive Two-Dimensional Gas Chromatography Using Flow Modulation with Methane Dopant." *Journal of Chromatography A* 1217 (11): 1830–37. doi:10.1016/j.chroma.2010.01.027.

Klee, Matthew S., Jack Cochran, Mark Merrick, and Leonid M. Blumberg. 2015. "Evaluation of Conditions of Comprehensive Two-Dimensional Gas Chromatography That Yield a near-Theoretical Maximum in Peak Capacity Gain." *Journal of Chromatography A* 1383 (February): 151–59. doi:10.1016/j.chroma.2015.01.031.

Koek, Maud M., Bastiaan Muilwijk, Leo L. P. van Stee, and Thomas Hankemeier. 2008. "Higher Mass Loadability in Comprehensive Two-Dimensional Gas Chromatography–mass Spectrometry for Improved Analytical Performance in Metabolomics Analysis." *Journal of Chromatography A*, Trends and Developments in Gas Chromatography, 1186 (1–2): 420–29. doi:10.1016/j.chroma.2007.11.107.

Krakowska, Barbara, Ivana Stanimirova, Joanna Orzel, Michal Daszykowski, Ireneusz Grabowski, Grzegorz Zaleszczyk, and Miroslaw Sznajder. 2014. "Detection of Discoloration in Diesel Fuel Based on Gas Chromatographic Fingerprints." *Analytical and Bioanalytical Chemistry* 407 (4): 1159–70. doi:10.1007/s00216-014-8332-4.

Krupčík, Ján, Pavel Májek, Roman Gorovenko, Jaroslav Blaško, Robert Kubinec, and Pat Sandra. 2015. "Considerations on the Determination of the Limit of Detection and the Limit of Quantification in One-Dimensional and Comprehensive Two-Dimensional Gas Chromatography." *Journal of Chromatography A* 1396 (May): 117–30. doi:10.1016/j.chroma.2015.03.084.

Lee, Andrew L., Keith D. Bartle, and Alastair C. Lewis. 2001. "A Model of Peak Amplitude Enhancement in Orthogonal Two-Dimensional Gas Chromatography." *Analytical Chemistry* 73 (6): 1330–35. doi:10.1021/ac001120s.

Leek, Jeffrey T., and John D. Storey. 2011. "The Joint Null Criterion for Multiple Hypothesis Tests." *Statistical Applications in Genetics and Molecular Biology* 10 (1): 1–22. http://www.degruyter.com/view/j/sagmb.2011.10.issue-1/sagmb.2011.10.1.1673/sagmb.2011.10.1.1673.xml.

Li, Xiang, Xin Lu, Jing Tian, Peng Gao, Hongwei Kong, and Guowang Xu. 2009. "Application of Fuzzy c-Means Clustering in Data Analysis of Metabolomics." *Analytical Chemistry* 81 (11): 4468–75. doi:10.1021/ac900353t.

Liu, Zaiyou, and John B. Phillips. 1991. "Comprehensive Two-Dimensional Gas Chromatography Using an On-Column Thermal Modulator Interface." *Journal of Chromatographic Science* 29 (6): 227–31. doi:10.1093/chromsci/29.6.227.

Lu, Hongmei, Yizeng Liang, Warwick B. Dunn, Hailin Shen, and Douglas B. Kell. 2008. "Comparative Evaluation of Software for Deconvolution of Metabolomics Data Based on GC-TOF-MS." *TrAC Trends in Analytical Chemistry*, Metabolomics, 27 (3): 215–27. doi:10.1016/j.trac.2007.11.004.

Ma, Chenfei, Huahong Wang, Xin Lu, Hong Wang, Guowang Xu, and Benye Liu. 2009. "Terpenoid Metabolic Profiling Analysis of Transgenic Artemisia Annua L. by Comprehensive Two-Dimensional Gas Chromatography Time-of-Flight Mass Spectrometry." *Metabolomics* 5 (4): 497–506. doi:10.1007/s11306-009-0170-6.

Mahé, Laure, Marion Courtiade, Cyril Dartiguelongue, Jérémie Ponthus, Vincent Souchon, and Didier Thiébaut. 2012. "Overcoming the High-Temperature Two-Dimensional Gas Chromatography Limits to Elute Heavy Compounds." *Journal of Chromatography A* 1229 (March): 298–301. doi:10.1016/j.chroma.2012.01.030.

Marney, Luke C., W. Christopher Siegler, Brendon A. Parsons, Jamin C. Hoggard, Bob W. Wright, and Robert E. Synovec. 2013a. "Tile-Based Fisher-Ratio Software for Improved Feature Selection Analysis of Comprehensive Two-Dimensional Gas Chromatography–time-of-Flight Mass Spectrometry Data." *Talanta* 115 (October): 887–95. doi:10.1016/j.talanta.2013.06.038.

Marriott, Philip, and Robert Shellie. 2002. "Principles and Applications of Comprehensive Two-Dimensional Gas Chromatography." *TrAC Trends in Analytical Chemistry* 21 (9–10): 573–83. doi:10.1016/S0165-9936(02)00814-2.

Martín-Alberca, Carlos, Carmen García-Ruiz, and Olivier Delémont. 2015a. "Study of Acidified Ignitable Liquid Residues in Fire Debris by Solid-Phase Microextraction with Gas Chromatography and Mass Spectrometry." *Journal of Separation Science* 38 (18): 3218–27. doi:10.1002/jssc.201500337.

Martín-Alberca, Carlos, María López-López, and Carmen García-Ruiz. 2015. "Analysis of Pre-Ignited Improvised Incendiary Devices Using Portable Raman." *Talanta* 144 (November): 612–18. doi:10.1016/j.talanta.2015.06.072.

Massart, Desiré L. 1988. *Chemometrics: A Textbook*. Amsterdam; New York; New York, NY, U.S.A.: Elsevier ; Distributors for the U.S. and Canada, Elsevier Science Pub. Co.

Milton L. Lee. 1984. Open Tubular Column Gas Chromatography: Theory and Practice. New York: Wiley.

Mohler, Rachel E., Kenneth M. Dombek, Jamin C. Hoggard, Karisa M. Pierce, Elton T. Young, and Robert E. Synovec. 2007a. "Comprehensive Analysis of Yeast Metabolite GC×GC–TOFMS Data: Combining Discovery-Mode and Deconvolution Chemometric Software." *Analyst* 132 (8): 756–67. doi:10.1039/B700061H.

Mohler, Rachel E., Kenneth M. Dombek, Jamin C. Hoggard, Elton T. Young, and Robert E. Synovec. 2006. "Comprehensive Two-Dimensional Gas Chromatography Time-of-Flight Mass Spectrometry Analysis of Metabolites in Fermenting and Respiring Yeast Cells." *Analytical Chemistry* 78 (8): 2700–2709. doi:10.1021/ac052106o.

Mohler, Rachel E., Benjamin P. Tu, Kenneth M. Dombek, Jamin C. Hoggard, Elton T. Young, and Robert E. Synovec. 2008. "Identification and Evaluation of Cycling Yeast Metabolites in Two-Dimensional Comprehensive Gas Chromatography–time-of-Flight-Mass Spectrometry Data." *Journal of Chromatography A*, Trends and Developments in Gas Chromatography, 1186 (1–2): 401–11. doi:10.1016/j.chroma.2007.10.063.

Mondello, Luigi, Miguel Herrero, Tiina Kumm, Paola Dugo, Hernan Cortes, and Giovanni Dugo. 2008. "Quantification in Comprehensive Two-Dimensional Liquid Chromatography." *Analytical Chemistry* 80 (14): 5418–24. doi:10.1021/ac800484y.

Mondello, Luigi, Peter Quinto Tranchida, Paola Dugo, and Giovanni Dugo. 2008. "Comprehensive Two-Dimensional Gas Chromatography-Mass Spectrometry: A Review." *Mass Spectrometry Reviews* 27 (2): 101–24. doi:10.1002/mas.20158.

Mostafa, Ahmed, Matthew Edwards, and Tadeusz Górecki. 2012. "Optimization Aspects of Comprehensive Two-Dimensional Gas Chromatography." *Journal of Chromatography A*, Hyphenated and Multidimensional Chromatography Techniques, 1255 (September): 38–55. doi:10.1016/j.chroma.2012.02.064.

Nadeau, Jeremy S., Ryan B. Wilson, Jamin C. Hoggard, Bob W. Wright, and Robert E. Synovec. 2011. "Study of the Interdependency of the Data Sampling Ratio with Retention Time Alignment and Principal Component Analysis for Gas Chromatography." *Journal of Chromatography A* 1218 (50): 9091–9101. doi:10.1016/j.chroma.2011.10.031.

Organtini, Kari L., Anne L. Myers, Karl J. Jobst, Jack Cochran, Brian Ross, Brian McCarry, Eric J. Reiner, and Frank L. Dorman. 2014. "Comprehensive Characterization of the Halogenated Dibenzo-P-Dioxin and Dibenzofuran Contents of Residential Fire Debris Using Comprehensive Two-Dimensional Gas Chromatography Coupled to Time of Flight Mass Spectrometry." *Journal of Chromatography A* 1369 (November): 138–46. doi:10.1016/j.chroma.2014.09.088.

Parsons, Brendon A., Luke C. Marney, W. Christopher Siegler, Jamin C. Hoggard, Bob W. Wright, and Robert E. Synovec. 2015. "Tile-Based Fisher Ratio Analysis of Comprehensive Two-Dimensional Gas Chromatography Time-of-Flight Mass Spectrometry (GC × GC–TOFMS) Data Using a Null Distribution Approach." *Analytical Chemistry* 87 (7): 3812–19. doi:10.1021/ac504472s.

Parsons, Brendon A., David K. Pinkerton, Bob W. Wright, and Robert E. Synovec. 2016. "Chemical Characterization of the Acid Alteration of Diesel Fuel: Non-Targeted Analysis by Two-Dimensional Gas Chromatography Coupled with Time-of-Flight Mass Spectrometry with Tile-Based Fisher Ratio and Combinatorial Threshold Determination." *Journal of Chromatography A* 1440 (April): 179–90. doi:10.1016/j.chroma.2016.02.067.

Pasikanti, Kishore Kumar, Juwita Norasmara, Shirong Cai, Ratha Mahendran, Kesavan Esuvaranathan, Paul C. Ho, and Eric Chun Yong Chan. 2010. "Metabolic Footprinting of Tumorigenic and Nontumorigenic Uroepithelial Cells Using Two-Dimensional Gas Chromatography Time-of-Flight Mass Spectrometry." *Analytical and Bioanalytical Chemistry* 398 (3): 1285–93. doi:10.1007/s00216-010-4055-3.

Pc, Carvalho, Hewel J, Barbosa Vc, and Yates JR 3rd. 2007. “Identifying Differences in Protein Expression Levels by Spectral Counting and Feature Selection., Identifying Differences in Protein Expression Levels by Spectral Counting and Feature Selection.” *Genetics and Molecular Research : GMR, Genetics and Molecular Research : GMR* 7, 7 (2, 2): 342, 342–56. doi:10.4238/vol7-2gmr426.

Peroni, Daniela, and Hans-Gerd Janssen. 2014. “Comprehensive Two-Dimensional Gas Chromatography under High Outlet Pressure Conditions: A New Approach to Correct the Flow-Mismatch Issue in the Two Dimensions.” *Journal of Chromatography A* 1332 (March): 57–63. doi:10.1016/j.chroma.2014.01.051.

Peroni, Daniela, Andjoe A.S. Sampat, Wil van Egmond, Sjaak de Koning, Jack Cochran, Roy Lautamo, and Hans-Gerd Janssen. 2013. “Comprehensive Two-Dimensional Gas Chromatography with a Multi-Capillary Second Dimension: A New Column-Set Format for Simultaneous Optimum Linear Velocity Operation.” *Journal of Chromatography A*, September. doi:10.1016/j.chroma.2013.07.097.

Pierce, Karisa M., Jamin C. Hoggard, Janiece L. Hope, Petrie M. Rainey, Andrew N. Hoofnagle, Rhona M. Jack, Bob W. Wright, and Robert E. Synovec. 2006. “Fisher Ratio Method Applied to Third-Order Separation Data To Identify Significant Chemical Components of Metabolite Extracts.” *Analytical Chemistry* 78 (14): 5068–75. doi:10.1021/ac0602625.

Pierce, Karisa M., Benjamin Kehimkar, Luke C. Marney, Jamin C. Hoggard, and Robert E. Synovec. 2012a. “Review of Chemometric Analysis Techniques for Comprehensive Two Dimensional Separations Data.” *Journal of Chromatography A* 1255 (September): 3–11. doi:10.1016/j.chroma.2012.05.050.

Pierce, Karisa M., Jeremy S. Nadeau, and Robert E. Synovec. 2012. “Chapter 17 - Data Analysis Methods.” In *Gas Chromatography*, edited by Colin F. Poole, 415–34. Amsterdam: Elsevier. http://www.sciencedirect.com/science/article/pii/B9780123855404000171.

Pierce, Karisa M., and Stephen P. Schale. 2011. “Predicting Percent Composition of Blends of Biodiesel and Conventional Diesel Using Gas Chromatography–mass Spectrometry, Comprehensive Two-Dimensional Gas Chromatography–mass Spectrometry, and Partial Least Squares Analysis.” *Talanta*, Enhancing Chemical Separations with Chemometric Data Analysis, 83 (4): 1254–59. doi:10.1016/j.talanta.2010.07.084.

Pierce, Karisa M., Lianna F. Wood, Bob W. Wright, and Robert E. Synovec. 2005. “A Comprehensive Two-Dimensional Retention Time Alignment Algorithm To Enhance Chemometric Analysis of Comprehensive Two-Dimensional Separation Data.” *Analytical Chemistry* 77 (23): 7735–43. doi:10.1021/ac0511142.

Pinkerton, David K., Brendon A. Parsons, Todd J. Anderson, and Robert E. Synovec. 2015. “Trilinearity Deviation Ratio: A New Metric for Chemometric Analysis of Comprehensive Two-Dimensional Gas Chromatography Time-of-Flight Mass Spectrometry Data.” *Analytica Chimica Acta* 871 (April): 66–76. doi:10.1016/j.aca.2015.02.040.

Prebihalo, Sarah, Adrienne Brockman, Jack Cochran, and Frank L. Dorman. 2015. “Determination of Emerging Contaminants in Wastewater Utilizing Comprehensive

Two-Dimensional Gas-Chromatography Coupled with Time-of-Flight Mass Spectrometry." *Journal of Chromatography A* 1419 (November): 109–15. doi:10.1016/j.chroma.2015.09.080.

Pryor, William A., Gerald J. Gleicher, John P. Cosgrove, and Daniel F. Church. 1984. "Reaction of Polycyclic Aromatic Hydrocarbons (PAH) with Nitrogen Dioxide in Solution. Support for an Electron-Transfer Mechanism of Aromatic Nitration Based on Correlations Using Simple Molecular Orbital Theory." *The Journal of Organic Chemistry* 49 (26): 5189–94. doi:10.1021/jo00200a035.

Qiu, Yaqiong, Xin Lu, Tao Pang, Chenfei Ma, Xiang Li, and Guowang Xu. 2008. "Determination of Radix Ginseng Volatile Oils at Different Ages by Comprehensive Two-Dimensional Gas Chromatography/time-of-Flight Mass Spectrometry." *Journal of Separation Science* 31 (19): 3451–3457. doi:10.1002/jssc.200800253.

Reichenbach, Stephen E., Mingtian Ni, Visweswara Kottapalli, and Arvind Visvanathan. 2004. "Information Technologies for Comprehensive Two-Dimensional Gas Chromatography." *Chemometrics and Intelligent Laboratory Systems* 71 (2): 107–20. doi:10.1016/j.chemolab.2003.12.009.

Reichenbach, Stephen E., Xue Tian, Akwasi A. Boateng, Charles A. Mullen, Chiara Cordero, and Qingping Tao. 2013. "Reliable Peak Selection for Multisample Analysis with Comprehensive Two-Dimensional Chromatography." *Analytical Chemistry* 85 (10): 4974–81. doi:10.1021/ac303773v.

Reichenbach, Stephen E., Xue Tian, Chiara Cordero, and Qingping Tao. 2012. "Features for Non-Targeted Cross-Sample Analysis with Comprehensive Two-Dimensional Chromatography." *Journal of Chromatography A*, Selected Papers from the 35th International Symposium on Capillary Chromatography, the 26th International Symposium on MicroScale Bioseparations and the 8th GC×GC Symposium, San Diego, CA, USA, 1-5 May 2011 35th International Symposium on Capillary Chromatography, 26th International Symposium on MicroScale Bioseparations and 8th GC×GC Symposium, 1226 (February): 140–48. doi:10.1016/j.chroma.2011.07.046.

Reichenbach, Stephen E., Xue Tian, Qingping Tao, Dwight R. Stoll, and Peter W. Carr. 2010. "Comprehensive Feature Analysis for Sample Classification with Comprehensive Two-Dimensional LC." *Journal of Separation Science* 33 (10): 1365–74. doi:10.1002/jssc.200900859.

Reid, Vanessa R., and Robert E. Synovec. 2008. "High-Speed Gas Chromatography: The Importance of Instrumentation Optimization and the Elimination of Extra-Column Band Broadening." *Talanta* 76 (4): 703–17. doi:10.1016/j.talanta.2008.05.012.

RYSER, HERBERT JOHN. 1963. *Combinatorial Mathematics*. 1sted. Vol. 14. Mathematical Association of America. http://www.jstor.org/stable/10.4169/j.ctt5hh8v6.

Samanipour, Saer, Petros Dimitriou-Christidis, Jonas Gros, Aureline Grange, and J. Samuel Arey. 2015. "Analyte Quantification with Comprehensive Two-Dimensional Gas Chromatography: Assessment of Methods for Baseline Correction, Peak Delineation, and

Matrix Effect Elimination for Real Samples." *Journal of Chromatography A* 1375 (January): 123–39. doi:10.1016/j.chroma.2014.11.049.

Sampat, Andjoe, Martin Lopatka, Marjan Sjerps, Gabriel Vivo-Truyols, Peter Schoenmakers, and Arian van Asten. 2016. "Forensic Potential of Comprehensive Two-Dimensional Gas Chromatography." *TrAC Trends in Analytical Chemistry* 80 (June): 345–63. doi:10.1016/j.trac.2015.10.011.

Schmarr, Hans-Georg, and Jörg Bernhardt. 2010. "Profiling Analysis of Volatile Compounds from Fruits Using Comprehensive Two-Dimensional Gas Chromatography and Image Processing Techniques." *Journal of Chromatography A* 1217 (4): 565–74. doi:10.1016/j.chroma.2009.11.063.

Seeley, John V., Frederick Kramp, and Christine J. Hicks. 2000. "Comprehensive Two-Dimensional Gas Chromatography via Differential Flow Modulation." *Analytical Chemistry* 72 (18): 4346–52. doi:10.1021/ac000249z.

Seeley, John V., and Stacy K. Seeley. 2013. "Multidimensional Gas Chromatography: Fundamental Advances and New Applications." *Analytical Chemistry* 85 (2): 557–78. doi:10.1021/ac303195u.

Shellie, Robert, Luigi Mondello, Philip Marriott, and Giovanni Dugo. 2002. "Characterisation of Lavender Essential Oils by Using Gas Chromatography–mass Spectrometry with Correlation of Linear Retention Indices and Comparison with Comprehensive Two-Dimensional Gas Chromatography." *Journal of Chromatography A* 970 (1–2): 225–34. doi:10.1016/S0021-9673(02)00653-2.

Siegler, W. Christopher, Brian D. Fitz, Jamin C. Hoggard, and Robert E. Synovec. 2011. "Experimental Study of the Quantitative Precision for Valve-Based Comprehensive Two-Dimensional Gas Chromatography." *Analytical Chemistry* 83 (13): 5190–96. doi:10.1021/ac200302b.

Soggiu, Alessio, Osvaldo Marullo, Enrico Capobianco, Paola Roncada, and Paola Roncada. 2009. "Empowering Spot Detection in 2DE Images by Wavelet Denoising." *In Silico Biology* 9 (3): 125–133. doi:10.3233/ISB-2009-0393.

Stadler, Sonja, Pierre-Hugues Stefanuto, Michał Brokl, Shari L. Forbes, and Jean-François Focant. 2013. "Characterization of Volatile Organic Compounds from Human Analogue Decomposition Using Thermal Desorption Coupled to Comprehensive Two-Dimensional Gas Chromatography–Time-of-Flight Mass Spectrometry." *Analytical Chemistry* 85 (2): 998–1005. doi:10.1021/ac302614y.

Stefanuto, P.-H., K. A. Perrault, R. M. Lloyd, B. Stuart, T. Rai, S. L. Forbes, and J.-F. Focant. 2015. "Exploring New Dimensions in Cadaveric Decomposition Odour Analysis." *Analytical Methods* 7 (6): 2287–94. doi:10.1039/C5AY00371G.

Stefanuto, Pierre-Hugues, Katelynn A. Perrault, Sonja Stadler, Romain Pesesse, Helene N. LeBlanc, Shari L. Forbes, and Jean-François Focant. 2015. "GC × GC–TOFMS and Supervised Multivariate Approaches to Study Human Cadaveric Decomposition

Olfactive Signatures." *Analytical and Bioanalytical Chemistry* 407 (16): 4767–78. doi:10.1007/s00216-015-8683-5.

Stevenson, Paul G., Mariam Mnatsakanyan, Georges Guiochon, and R. Andrew Shalliker. 2010. "Peak Picking and the Assessment of Separation Performance in Two-Dimensional High Performance Liquid Chromatography." *Analyst* 135 (7): 1541–50. doi:10.1039/B922759H.

Storey, John D. 2002. "A Direct Approach to False Discovery Rates." *Journal of the Royal Statistical Society: Series B (Statistical Methodology)* 64 (3): 479–498. doi:10.1111/1467-9868.00346.

Storey, John D. 2007. "The Optimal Discovery Procedure: A New Approach to Simultaneous Significance Testing." *Journal of the Royal Statistical Society: Series B (Statistical Methodology)* 69 (3): 347–368. doi:10.1111/j.1467-9868.2007.005592.x.

Tobias, Herbert J., Gavin L. Sacks, Ying Zhang, and J. Thomas Brenna. 2008. "Comprehensive Two-Dimensional Gas Chromatography Combustion Isotope Ratio Mass Spectrometry." *Analytical Chemistry* 80 (22): 8613–21. doi:10.1021/ac801511d.

Tomasi, Giorgio, Frans van den Berg, and Claus Andersson. 2004. "Correlation Optimized Warping and Dynamic Time Warping as Preprocessing Methods for Chromatographic Data." *Journal of Chemometrics* 18 (5): 231–41. doi:10.1002/cem.859.

Tranchida, Peter Q., Paola Donato, Francesco Cacciola, Marco Beccaria, Paola Dugo, and Luigi Mondello. 2013. "Potential of Comprehensive Chromatography in Food Analysis." *TrAC Trends in Analytical Chemistry*, Modern Food Analysis and Foodomics, 52 (December): 186–205. doi:10.1016/j.trac.2013.07.008.

Tranchida, Peter Q., Mariarosa Maimone, Flavio A. Franchina, Thiago Rodrigues Bjerk, Cláudia Alcaraz Zini, Giorgia Purcaro, and Luigi Mondello. 2016. "Four-Stage (Low-)Flow Modulation Comprehensive Gas Chromatography–quadrupole Mass Spectrometry for the Determination of Recently-Highlighted Cosmetic Allergens." *Journal of Chromatography A*, Mass Spectrometry: Inovation and Application - Part VIII, 1439 (March): 144–51. doi:10.1016/j.chroma.2015.12.002.

Trudgett, Mark J.E., Georges Guiochon, and R. Andrew Shalliker. 2011. "Theoretical Description of a New Analytical Technique: Comprehensive Online Multidimensional Fast Fourier Transform Separations." *Journal of Chromatography A* 1218 (22): 3545–54. doi:10.1016/j.chroma.2011.03.061.

van der Klift, Elbert J. C., Gabriel Vivó-Truyols, Frank W. Claassen, Frederique L. van Holthoon, and Teris A. van Beek. 2008. "Comprehensive Two-Dimensional Liquid Chromatography with Ultraviolet, Evaporative Light Scattering and Mass Spectrometric Detection of Triacylglycerols in Corn Oil." *Journal of Chromatography A* 1178 (1–2): 43–55. doi:10.1016/j.chroma.2007.11.039.

van der Westhuizen, Rina, Hein Potgieter, Nico Prinsloo, André de Villiers, and Pat Sandra. 2011. "Fractionation by Liquid Chromatography Combined with Comprehensive Two-Dimensional Gas Chromatography–mass Spectrometry for Analysis of Cyclics in

Oligomerisation Products of Fischer–Tropsch Derived Light Alkenes." *Journal of Chromatography A*, Selected Papers from the 34th ISCC and the 7th GCxGC Symposium34th International Symposium on Capillary Chromatography and 7th GCxGC Symposium, 1218 (21): 3173–79. doi:10.1016/j.chroma.2010.10.009.

Vasquez, N. Pérez, M. Crosnier de bellaistre-Bonose, N. Lévêque, E. Thioulouse, D. Doummar, T. Billette de Villemeur, D. Rodriguez, et al. 2015. "Advances in the Metabolic Profiling of Acidic Compounds in Children's Urines Achieved by Comprehensive Two-Dimensional Gas Chromatography." *Journal of Chromatography B* 1002 (October): 130–38. doi:10.1016/j.jchromb.2015.08.006.

Vendeuvre, Colombe, Fabrice Bertoncini, Laurent Duval, Jean-Luc Duplan, Didier Thiébaut, and Marie-Claire Hennion. 2004. "Comparison of Conventional Gas Chromatography and Comprehensive Two-Dimensional Gas Chromatography for the Detailed Analysis of Petrochemical Samples." *Journal of Chromatography A*, 8th International Symposium on Hyphenated Techniques in Chromatography and Hyphenated Chromatographic Analyzers, 1056 (1–2): 155–62. doi:10.1016/j.chroma.2004.05.071.

Vezzani, S., G. Castello, and D. Pierani. 1998. "Measurement and Prediction of Dead Times and Column Diameter in Capillary Gas Chromatography by Using Air, Methane and Some Solvents." *Journal of Chromatography A* 811 (1–2): 85–96. doi:10.1016/S0021-9673(98)00215-5.

Vial, Jérôme, Hicham Noçairi, Patrick Sassiat, Sreedhar Mallipatu, Guillaume Cognon, Didier Thiébaut, Béatrice Teillet, and Douglas N. Rutledge. 2009. "Combination of Dynamic Time Warping and Multivariate Analysis for the Comparison of Comprehensive Two-Dimensional Gas Chromatograms: Application to Plant Extracts." *Journal of Chromatography A*, 32nd International Symposium on Capillary Chromatography and 5th GCxGC Symposium, 1216 (14): 2866–72. doi:10.1016/j.chroma.2008.09.027.

Vial, Jérôme, Benoît Pezous, Didier Thiébaut, Patrick Sassiat, Béatrice Teillet, Xavier Cahours, and Isabelle Rivals. 2011. "The Discriminant Pixel Approach: A New Tool for the Rational Interpretation of GCxGC-MS Chromatograms." *Talanta* 83 (4): 1295–1301. doi:10.1016/j.talanta.2010.07.059.

Vis, Daniel J., Johan A. Westerhuis, Age K. Smilde, and Jan van der Greef. 2007. "Statistical Validation of Megavariate Effects in ASCA." *BMC Bioinformatics* 8 (1): 322. doi:10.1186/1471-2105-8-322.

Vivó-Truyols, Gabriel, and Hans-Gerd Janssen. 2010. "Probability of Failure of the Watershed Algorithm for Peak Detection in Comprehensive Two-Dimensional Chromatography." *Journal of Chromatography A* 1217 (8): 1375–85. doi:10.1016/j.chroma.2009.12.063.

Vogt, Leslie, Thomas Gröger, and Ralf Zimmermann. 2007. "Automated Compound Classification for Ambient Aerosol Sample Separations Using Comprehensive Two-Dimensional Gas Chromatography–time-of-Flight Mass Spectrometry." *Journal of Chromatography A* 1150 (1–2): 2–12. doi:10.1016/j.chroma.2007.03.006.

Wang, Bing, Aiqin Fang, John Heim, Bogdan Bogdanov, Scott Pugh, Mark Libardoni, and Xiang Zhang. 2010. "DISCO: Distance and Spectrum Correlation Optimization

Alignment for Two-Dimensional Gas Chromatography Time-of-Flight Mass Spectrometry-Based Metabolomics." *Analytical Chemistry* 82 (12): 5069–81. doi:10.1021/ac100064b.

Welke, Juliane Elisa, Vitor Manfroi, Mauro Zanus, Marcelo Lazzarotto, and Cláudia Alcaraz Zini. 2013a. "Differentiation of Wines according to Grape Variety Using Multivariate Analysis of Comprehensive Two-Dimensional Gas Chromatography with Time-of-Flight Mass Spectrometric Detection Data." *Food Chemistry* 141 (4): 3897–3905. doi:10.1016/j.foodchem.2013.06.100.

Wilson, R.B., J.C. Hoggard, and R.E. Synovec. 2012. "Fast, High Peak Capacity Separations in Gas Chromatography-Time-of-Flight Mass Spectrometry." *Analytical Chemistry* 84 (9): 4167–73. doi:10.1021/ac300481k.

Wilson, Ryan B., Jamin C. Hoggard, and Robert E. Synovec. 2013. "High Throughput Analysis of Atmospheric Volatile Organic Compounds by Thermal Injection – Isothermal Gas Chromatography – Time-of-Flight Mass Spectrometry." *Talanta* 103 (January): 95–102. doi:10.1016/j.talanta.2012.10.013.

Wilson, Ryan B., W. Christopher Siegler, Jamin C. Hoggard, Brian D. Fitz, Jeremy S. Nadeau, and Robert E. Synovec. 2011. "Achieving High Peak Capacity Production for Gas Chromatography and Comprehensive Two-Dimensional Gas Chromatography by Minimizing off-Column Peak Broadening." *Journal of Chromatography A*, Selected Papers from the 34th ISCC and the 7th GCxGC Symposium34th International Symposium on Capillary Chromatography and 7th GCxGC Symposium, 1218 (21): 3130–39. doi:10.1016/j.chroma.2010.12.108.

Wong, Yong Foo, Rachel N. West, Sung-Tong Chin, and Philip J. Marriott. 2015. "Evaluation of Fast Enantioselective Multidimensional Gas Chromatography Methods for Monoterpenic Compounds: Authenticity Control of Australian Tea Tree Oil." *Journal of Chromatography A* 1406 (August): 307–15. doi:10.1016/j.chroma.2015.06.036.

Woo, Sangsoon, Jeffrey T. Leek, and John D. Storey. 2011. "A Computationally Efficient Modular Optimal Discovery Procedure." *Bioinformatics* 27 (4): 509–15. doi:10.1093/bioinformatics/btq701.

Yang, Song, Jamin C. Hoggard, Mary E. Lidstrom, and Robert E. Synovec. 2013. "Gas Chromatography and Comprehensive Two-Dimensional Gas Chromatography Hyphenated with Mass Spectrometry for Targeted and Nontargeted Metabolomics." In *Metabolomics in Practice*, edited by Michael Lämmerhofer and Wolfram Weckwerth, 69–92. Wiley-VCH Verlag GmbH & Co. KGaA. http://onlinelibrary.wiley.com/doi/10.1002/9783527655861.ch4/summary.

Zhang, Dabao, Xiaodong Huang, Fred E. Regnier, and Min Zhang. 2008. "Two-Dimensional Correlation Optimized Warping Algorithm for Aligning GC×GC−MS Data." *Analytical Chemistry* 80 (8): 2664–71. doi:10.1021/ac7024317.